Research Report
Project Number: 930-373

Camber and Prestress Losses in High Performance Concrete Bridge Girders

Submitted to

Alabama Department of Transportation

Prepared by

James Michael Stallings
Sam Eskildsen

May 2001

1. Report No.	2. Government Accession No	3. Recipient's Catalog No.

4. Title and Subtitle	5. Report Date
Camber and Prestress Losses in High Performance Concrete Bridge Girders	May 2001
	6. Performing Organization Code

7. Author(s)	8. Performing Organization Report No.
James Michael Stallings Sam Eskildsen	

9. Performing Organization Name and Address	10. Work Unit No. (TRAIS)
Auburn University Highway Research Center 238 Harbert Engineering Center Auburn, AL 36849-5337	11. Contract or Grant No. ALDOT 930-373

12. Sponsoring Agency Name and Address	13. Type of Report and Period Covered
Alabama Department of Transportation Research & Development Bureau 1409 Coliseum Boulevard Montgomery, AL 36130-3050	14. Sponsoring Agency Code

15. Supplementary Notes

16. Abstract

Camber and strains were monitored for five AASHTO BT-54 girders of Alabama's HPC Showcase Bridge from release through completion of construction of the bridge. Camber of 31 girders was measured on a single day when the average girder age was 200-days. Specified release strength of the HPC girder concrete was 8,000 psi, and the specified 28-day strength was 10,000 psi. Cylinders of the HPC were made and match-cured during production of the girders for use in creep and shrinkage tests. Measured materials parameters and standard parameters were used in the Incremental Time Steps Method to calculate girder strains, camber and prestress losses up to the time of deck construction. Comparisons of the field measurements and values calculated using the measured materials parameters show good agreement. Error bands at plus 35% and minus 15% from the calculated cambers included all measured cambers for all ages to 300-days. Losses were measured from 1-day to approximately 300-days. For five girders with midspan strain gages, the average difference between the measured and calculated losses was 14%. For the three girders with quarter span strain gages, the average difference between the measured and calculated losses was 10%.

17. Key Words	18. Distribution Statement
bridges, bridge girders, prestressed concrete, high-performance concrete, camber, prestress losses, creep, shrinkage	

19. Security Classif. (of this report)	20. Security Classif. (of this Page)	21. No. of Pages	22. Price
		116	

ACKNOWLEDGEMENT

Material contained herein was obtained in connection with a research project, "High Performance Concrete Bridge Showcase," ALDOT 930-373, conducted by the Auburn University Highway Research Center. Funding for the project was provided by the Federal Highway Administration and the Alabama Department of Transportation. The funding, cooperation, and assistance of many people from each of these organizations are gratefully acknowledged. The authors also acknowledge the high level of interest and assistance provided by Sherman Prestressed Concrete.

DISCLAIMER

TABLE OF CONTENTS

List of Figures

Lists of Tables

CHAPTER ONE

Introduction

Eccentrically prestressed bridge girders deflect upward under the combined action of the prestressing force and the self-weight of the girder. This upward deflection is called camber. Creep and shrinkage of the concrete, and strand relaxation are time-dependent phenomena which cause the prestressing force to decrease with time. Creep of the concrete also has a direct multiplying affect on the upward deflection due to the prestressing force as well as the downward deflection due to self-weight. Accurate estimates of camber require an appropriate accounting for the time-dependent losses of prestress and the direct effects of creep.

Calculated predictions of girder camber are made during the design of a bridge. Camber of the girders affects the positioning of the deck forms during construction. The ability to accurately predict the camber at the design stage is desirable since camber affects the construction process.

Prestress losses are also calculated during the design process. The larger the losses, the larger the required initial prestress for resistance to applied loads. Use of overly conservative methods for calculating losses can limit the span lengths of girders and lead to excessive camber as a result of specifying an unnecessarily large initial prestress.

The use of high-performance concrete (HPC), or high-strength concrete, in bridge girders can allow the use of longer span lengths as is the case with Alabama's HPC

Showcase Bridge. Longer span lengths require a higher prestressing force. The combination of longer span lengths and higher prestressing force may lead to large calculated cambers. Significant overestimates of camber during the design stage may falsely discourage the use of long spans. Ultimately this makes bridge construction more expensive.

High-performance concrete research in North America has shown that HPC tends to exhibit less creep and shrinkage than conventional concretes. This improved creep and shrinkage performance results in reduced time-dependent effects on camber and prestress losses. Methods for estimating camber and prestress losses that were developed for conventional concretes may not provide accurate results for HPC bridge girders.

Scope

The research reported in subsequent chapters started as an effort to identify or create a reliable and useable method to predict camber and prestress losses for HPC girders. As the work progressed, currently available methods were found to be reasonably well developed and new methods were not required. The goal of the work presented here is to investigate the accuracy of available methods for the prediction of camber and prestress losses in AASHTO girders made with HPC. To this end, laboratory tests were performed to determine the creep, shrinkage, and elastic properties of HPC used in the production of the girders of Alabama's HPC Showcase Bridge. Field measurements of girder camber and strains for five HPC girders were made for approximately one year. Calculated cambers, strains, and prestress losses are compared to measured values. Based on the length of time for which field measurements were

made, the focus of this report is the prediction of camber and prestress losses up to the time of placement of the bridge deck slab.

CHAPTER TWO

Literature Review

Introduction

Camber in prestressed concrete bridge girders is the product of a number of factors. The prestressing force itself leads to initial camber. The effects of shrinkage, creep, elastic deformation, relaxation of the strand, and thermal gradients all lead to changes in this initial camber. In this chapter, each of these effects will be discussed. Several methods exist for estimating the camber of prestressed girders, and in the last section of this chapter these methods are discussed.

Shrinkage

"Shrinkage designates the time-dependent strains which concrete undergoes at constant temperature without any external strains"(Smerda 1988). There are four types of shrinkage: Plastic shrinkage, autogenous shrinkage, drying shrinkage, and carbonation shrinkage.

Plastic shrinkage occurs as concrete sets. While the concrete is still in a plastic state, water can be removed from the surfaces of the concrete by evaporation or suction resulting from contact with another medium such as soil.

Autogenous shrinkage occurs after setting has taken place. Concrete continues to hydrate even when no moisture from the external environment is available. Water from the capillary pores, in a process of self-desiccation, is used to continue hydration of the

cement. Autogenous shrinkage is very small, of the order of $40x10^{-6}$ in./in. during the first year. As a consequence of the small magnitude of autogenous shrinkage it is commonly included as part of the next type of shrinkage: drying shrinkage (Neville 1996).

Drying shrinkage is caused by the removal of water when concrete is stored in air at a relative humidity of less than 100%. The loss of free water to unsaturated air begins the process of drying shrinkage but does not contribute greatly to the shrinkage. Free water is not involved in hydration, is not bound into the cement paste electrically, or physically absorbed into the constituents of the concrete mix. It is the loss of absorbed water (after all free water is depleted) to the atmosphere that results in drying shrinkage. In this context, water retained by electrostatic adhesion, or physical absorption is termed absorbed water. For reasons that are unclear, drying shrinkage is not fully reversible (Bazant 1982).

Carbonation occurs first at the surface of concrete and progresses deeper with time. The mechanisms of carbonation are not fully established. However, Neville (1996) suggests that carbonation shrinkage is likely due to the dissolving of $Ca(OH)_2$ and movement of $CaCO_3$ to spaces free of compressive stress induced by drying shrinkage. The effects of drying shrinkage and carbonation shrinkage are not independent.

The combined effect of drying shrinkage and carbonation shrinkage is strongly affected by the sequence in which they occur. If they occur at the same time the combined shrinkage is much less than the case of drying followed by carbonation.

ACI 209R-92 (1992) states that approximately 80% of all shrinkage will occur during the first year. T he committee also suggested that the average value of ultimate shrinkage is on the order of 780×10^{-6} in./in. for normal performance concretes.

Factors Affecting Shrinkage

Nawy (1989) lists seven factors that influence the shrinkage of concrete: Aggregate, water to cement (w/c) ratio, size of the concrete element, ambient conditions, amount of reinforcement, admixtures, and type of cement.

Shrinkage of the neat cement paste is restrained by the presence of aggregate. Neville (1996) proposes the following relationship between aggregate content and free shrinkage of the neat cement paste:

$$S_c = S_p(1-a)^n \qquad (2\text{-}1)$$

where S_c is the concrete shrinkage; S_p is the shrinkage of the neat cement paste; a is the total percent aggregate content; and n is a parameter having values between 1.2 and 1.7 .

The w/c ratio strongly affects the amount of shrinkage. A higher w/c ratio results in a greater magnitude of shrinkage. A higher w/c ratio corresponds to a more porous concrete, which favors the conditions for moisture transfer between the concrete and surrounding environment (Rusch 1983). Generally, as the w/c ratio rises so does the water content. At large water contents some aggregate volume is lost along with the restraint it provided thereby allowing increased shrinkage (Neville 1996).

The ambient conditions around exposed concrete surfaces exert a large influence on the magnitude of shrinkage. It follows that the amount of exposed surface would therefore be a consideration. The total volume of concrete plays an important role as

well. The period during which the member can be expected to undergo significant shrinkage is longer for more volumous members. In a large member it takes more time for drying shrinkage to initiate toward the center of the mass (Nawy 1989).

The relative humidity and temperature affects the magnitude of shrinkage. Shrinkage is greater at lower relative humidity (Neville 1996). Lower relative humidity creates a condition of greater moisture transfer from the concrete and therefore increases shrinkage.

Reinforcement in concrete does not reduce the amount of shrinkage per se. It restrains the concrete from shrinking as it would if it were free to deform. Reinforcement restrains the shrinkage in a manner similar to the restraint offered to the neat cement paste by aggregate (Nawy 1989).

Fly ash and granulated blast furnace slag have been shown to increase the magnitude of shrinkage when used as a replacement for cement. When silica fume is used as a replacement the resulting concrete tends to show an increase in the long-term shrinkage. Superplasticisers can increase the magnitude of shrinkage up to 20%, while entrained air seems to have little effect on concrete shrinkage (Neville 1996).

Some suggest that cement type has little effect on shrinkage. However, cement content, and w/c ratio, do impact shrinkage (Smerda 1988). As the cement content is increased at a constant w/c the magnitude of shrinkage increases.

Methods to Predict Shrinkage

A multitude of models exist for the prediction of shrinkage: The CEB-FIB, ACI, Banzant and Panula, and Concrete Society methods among others (Neville 1983). The ACI method has been chosen for use in this research.

The method recommended by ACI 209R-92 (1992) models shrinkage using the following basic relationship:

$$\varepsilon_{sh}(t) = \frac{t^{\alpha}}{f + t^{\alpha}} (\varepsilon_{sh})_u \gamma_{sh} \tag{2-2}$$

where $(\varepsilon_{sh})_u$ is the ultimate shrinkage value. In the absence of test data ACI 209R-92 recommends $(\varepsilon_{sh})_u = 780 \times 10^{-6}$ in./in.; $\alpha = 1.0$; and $f = 55$. A value for γ_{sh} is obtained by multiplying the factors outlined below.

$$\gamma_{sh} = \gamma_{la}\,\gamma_{\lambda}\,\gamma_{vs}\,\gamma_{s}\,\gamma_{\psi}\,\gamma_{c}\,\gamma_{\alpha} \tag{2-3}$$

For loading ages later than one to three days for steam-cured concrete the loading age correction factor, γ_{la}, is given as

$$\gamma_{la} = 1.13(t_{la})^{-0.118} \tag{2-4}$$

where t_{la} is the loading age in days. If the average ambient relative humidity is greater than 40% the following correction factor applies

$$\gamma_{\lambda} = 1.4\text{-}0.010\lambda \qquad \text{for } 40 \le \lambda < 80 \tag{2-6a}$$

$$\gamma_{\lambda} = 3.0\text{-}0.030\lambda \qquad \text{for } 80 > \lambda \le 100 \tag{2-6b}$$

where λ is the average relative humidity. If the volume to surface ratio is other than 1.5 in. the following volume-surface ratio correction factor, γ_{vs}, must be used:

$$\gamma_{vs} = 1.2e^{(-0.12\ v/s)} \tag{2-7}$$

where v/s is the volume to surface ratio in inches. Eqn. 2-3 also requires several correction factors based on concrete composition. For slump:

$$\gamma_s = 0.89s \tag{2-8}$$

where s is the slump in inches. The fine aggregate percentage correction factor is:

$$\gamma_\psi = 0.30 + 0.014\psi \quad \text{for } \psi \leq 50\% \tag{2-9a}$$

$$\gamma_\psi = 0.90 + 0.002\psi \quad \text{for } \psi > 50\% \tag{2-9b}$$

where ψ is the fine aggregate percentage. Cement content is accounted for using γ_c:

$$\gamma_c = 0.75 + .00036c \tag{2-10}$$

where c is the cement content in pounds per cubic yard. The last correction factor is the air content correction factor:

$$\gamma_\alpha = 0.95 + 0.008\alpha \tag{2-11}$$

where α is the air content in percent.

Creep

Creep is the gradual increase in strain under constant stress. Using this definition strain in a loaded concrete sample may be separated into three distinct parts: Creep strain, shrinkage strain, and elastic strain. This interpretation implies the three are directly additive and not interrelated (Neville 1983). This is, of course, a simplification.

Creep and shrinkage are not fully independent. Shrinkage has been shown to increase creep when the shrinkage is restrained. However, when shrinkage is not restrained the interaction between creep and shrinkage is minimal (Neville 1983). Because the modulus of elasticity of concrete increases with age, the portion of the total deformation defined as elastic decreases with age as shown by Figure 2.1. Although

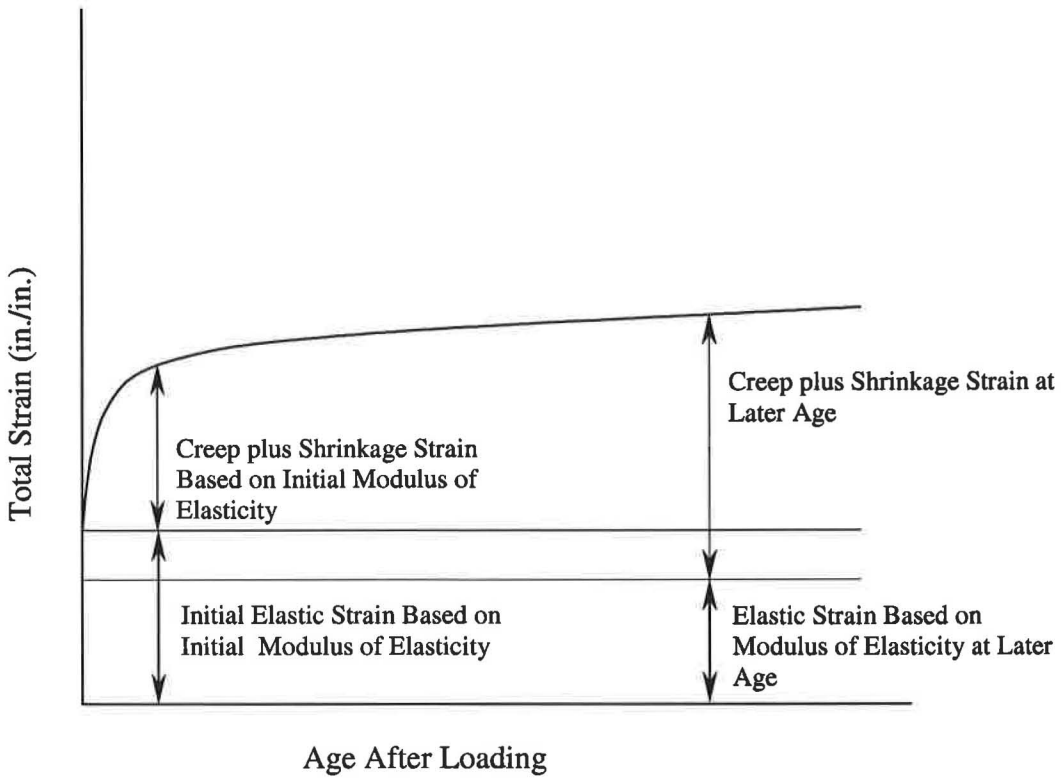

Figure 2.1 Change in Elastic Strain with Time

these errors are recognized, the common assumption that creep and shrinkage are additive is made in this research.

Factors Affecting Creep

Stress state, age at loading, curing method, ambient conditions, and concrete composition all affect the creep properties of concrete. Creep in normal performance concrete has been shown to be directly proportional to stress up to 40% of the compressive strength of the concrete. Linearity has been observed after stresses in excess of 40%, however, as micro-cracking is thought to initiate at the 40% level a limiting value of 40% is conservative (Neville 1996).

Neville (1983) and Smerda (1988) report ultimate creep in tension and ultimate creep in compression to be equivalent for the same stress level, with Neville indicating that tensile creep develops quicker than compressive creep during the early months of loading. The upper limit of linearity for tensile creep appears to be similar to that of concrete in compression, 40% of the ultimate tensile strength. It is interesting to note that most test data is for tension due to concentric loading, virtually no data exists on tensile creep due to bending stresses. Given the sensitivity of concrete properties to cracking, and the widespread use of the creep coefficient as a multiplier for deflections in concrete beams, more information on tensile creep due to bending would be beneficial.

Concrete that has been allowed to age unloaded exhibits lower long-term creep values compared to similar concrete loaded at an earlier age. The time dependent distribution, or initial rate, of creep also changes (Smerda 1988). Steam curing reduces creep by 30% to 50% below the creep for similar concrete that is moist cured (Neville

1983). Steam curing accelerates hydration. In this way the effect of steam curing may simply be the result of higher early strength attained by steam cured concrete. A stronger early-age concrete will exhibit reduced creep.

Ambient conditions after initial curing affect the rate and magnitude of creep. A lower relative humidity produces a greater rate of creep and greater long-term creep values. The effect of relative humidity is the result of the imbalance between the cement paste's moisture content and ambient moisture content. In other words, a low ambient relative humidity will draw moisture from the cement paste. Once the paste reaches equilibrium with the ambient conditions creep values are no longer affected by relative humidity (Neville 1983).

The influence of relative humidity is a function of the size of the member and the amount of exposed surface. Concrete on the outer surface undergoes drying while deeper portions of the concrete mass cure under conditions of high humidity (where creep is reduced). Thus, in masses with a large volume to surface ratio, creep is reduced.

Creep is influenced by cement and aggregate content. The volumetric content of aggregate, unhydrated cement, and creep coefficient (creep at time equals infinity/elastic strain) are related as follows:

$$\log \frac{c_p}{c} = \alpha \frac{1}{1-g-u} \tag{2-12a}$$

$$\alpha = \frac{3(1-\mu)}{1+\mu+2(1-2\mu_a)\frac{E}{E_a}} \tag{2-12b}$$

where c_p is the creep coefficient of the neat cement paste; c is the creep coefficient of concrete; g is the volumetric content of total aggregate in percent; u is the volumetric content of unhydrated cement; μ_a is Poisson's ratio of coarse aggregate; μ is Poisson's ratio of hardened cement paste; E_a is the modulus of elasticity of aggregate; and E is the modulus of elasticity for the surrounding cement paste (Neville 1996).

From Eqn.(2-12) we see the relationship of creep to aggregate volume. An increase in the aggregate content from 65% to 75% percent will yield a decree in the creep coefficient (creep strain/elastic strain) of ten percent. The equation also demonstrates the effect of the aggregate's modulus of elasticity. A greater modulus will offer more restraint to the creep of the cement paste, reducing the creep values (Neville 1983).

Admixtures such as air entraining agents, superplasticisers, silica fume, and fly ash can have an affect on the creep properties of concrete. Neville states that air entrainment in and of its self does not influence creep. The addition of air entrainment does, however, affect the mix properties and thus indirectly affect the creep properties of concrete.

Superplasticisers have been shown to slightly increase creep. But, the inclusion of a superplasticier allows for a lower water to cement ratio and better workability leading to superior compaction--both factors that reduce creep. Long-term creep is reduced by the addition of fly ash and silica fume.

Creep Model

As with shrinkage several techniques have been developed to model creep. Logarithmic, exponential, and various power expressions have all been proposed. In following as with the preceding section on shrinkage, the method presented in ACI 209R-92 (1992) for predicting creep will be considered here.

The ACI 209R-92 (1992) method for predicting creep is based on the same form of mathematical relation as that for shrinkage. The creep coefficient (creep strain divided by initial elastic strain) as a function of time is:

$$C(t) = \frac{t^{\varphi}}{d + t^{\varphi}} C_u \gamma_c \qquad (2\text{-}13)$$

where C_u is the ultimate creep coefficient (creep coefficient at time equals infinity). In the absence of test data ACI 209R-92 (1992) recommends $C_u = 2.35$; $\varphi = 0.6$; and $d = 10$. A value for γ_c is obtained by multiplying the factors outlined below as shown in Eqn. 2-14.

$$\gamma_c = \gamma_{la}\,\gamma_\lambda\,\gamma_{vs}\,\gamma_s\,\gamma_\psi\,\gamma_\alpha \qquad (2\text{-}14)$$

For loading ages later than one to three days for steam-cured concrete the loading age correction factor, γ_{la}, is given as

$$\gamma_{la} = 1.25(t_{la})^{-0.118} \qquad (2\text{-}15)$$

where t_{la} is the loading age in days. If the average ambient relative humidity is greater than 40% the following correction factor applies

$$\gamma_\lambda = 1.27\text{-}0.0067\lambda \qquad \text{for } \lambda > 40 \qquad (2\text{-}16)$$

where λ is the average relative humidity. If the volume to surface ratio is other than 1.5 in., the volume-surface ratio correction factor, γ_{vs}, must be used:

$$\gamma_{vs} = \frac{2}{3}\left(1+1.13e^{(-0.54v/s)}\right) \tag{2-17}$$

where v/s is the volume to surface ratio in inches. Eqn. 2-14 also requires several correction factors based on the concrete composition. For slump:

$$\gamma_s = 0.82 + 0.067s \tag{2-18}$$

where s is the slump in inches. The fine aggregate percentage correction factor is:

$$\gamma_\psi = 0.88 + 0.0024\psi \tag{2-19}$$

where, ψ is fine aggregate percentage. The last correction factor is the air content correction factor:

$$\gamma_\alpha = 0.46 + 0.09\alpha \quad \gamma_\alpha \geq 1.0 \tag{2-20}$$

where α is the air content in percent.

Modeling Creep and Shrinkage Data

Farrington et al. (1996) modified the coefficients of the ACI 209R-92 (1992) equations to model creep and shrinkage of HPC. Using least squares regression the Farrington et al. fitted Eqn. 2-2 and 2-13 to HPC creep and shrinkage data. They chose to investigate changes in f, d, $(\varepsilon_{sh})_u$, and C_u while keeping values of α and φ equal to the values suggested by ACI 209R-92 (α=1 and φ=0.6). The researchers tested cylinders cured under different conditions and loaded at different ages. Table 2.1 shows the results obtained for steam-cured cylinders loaded at one day.

Table 2.1 Values Reported by Farrington et al.(1996) for Modeling Creep and Shrinkage

Type of Concrete	f	d	$(\varepsilon_{sh})u$ (in./in.)	Cu
Steam-Cured, loaded at one day	19	-	450	-
Steam-Cured, loaded at one day	-	7	-	2.31
Steam-Cured, loaded at one day	-	7	-	1.75
Steam-Cured, loaded at one day	-	5	-	1.84

- Data Not Available

Modulus of Elasticity

The modulus of elasticity is related to the compressive strength of the concrete. The correct form of the relationship remains the subject of debate. The ACI 318-95 building code suggests the modulus is a function of the unit weight of the concrete.

$$E_c = 33w^{1.5}\sqrt{f_c'} \tag{2-21}$$

Eqn. 2-21 was developed for compressive strengths up to about 6,000 psi. Beyond the 6,000 psi limit Eqn. 2-21 over predicts the modulus of elasticity. For strengths above 6,000 psi ACI 363R-92 (1992) concludes a better fit is obtained using:

$$E_c = (40{,}000\sqrt{f_c'} + 10^6)\left(\frac{w}{145}\right)^{1.5} \tag{2-22}$$

A number of other methods, equations, etc. are available. The common link in these methods is the dependence of the modulus on the concrete strength. Neville (1998) states "all that can be said reliably is that the increase in modulus of elasticity is progressively lower than the increase in compressive strength."

Relaxation of Steel Prestressing Strands

Tendon relaxation is very similar to concrete creep except that creep is the gradual increase in strain under constant stress, while steel relaxation is the gradual loss of stress under constant strain (Nawy 1989). The equation used to predict the relaxation of stress relieved prestressing strands is:

$$\Delta f_{pR} = \left(\frac{(\log t_2 - \log t_1)}{10}\right)\left(\frac{f_{pi}}{f_{py}} - 0.55\right) \tag{2-22}$$

where f_{pi} is the initial prestress level; f_{py} is the yeild stress; t_1 and t_2 are the times at the beginning and the end of a period of relaxation measured in hours. For low relaxation strands the constant 10 in the denominator becomes 45.

Camber, Deflection and Prestress Losses

Short-term deflections of prestressed concrete members can be calculated using classical methods for linear elastic beams. Long-term deflections and deformations are a more complex issue. While section properties, loading information, and elastic modulus are sufficient for short-term analysis, long-term analysis requires considerably more information about the material and ambient conditions as well as the section and elastic properties.

Several methods are listed in ACI 435R-95 (1995) for calculating long-term deflection and camber in prestressed concrete members: The PCI Multipliers Method, Incremental Time-Steps Method, Approximate Time-Steps Method, Axial Strain and Curvature Method, Prestress Loss Method, and CEB-FIP Model Code Method.

The PCI multiplier method estimates long-term camber and deflection by multiplying short-term deflections by factors ranging from 1.80 to 3.00. The suggested multipliers are shown in Table 4.6.2 of *The PCI Design Handbook* (PCI 1992) which is reproduced in Figure 2.2.

The Incremental Time-Steps Method is based on calculation of deflection due to time-dependent creep, shrinkage, and relaxation losses. The procedure is incremental, tedious, and time consuming, lending itself to computer solution. The strain distributions, at the ends and midspan, prestressing forces, creep loss, shrinkage loss, and

		Without Composite Topping	With Composite Topping
At erection:			
(1)	Deflection (downward) component – apply to the elastic deflection due to the member weight at release of prestress	1.85	1.85
(2)	Camber (upward) component – apply to the elastic camber due to prestress at the time of release of prestress	1.80	1.80
Final:			
(3)	Deflection (downward) component – apply to the elastic deflection due to the member weight at release of prestress	2.70	2.40
(4)	Camber (upward) component – apply to the elastic camber due to prestress at the time of release of prestress	2.45	2.20
(5)	Deflection (downward) – apply to elastic deflection due to superimposed dead load only	3.00	3.00
(6)	Deflection (downward) – apply to elastic deflection caused by the composite topping	-	2.30

Figure 2.2 PCI Multipliers

steel relaxation are calculated for each time increment (Nawy 1989). Curvature at the end and midspan is determined from the computed strain distributions. Using the computed curvatures moment area is applied to evaluate the camber.

The Approximate Time-Steps Method is based on the summation of deflections due to the various time dependent factors. Unlike the Incremental Time Steps Method, the summation of factors is done only twice; immediately after release and at the final condition. This method yields comparable results to the PCI Multiplier Method. The Approximate Time-Steps Method is a compromise between complexity and efficiency of calculation.

The Axial Strain and Curvature Method is a procedure for the analysis of instantaneous and long-term stresses and strains in reinforced concrete cross-sections, with or without prestressing but considering cracking. The slope of the strain diagram is set equal to curvature, which can be used to calculate the change in deflection. The method does not require determination of prestress losses, but introduces an aging coefficient that adjusts the modulus of concrete, E_c, between initial release and the time under consideration.

The Prestress Loss Method assumes that sustained dead load due to self weight does not produce cracking. Therefore the effects of creep, shrinkage, and relaxation are considered only for uncracked cross sections. The method provides stress loss coefficients for creep and shrinkage effects. A set of multipliers are applied to the deflections due to initial prestress, member self-weight, superimposed dead load, and time-dependent prestress loss.

Prestress Losses by ASSHTO LRFD

ASSHTO LRFD (1993) provides two methods for estimating prestress losses. The first is the AASHTO 'lump sum' method. In the lump sum method, prestress loss is composed of two parts. The first is elastic shortening. The second represents the remaining time dependent prestress losses. One equation is given for each. The values are then added to give the total lump sum prestress loss.

ASSHTO LRFD also provides a method for "refined estimates of the time-dependent losses" in prestressed girders. Section 5.9.5.1 gives the following equation for estimating the total prestress loss in pretension members:

$$\Delta f_{PT} = \Delta f_{pES} + \Delta f_{pSR} + \Delta f_{pCR} + \Delta f_{pR} \tag{2-23}$$

where Δf_{PT} is the total prestress loss in ksi; Δf_{pES} is the loss due to elastic shortening in ksi; Δf_{pSR} is the loss due to shrinkage in ksi; Δf_{pCR} is the loss due to creep of the concrete in ksi; and Δf_{pR} is the loss due to relaxation of the steel in ksi.

Section 5.9.5.2.3a gives the following equation for evaluation of Δf_{pES}:

$$\Delta f_{pES} = \frac{E_p}{E_{ci}} f_{cgp} \tag{2-24}$$

where E_p is the modulus of elasticity of prestressing steel in ksi; E_{ci} is the modulus of elasticity of the concrete at transfer in ksi; f_{cgp} is the sum of concrete stresses at the center of gravity of the prestressing tendons due to the prestressing force at transfer and the self weight of the member at the section of maximum moment in ksi.

AASHTO LRFD section 5.9.5.4.2 gives the following equation for Δf_{pSR} :

$$\Delta f_{pSR} = (17.0 - 0.150H) \tag{2-25}$$

where H is the average annual ambient relative humidity. Section 5.9.5.2.4.3 gives the following equation for Δf_{pCR}:

$$\Delta f_{pCR} = 12.0 f_{cgp} - 7.0\Delta f_{cdp} \tag{2-26}$$

where f_{cgp} is the concrete stress at the center of gravity of prestressing steel at transfer in ksi; Δf_{cdp} is the change in concrete stress at the center of gravity of the prestressing steel due to permanent loads, except the load acting at the same time the prestressing force is applied. Values of Δf_{cdp} should be calculated at the same section for which f_{cgp} is calculated. Section 5.9.5.4.4 separates the losses due to relaxation, Δf_{pR}, into two parts. First the relaxation of the strands prior to transfer are calculated:

$$\Delta f_{pR1} = \frac{\log(24t)}{40.0}\left[\frac{f_{pi}}{f_{py}} - 0.55\right] f_{pj} \tag{2-27}$$

where t is the time estimated in days from strand stressing to transfer; f_{pj} is the initial stress in the tendons at the end of stressing in ksi; and f_{py} is the specified yield strength of the prestressing steel in ksi. Relaxation losses after transfer are computed from the following:

$$\Delta f_{pR2} = 0.3(20.0 - 0.4\Delta f_{pES} - 0.2(\Delta f_{pSR} + \Delta f_{pCR})) \tag{2-28}$$

The total relaxation loss is:

$$\Delta f_{pR} = \Delta f_{pR1} + \Delta f_{pR2} \tag{2-29}$$

CHAPTER THREE

Bridge and Girder Instrumentation

Introduction

Measurements of actual girder temperature gradients, prestress losses, and camber are needed to evaluate the methods for calculating camber and prestress losses proposed in subsequent chapters. Instrumentation for making these measurements (and other types of measurements) was installed in the span between Bent 5 and Bent 6 of the Uphapee Creek HPC Showcase Bridge in Macon County, Alabama. Sensors were installed in the deck and in all five BT-54 girders in the bridge span. A plan view of the deck showing the general location of the sensors in the deck, the overall geometry, and the girder numbering is provided in Figure 3.1. Electrical resistance strain gages installed in the concrete deck were mounted on pieces of 0.5-in. diameter reinforcing bar 4 ft in length. These pieces of reinforcing bar were installed parallel and transverse to the girders near the top and bottom of the deck slab as shown in Figures 3.1 and 3.2. Figure 3.2 shows a transverse cross section through the deck slab. The location of the #4 bars shown matches the location of the instrumented bars that were oriented parallel to the girders. The location of the #5 bars shown matches the location of the instrumented bars that were oriented perpendicular to the girders. The girders were instrumented with vibrating wire strain gages, thermocouples, and electrical resistance strain gages. Girder details are

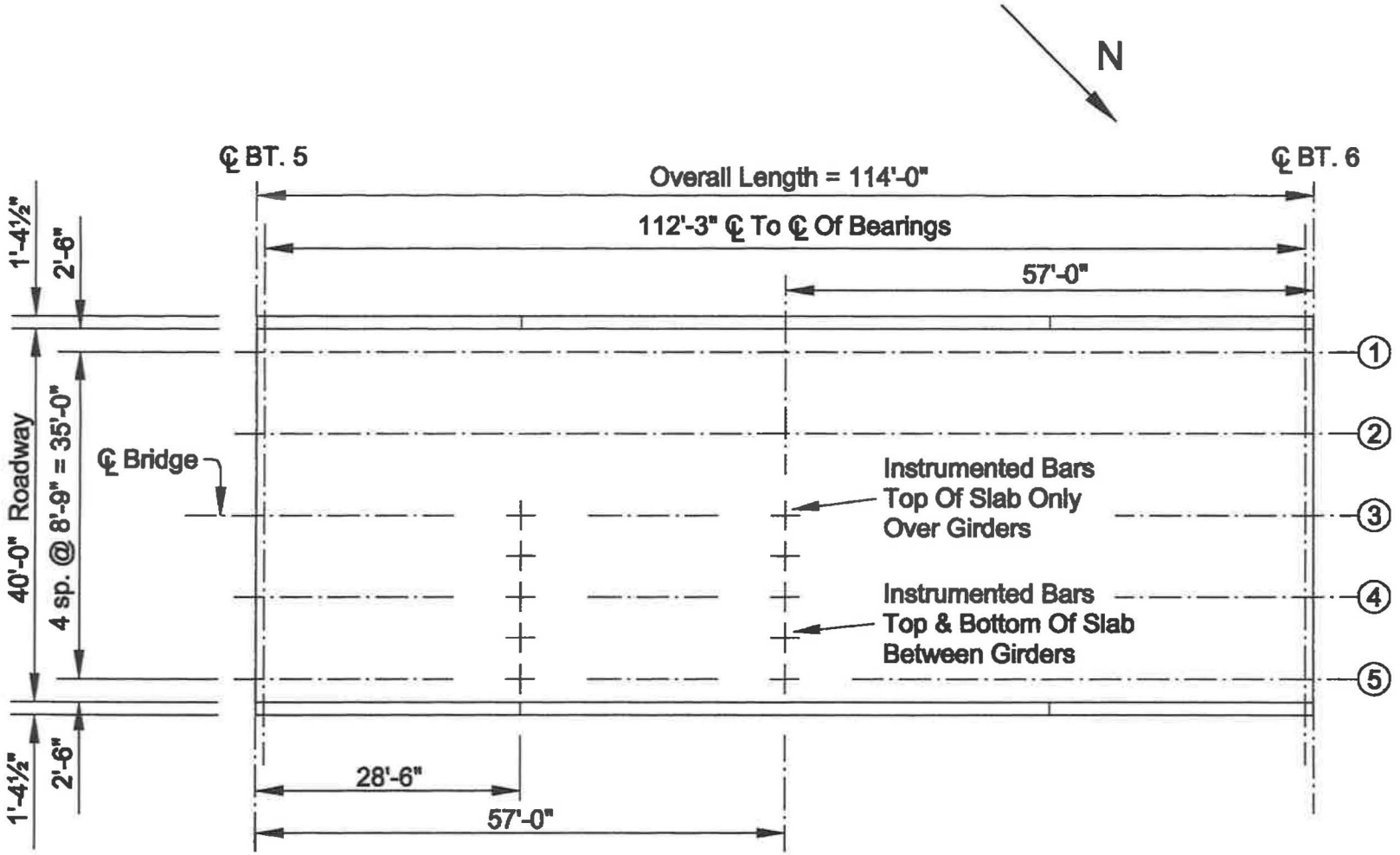

Figure 3.1 Bridge Geometry and Locations of Electrical Resistance Strain Gages in Deck

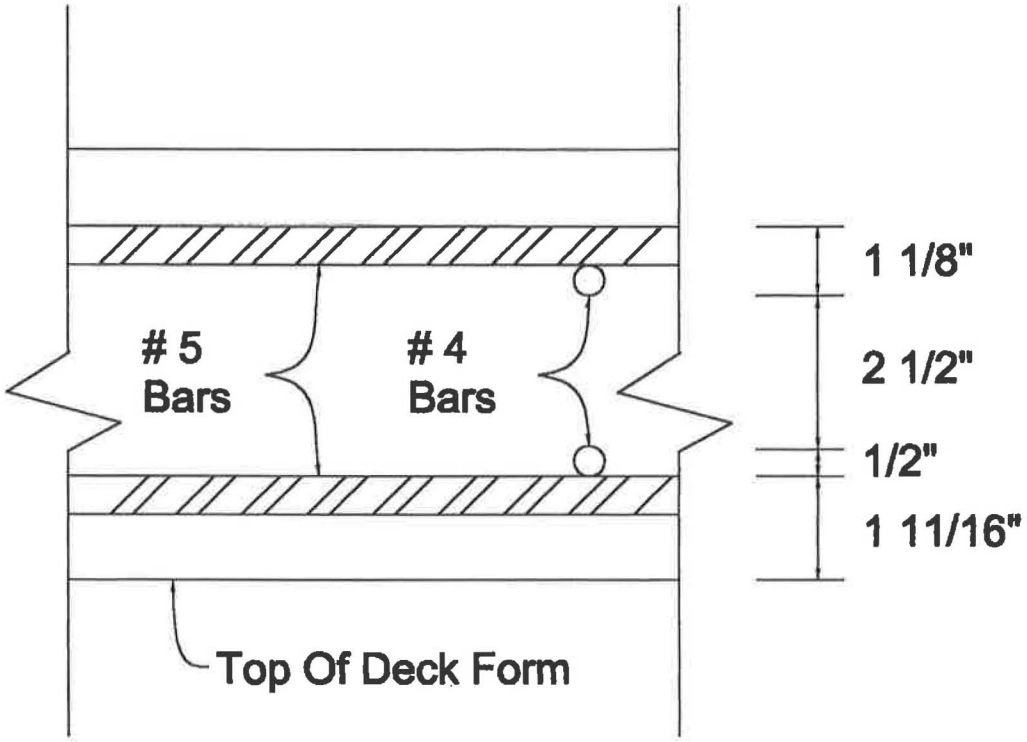

Figure 3.2 Depths of Reinforcement in Deck

shown in Figures 3.3 and 3.4. Locations of sensors in the girders are shown in Figure 3.5 and Table 3.1.

Data Acquisition

An automatic data acquisition system, Campbell Scientific's CR10X, was used to record all temperature and strain data. The CR10X is a 12 volt datalogger consisting of a detachable wiring panel and a measurement and control module. The datalogger is shown in Figures 3.6 and 3.7. The CR10X was mounted at the bridge site in an 18x18x6 in. electrical box attached to a diaphragm at midspan.

To increase the number of sensors that could be monitored by the datalogger, two different types of multiplexers were used with the CR10X: Two AM25Ts (used to multiplex a total of 50 thermocouples) and one AM416 (used to multiplex 16 vibrating wire strain gages). The datalogger support software, PC208W, was used to monitor and collect data from the CR10X.

Girder Instrumentation

The strain at different locations in the girders was measured using Geokon's Model 4911 Vibrating Wire Rebar Strain Meter, referred to subsequently as a vibrating wire strain gage. Each gage was purchased preassembled for direct embedment in concrete (see Figure 3.8). The vibrating wire strain gage consists of two lengths of steel reinforcing bar welded onto each end of a steel cylinder which contains the vibrating wire strain gage element with an electronic "plucking" coil. Each vibrating wire gage was connected to the CR10X which provided the necessary excitation to pluck the vibrating

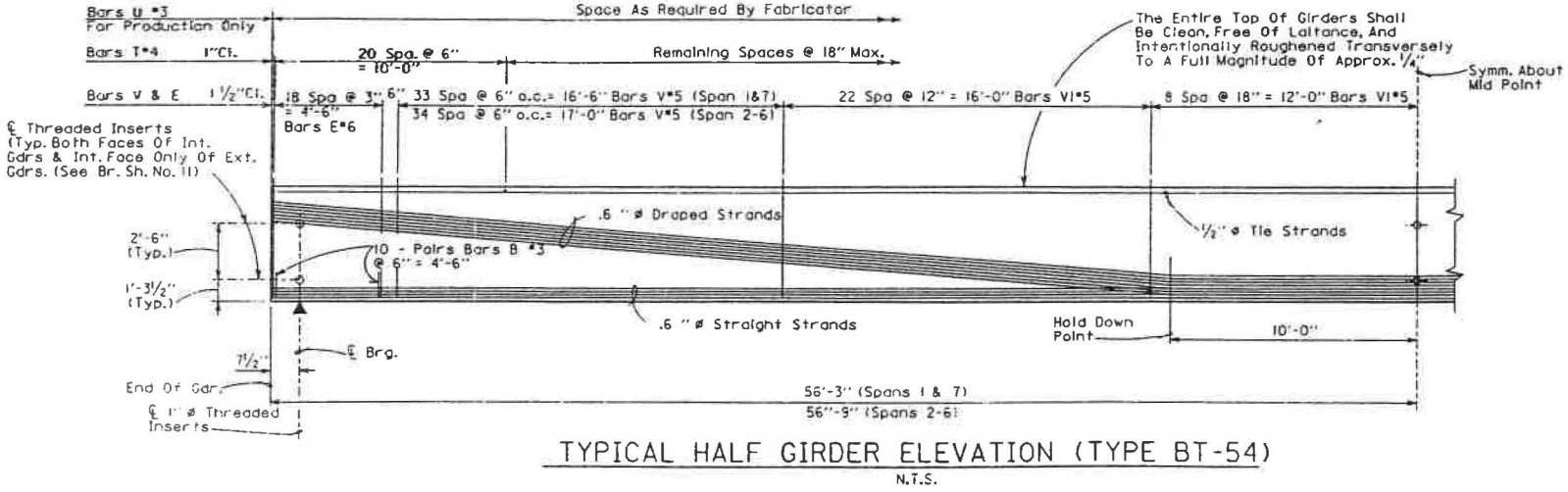

Figure 3.3 Typical Elevation of HPC Girder

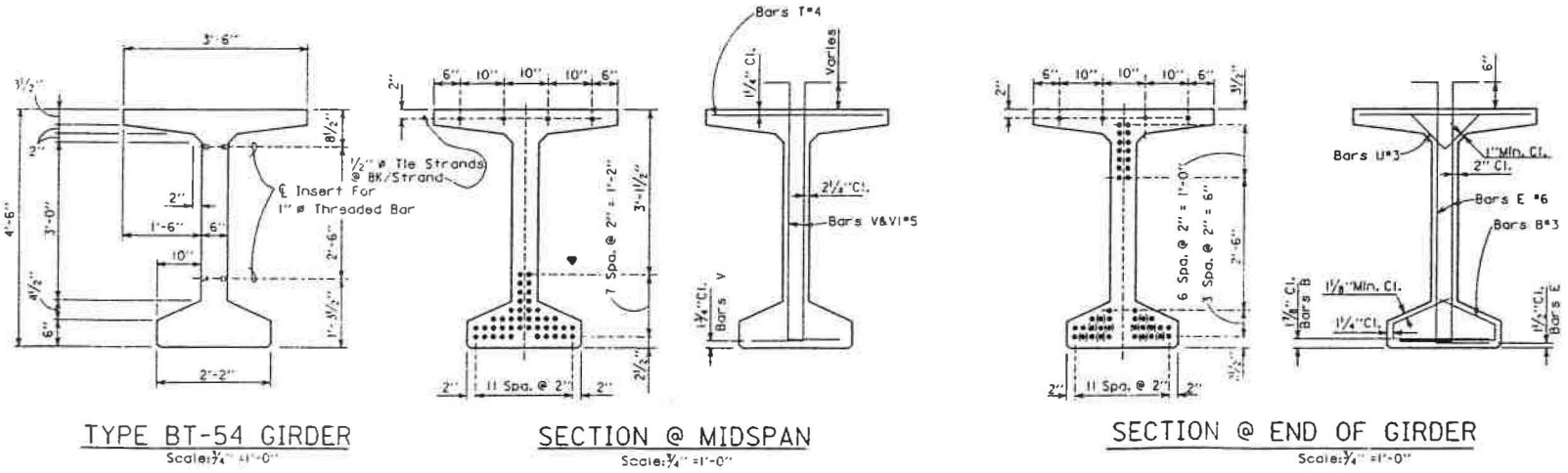

Figure 3.4 Typical Cross-Sections of HPC Girder

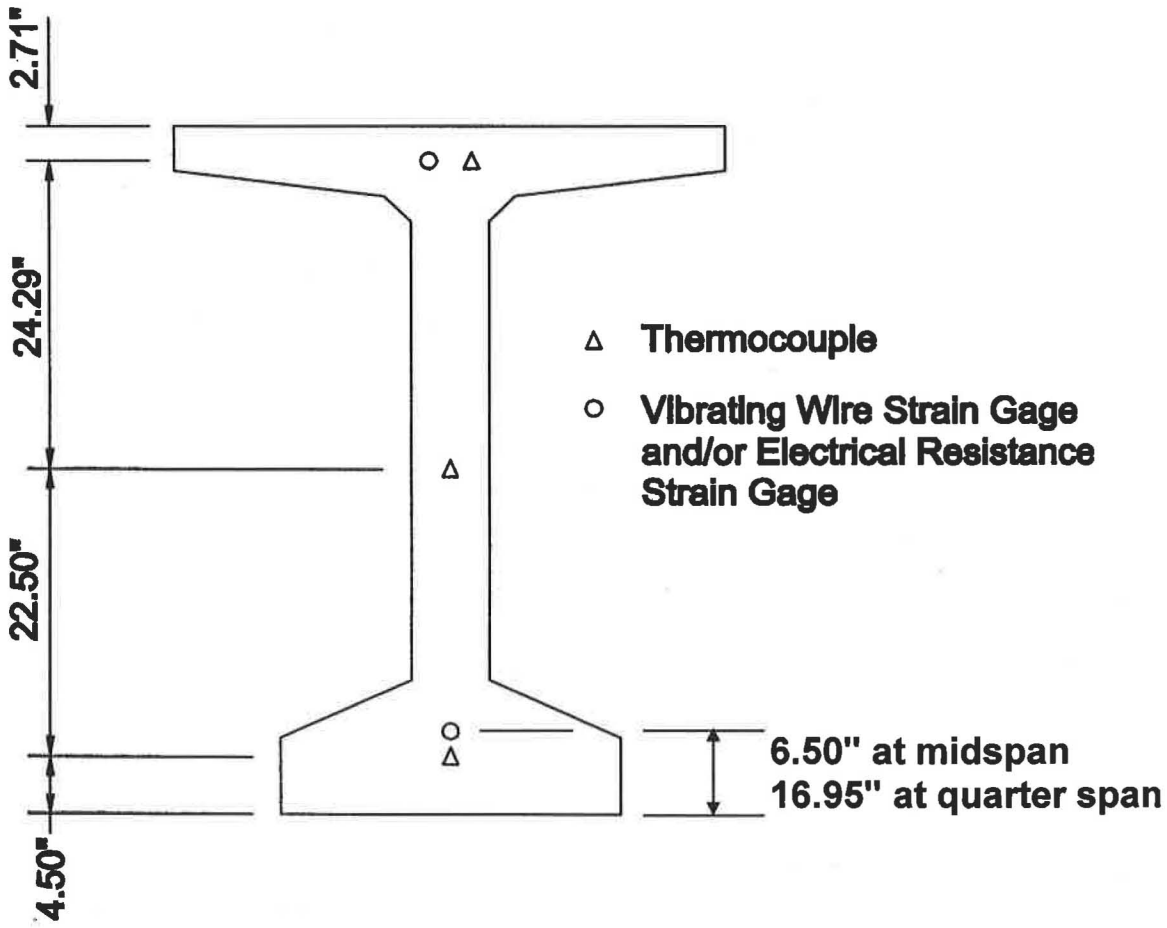

Figure 3.5 Instrumentation in HPC Girders

Figure 3.6 CR10X Being Used to Collect Data at Prestressing Yard

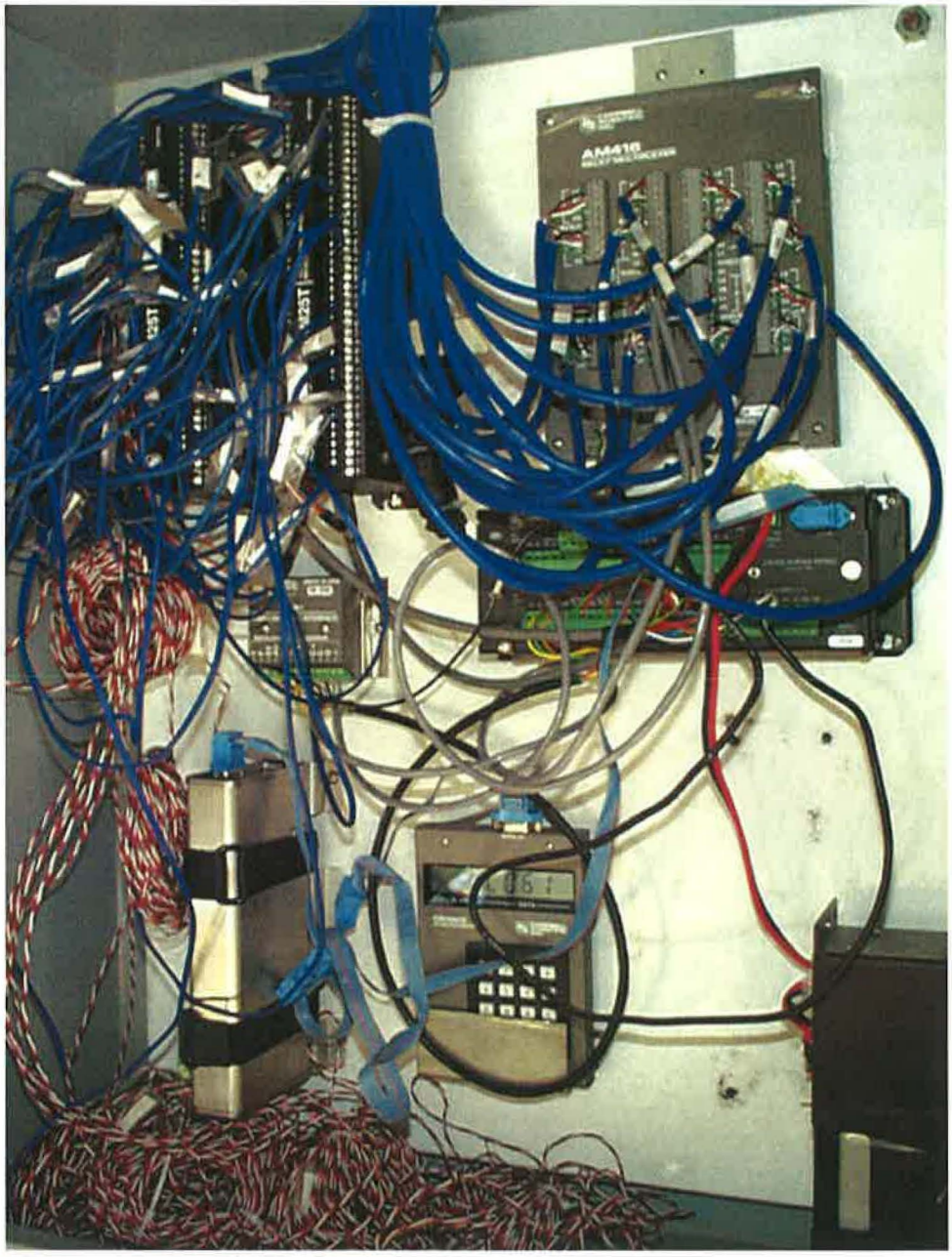

Figure 3.7 CR10X Mounted in Box on Diaphram at Midspan

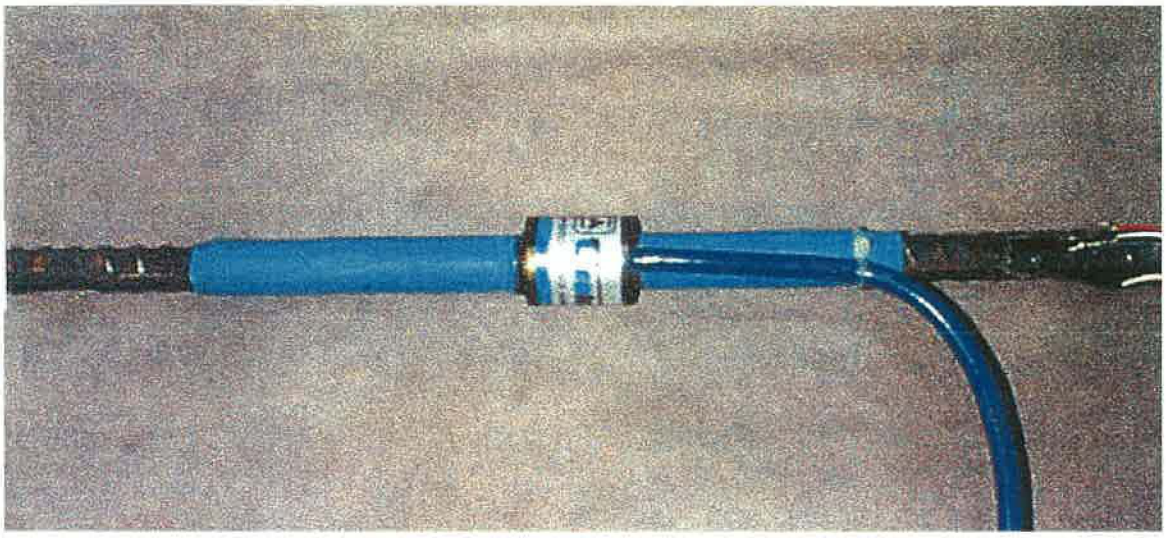

Figure 3.8 Vibrating Wire Strain Gage Unit

Table 3.1 Location of Instrumentation in Girders

Girder	Midspan		Quarter Span (28.375 ft. from Midspan)		End
	Thermocouples	Vibrating Wire Strain Gages	Thermocouples	Vibrating Wire Strain Gages	Thermocouples
1(west side)	X	X			
2	X	X			
3	X	X	X	X	X
4	X	X	X	X	X
5	X	X	X	X	X

Note: At vibrating wire strain gage locations there are always two gages, one at the prestresssing center of gravity and one at the top flange center of gravity. At each thermocouple location two thermocouples are present as shown in Figure 3.5.

wire element at its resonant frequency. As stated by the manufacturer (Geokon 1998), "The advantage of the VW device over conventional electrical resistance gages is in the VW's long-term stability and use of a frequency, rather than a voltage, as the output signal. Frequencies may be transmitted over long cable lengths without appreciable degradation caused by variations in cable resistance, contact resistance, or leakage to ground." A thermistor is included in each vibrating wire strain gage as a standard feature and permits measurement of temperature at the strain gage location. Two electrical resistance strain gages were added to five of the vibrating wire gage bars for use in future live load testing. One of the bars with the electrical resistance gages was installed in each girder at the centroid of the prestressing strands. Figure 3.9 shows the waterproofing material used to cover the electrical resistance strain gages.

The electrical resistance strain gages were 350 Ohm gages with a gage length of 0.25 in., and were manufactured by The Measurements Group. The gages were wired for use as quarter-bridges and had a gage factor of 2.075.

Temperatures at various locations in the girder and deck cross sections were monitored using Type T thermocouples. The vibrating wire strain gages and Type T thermocouples were placed in the five girders prior to casting. Figure 3.10 pictures placement of a bar instrumented with vibrating wire gage prior to casting. Figure 3.11 shows a typical thermocouple attached to a stirrup in the girder web. Thermocouples were placed in the deck several days prior to deck casting. Figure 3.12 shows a typical group of deck thermocouples. Unfortunately, attempts to calculate girder deflections

Figure 3.9 Black Waterproofing Material over Electrical Resistance Strain Gages

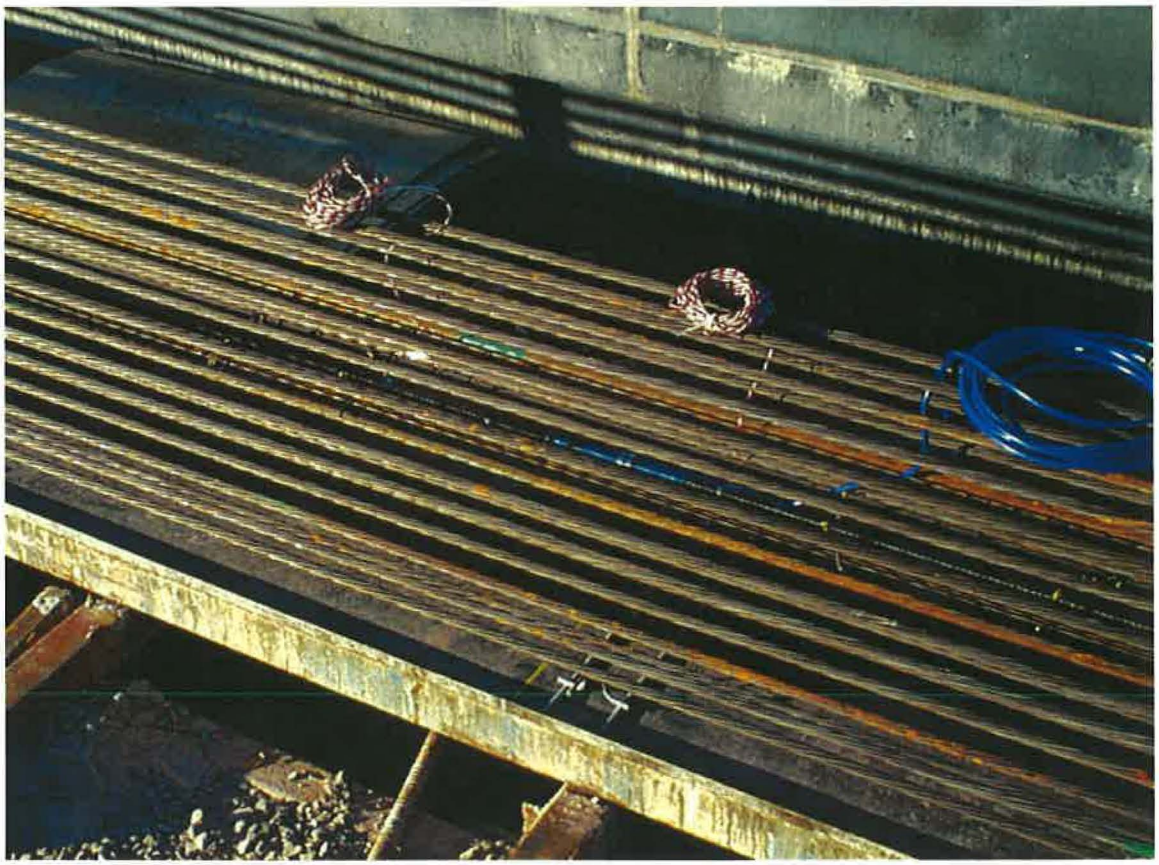

Figure 3.10 Instrumented Rebar with Surrounding Prestress Tendons

Figure 3.11 Thermocouple Located in Girder

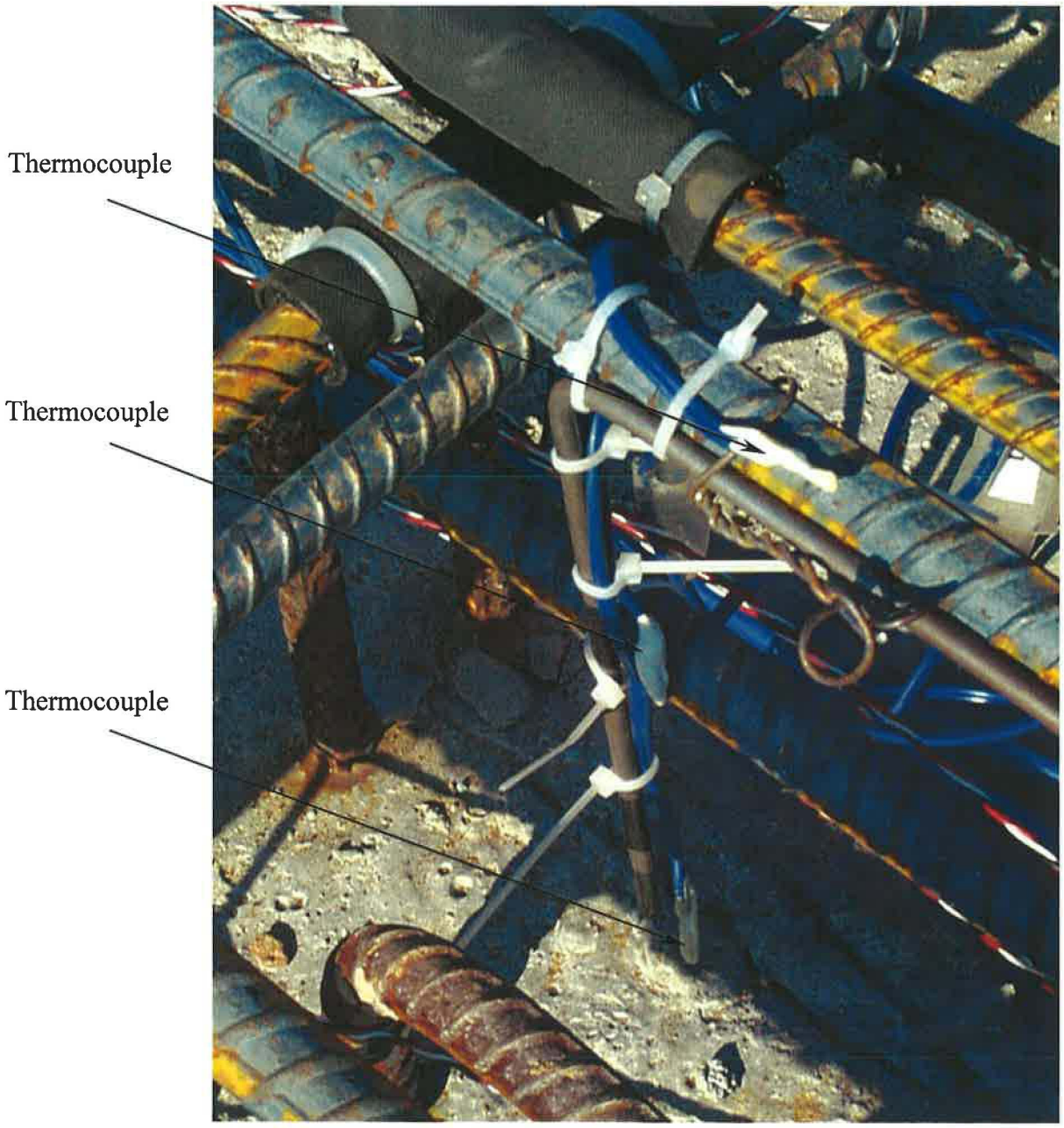

Figure 3.12 Thermocouples in Deck

using the measured temperatures were unsuccessful. No thermocouple data is reported here.

Girder camber was determined using surveying methods. Using a surveyor's level and carpenter's tape (1/16" divisions) camber at midspan was recorded at selected times after release of the prestressing force.

CHAPTER FOUR

Field and Laboratory Measurements

Camber of BT-54s

Camber of the five instrumented AASHTO BT-54 girders in the HPC Showcase bridge was monitored from release through completion of construction. Additionally, camber of 26 of the remaining 30 HPC girders in the Uphapee Creek bridge was measured on a single day to determine the variability of camber from girder to girder.

Fabrication of Girders 1 and 2 of the instrumented span was completed with release of the prestress force on December 18, 1998. Release for Girders 3 and 4 was on January 28, 1999, and release of Girder 5 occurred February 3, 1999. Table 4.1 lists the ages of the instrumented girders at the time the deck slab and barrier rails were cast. Casting of the deck was accomplished in 3 separate pours over a 15 day period (11/15/99 through 11/30/99).

The girder camber was determined using a surveyor's level and carpenter's tape. Data during the first 100 days of measurement activity were collected at various times of the day. Subsequent data were recorded in the morning in an attempt to minimize scatter in the readings due to thermal effects.

Figures 4.1a through 4.1e depict camber at various ages for the five instrumented girders. Figure 4.1f displays all of the camber data for the instrumented girders on one graph. Table 4.2 provides a summary of camber values at an age of 1-day (after release), prior to shipping, and after casting the deck and barriers. Figure 4.2 contains the results

Table 4.1 Age of Girders During Deck Construction

Girder Number	Age (days)	
	Casting of Deck	Casting of Barriers
1	332 to 347	398
2	332 to 347	398
3	291 to 306	357
4	291 to 306	357
5	285 to 300	351

of the one time survey of 31 of the 35 HPC girders. In Figure 4.2 camber from instrumented Girders 3 through 5 are plotted at approximately 200 days and are near the lower bound of the measured cambers, while the cambers of Girders 1 and 2 are closer to the average value. The Authors have been unable to pinpoint any specific differences in the girders that clearly explain produced these differences. Figure 4.2 illustrates that there is a noticeable amount of variability in the cambers of the 31 girders produced under the same material specifications.

Strain Measurements from BT-54s

Data from the vibrating wire strain gages were recorded by the CR-10X at selected times both before and after release of the five instrumented girders. Baseline data were taken immediately before release. After release, strain measurements were taken every three minutes for twelve hours for the first day, once daily for a week, weekly for a month, and subsequently at various times. Strain data are shown in Figures 4.3 and 4.4. Each vibrating wire strain gage contained an internal temperature sensor. Coversion of the raw measurements to the strains plotted in Figures 4.1 through 4.4 included an adjustment to account for changes in temperature of the gage. This adjustment did not account for strains resulting from thermal gradients.

Some data were lost due to technical problems with the CR-10X. Data taken with the CR-10X during construction of the deck were unusable, thus the absence of data in that period. A summary of vibrating wire strain gage data is provided in Table 4.3. Data were summarized for the following critical times: age of 1-day, the last date collected before casting of the deck, before casting of the barriers, and after the barriers were cast.

Figure 4.1 (a) Camber of Girder 1

Figure 4.1 (b) Camber of Girder 2

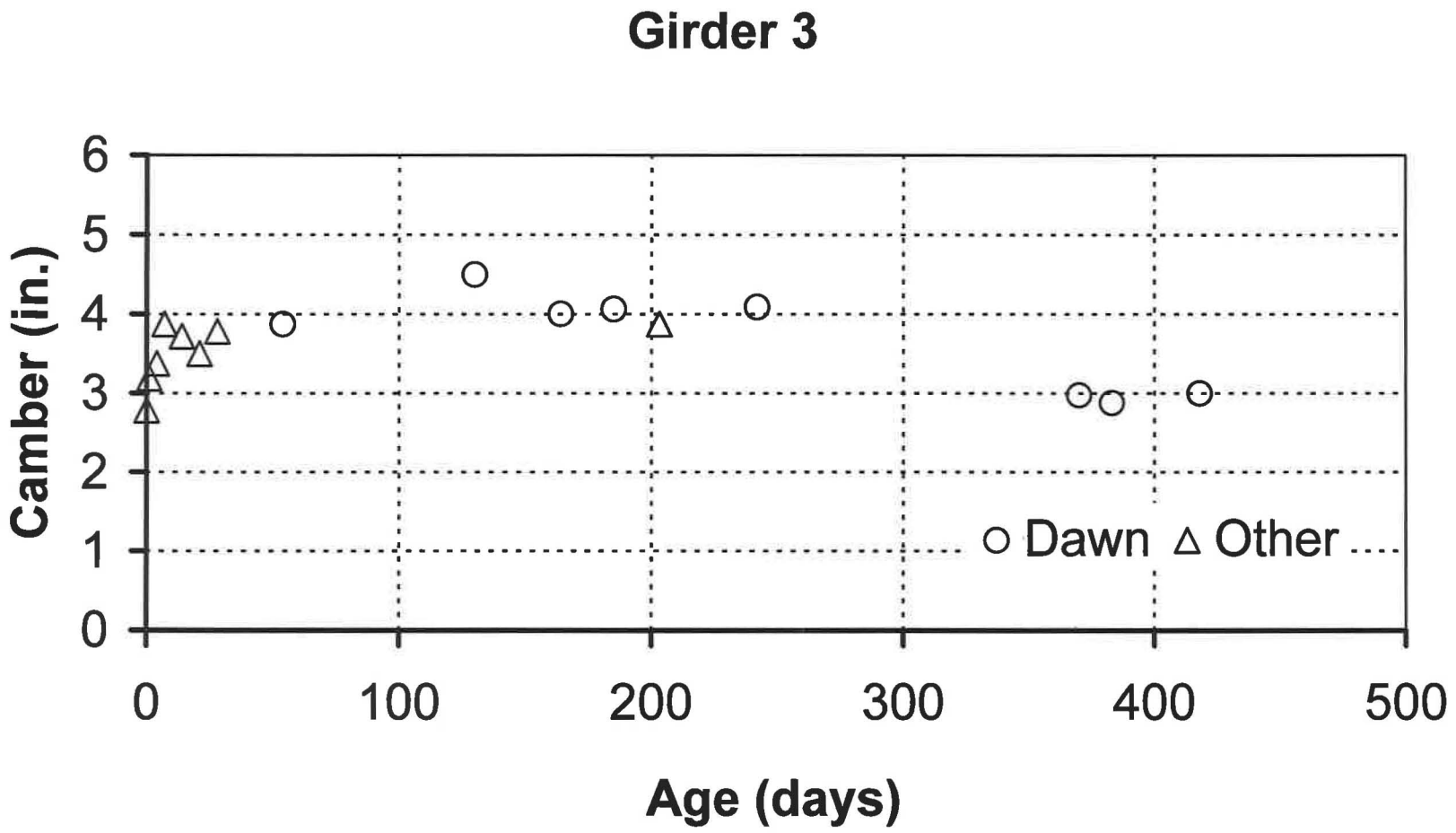

Figure 4.1 (c) Camber of Girder 3

Figure 4.1 (d) Camber of Girder 4

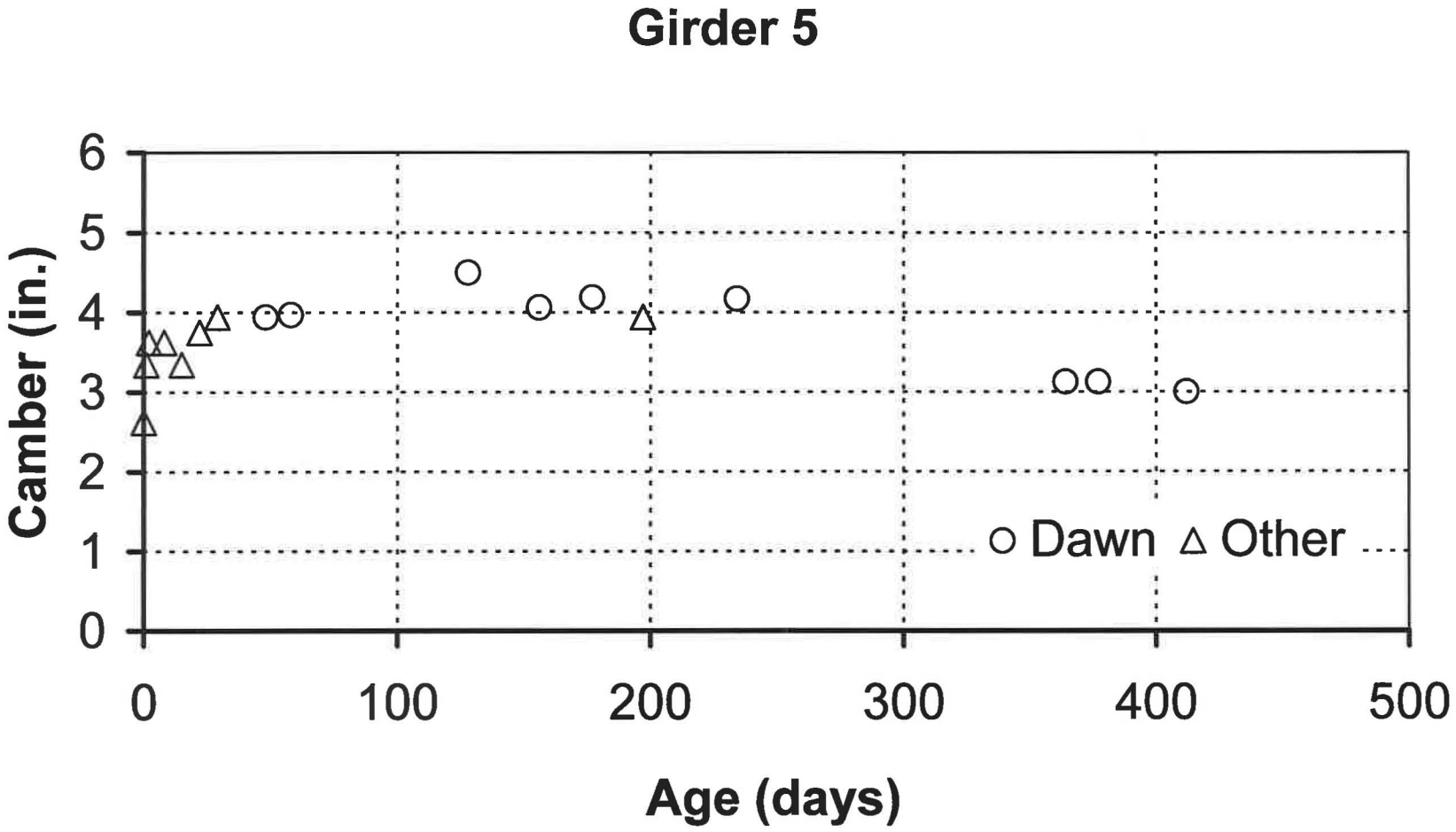

Figure 4.1 (e) Camber of Girder 5

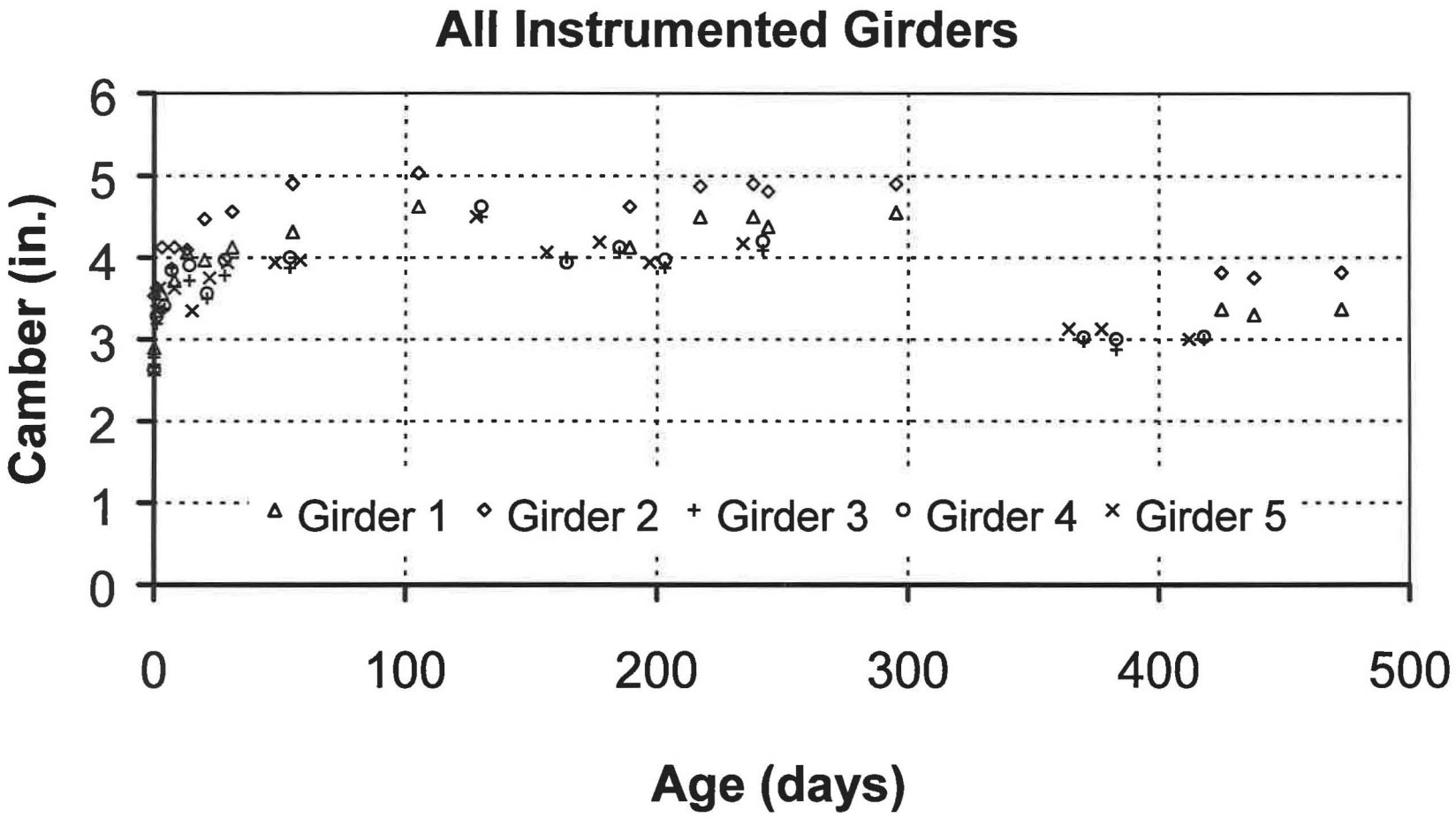

Figure 4.1 (f) Camber of All Instrumented Girders

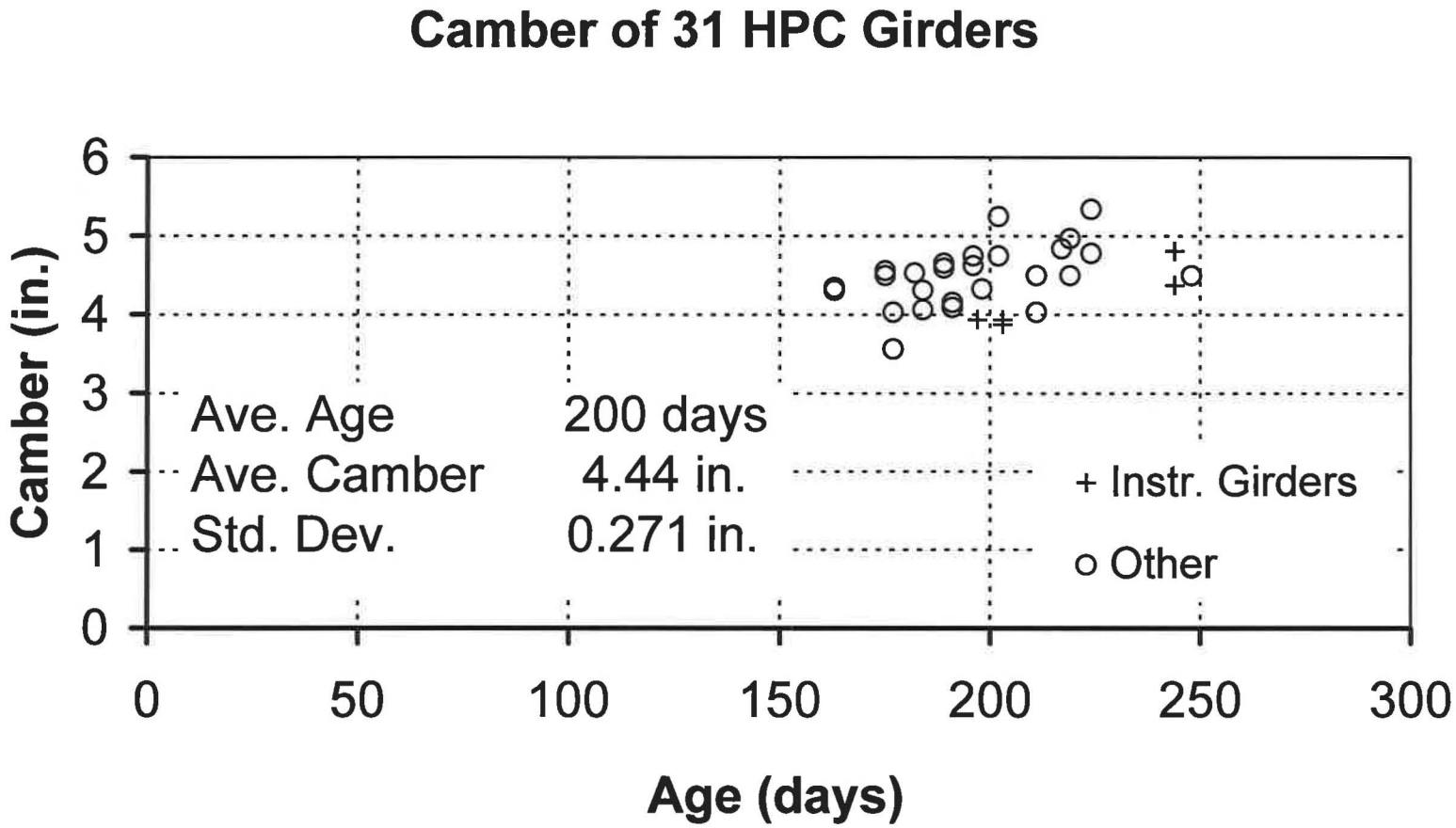

Figure 4.2 Camber of 31 HPC Girders Measured on the Same Day (8/19/00).

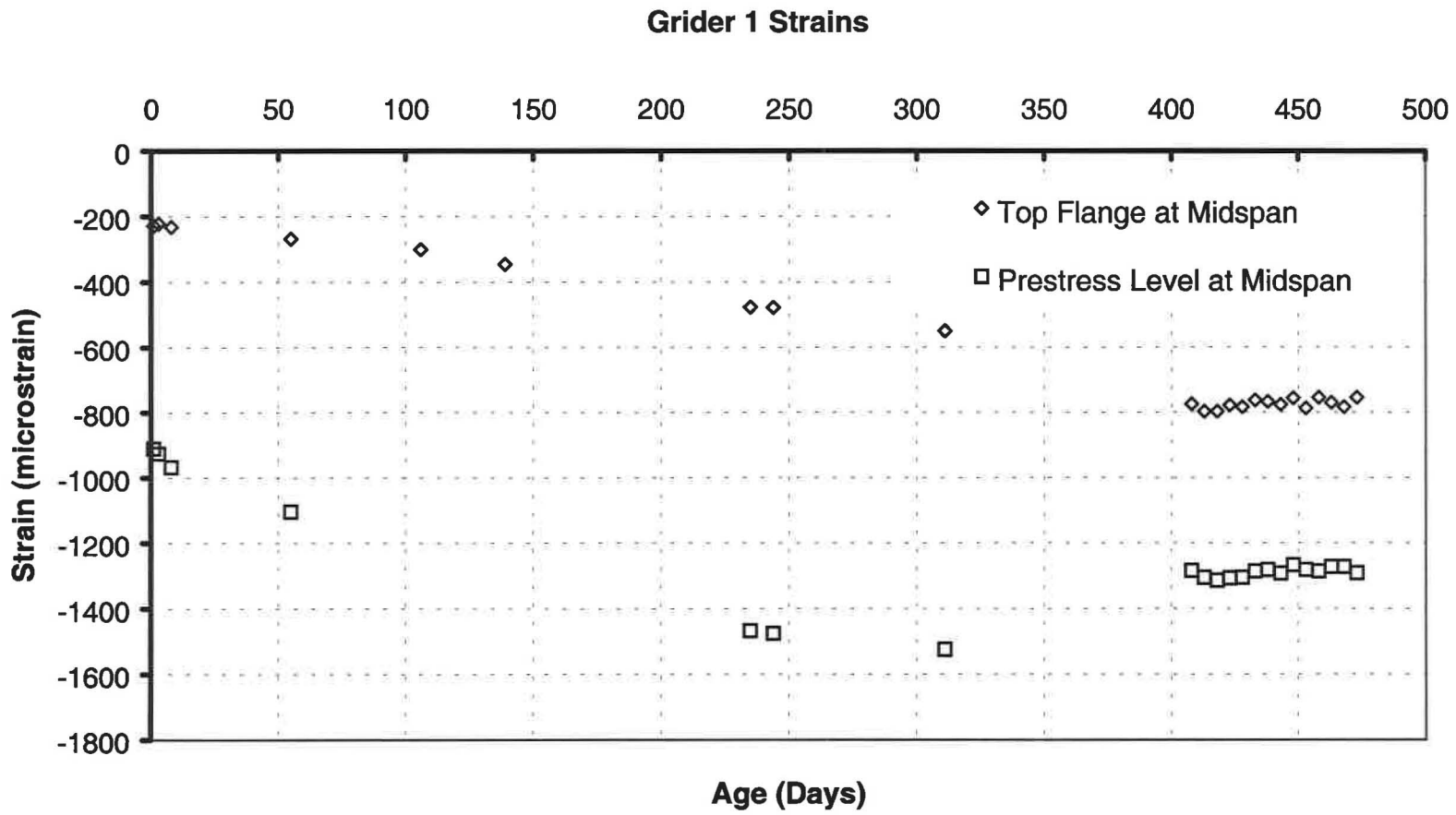

Figure 4.3(a) Vibrating Wire Strain Gage Data from Girder 1

Figure 4.3(b) Vibrating Wire Strain Gage Data from Girder 2

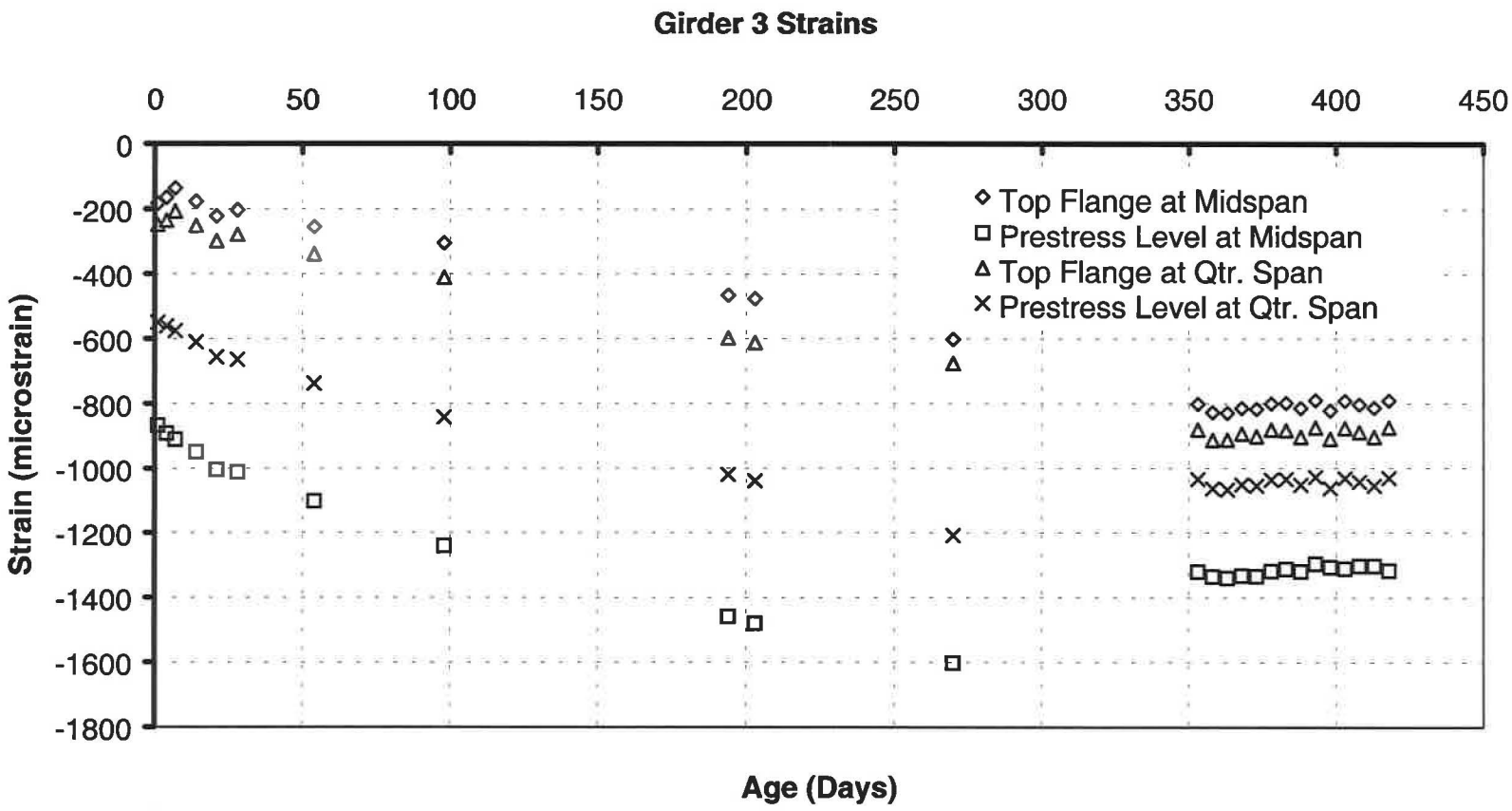

Figure 4.3(c) Vibrating Wire Strain Gage Data from Girder 3

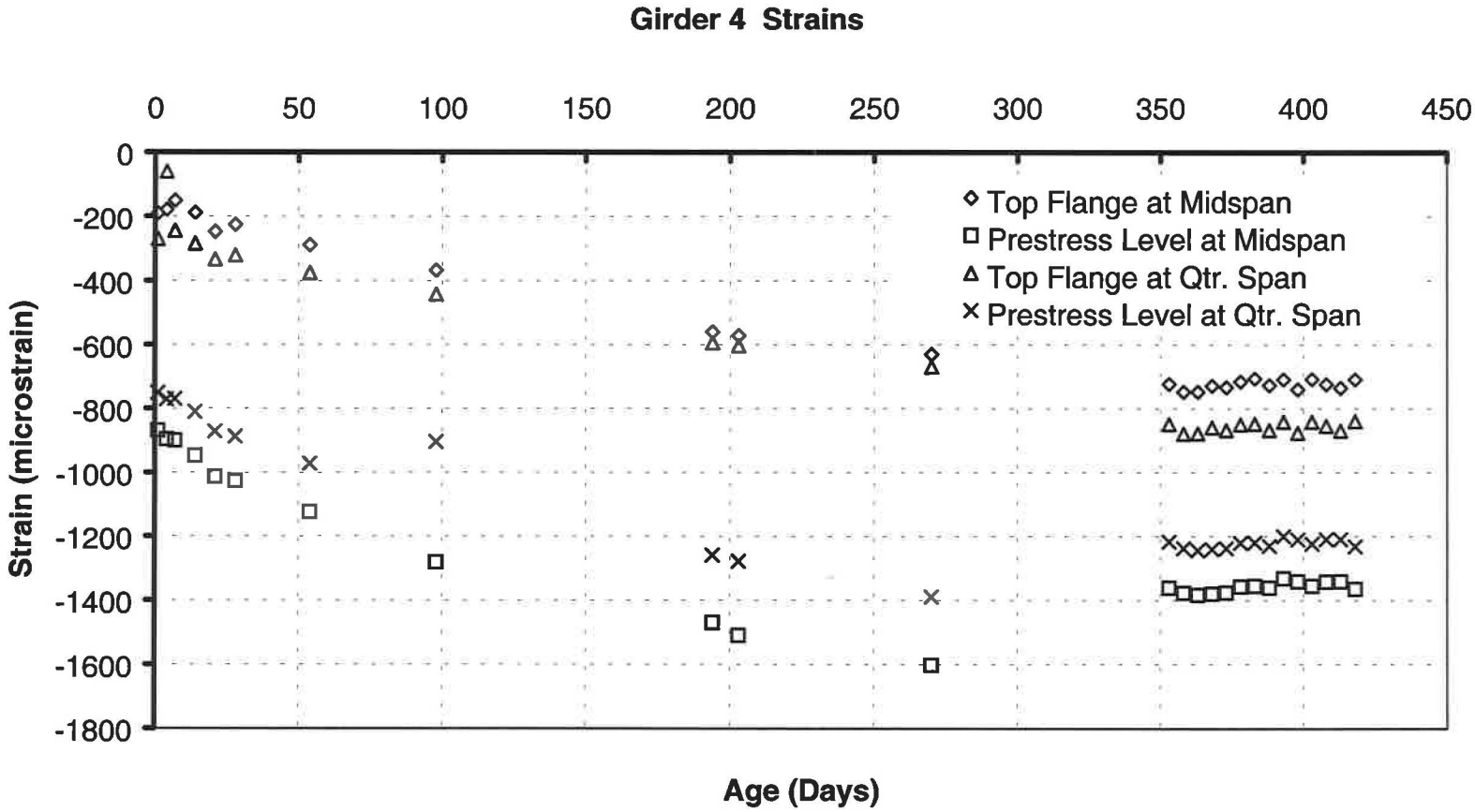

Figure 4.3(d) Vibrating Wire Strain Gage Data from Girder 4

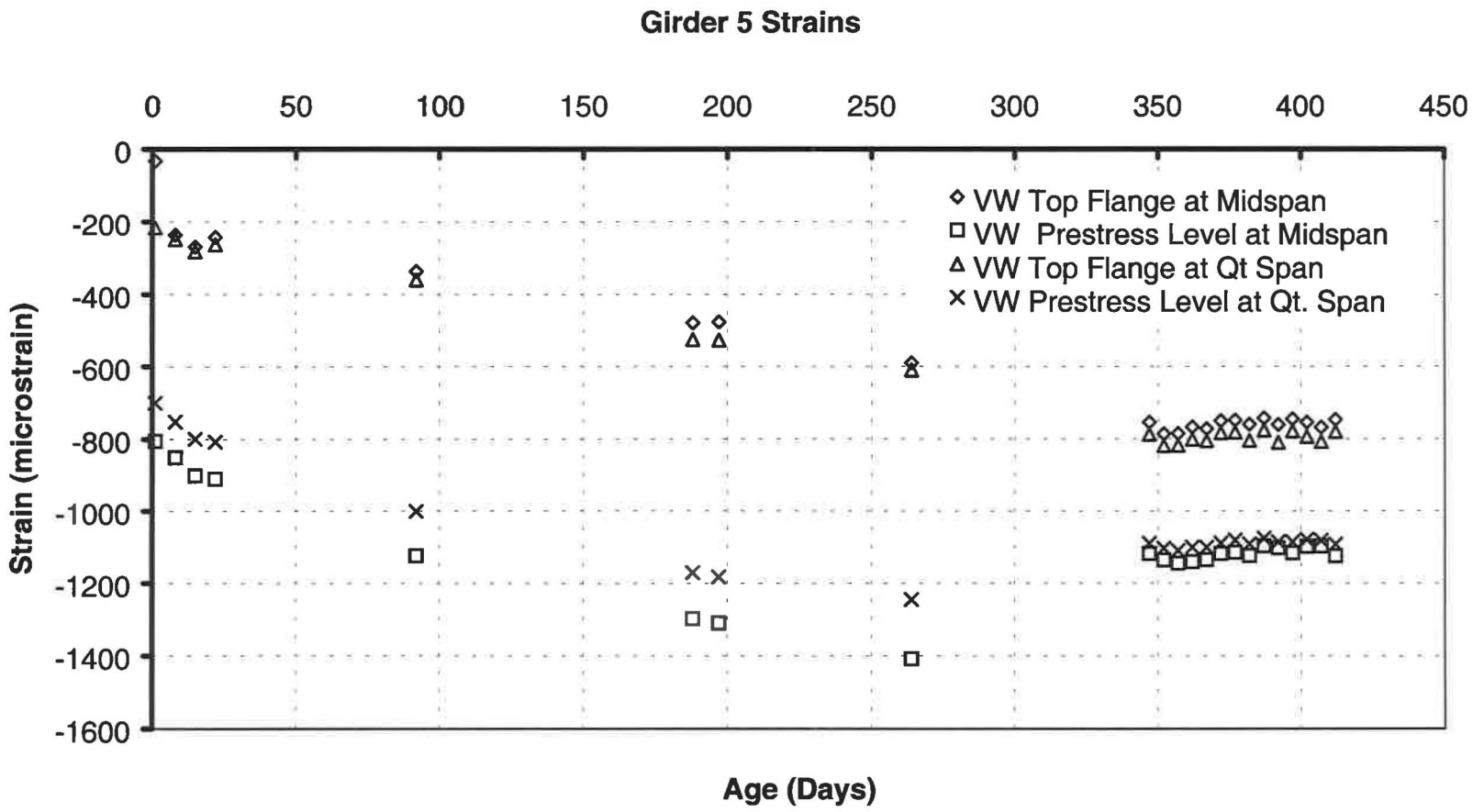

Figure 4.3(e) Vibrating Wire Strain Gage Data from Girder 5

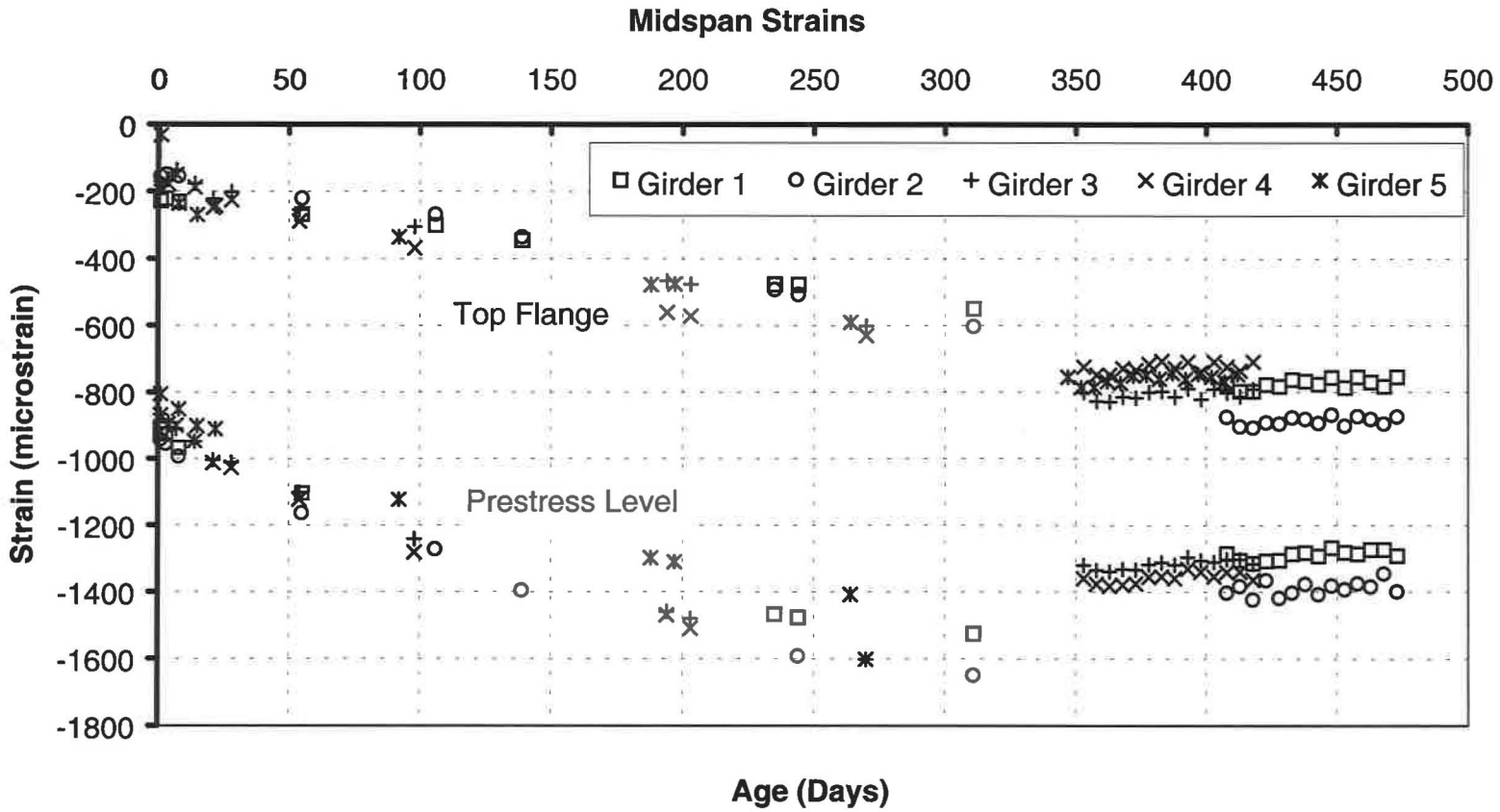

Figure 4.4 Midspan Strain Data from Five Instrumented Girders

Table 4.2 Summary of Camber Data

Girder No.	Age (days)	Stage	Midspan Camber (in.)
1	1	On Yard	3.34
	295	On Yard	4.55
	425	After Barriers	3.37
2	1	On Yard	3.63
	295	On Yard	4.90
	425	After Barriers	3.81
3	1	On Yard	3.19
	242	On Yard	4.09
	370	After Barriers	2.98
4	1	On Yard	3.28
	242	On Yard	4.20
	370	After Barriers	3.03
5	1	On Yard	3.34
	234	On Yard	4.17
	364	After Barriers	3.13

Laboratory Creep and Shrinkage Tests on Bridge Girder HPC

In conjunction with the field instrumentation of the HPC girders, laboratory tests were preformed to determine the creep and shrinkage properties of the high-performance concrete used in the girders. Additional descriptions of these tests is given by Glover and Stallings (2000). The ASTM C512 (ASTM 1994) procedure for creep testing of concrete in compression was used to conduct the test. Two loading frames similar to that depicted in the ASTM method were assembled to facilitate the test. Figure 4.5 shows two loading frames.

ASTM C512 calls for the concrete cylinders to be tested while placed end to end with half cylinders at each extremity. Tests at Auburn used four full 4x8 cylinders sulfur capped and placed in the creep frame with the sulfur capped ends bearing on one another and plates at either end. No half cylinders were used. The concrete cylinders used in this test were made by Auburn graduate student Jim Glover during the production of the HPC girders. The test cylinders were match-cured until release of the prestress force into the girders and then transported to Auburn. Release of the prestress force occurred at an age of approximately 18-24 hours.

Two of the match-cured 4x8 cylinders were broken to determine the compressive strength at the time of loading. The four sulfur capped cylinders in the creep frame were then loaded to 45% of the concrete compressive strength by way of a hydraulic ram as depicted in Figure 4.5. ASTM calls for the cylinders to be tested at no more than 45% of the compressive strength. Measurements after the jack was removed indicate the final

Figure 4.5 Creep Frame Shown with Jack and Load Cell in Place

Table 4.3 Summary of Strain Data

Girder No.	Age (days)	Stage	Quarter Span Strains (microstrain)		Midspan Strains (microstrain)	
			Top Flange	Bottom Flange	Top Flange	Bottom Flange
1	1	On Yard	-	-	-228	-910
	311	Before Deck	-	-	-550	-1525
	408	After Barriers	-	-	-775	-1285
2	1	On Yard	-	-	-156	-943
	311	Before Deck	-	-	-603	-1650
	408	After Barriers	-	-	-876	-1404
3	1	On Yard	-248	-549	-183	-866
	270	Before Deck	-675	-1209	-602	-1602
	353	Before Barriers	-881	-1036	-801	-1320
	358	After Barriers	-914	-1064	-828	-1335
4	1	On Yard	-271	-751	-191	-867
	270	Before Deck	-670	-1389	-630	-1602
	353	Before Barriers	-848	-1217	-724	-1360
	358	After Barriers	-879	-1238	-748	-1377
5	1	On Yard	-216	-700	-33	-806
	264	Before Deck	-610	-1245	-590	-1408
	347	Before Barriers	-788	-1090	-754	-1118
	357	After Barriers	-819	-1109	-786	-1145

- Measurement not made

axial force in the cylinders produced an axial stress equal to 42% of the compressive strength.

Strains in the loaded cylinders in the creep frame were collected using digital calipers and shop fabricated Demec points. The cylinders were fitted with three sets of these points. Each set of points was placed to provide an approximate gage length of five inches with the Demec pairs placed 120 degrees apart around the circumference of the cylinders as shown in Figure 4.6. Two additional cylinders were fitted with Demec points and placed on a shelf near the creep frames. These two cylinders provided shrinkage data. Measurements for each of the cylinders were made at approximately the following times: daily for a week, weekly for a month, monthly until the end of the first six months, then every other month.

Total strains measured for the four individual cylinders in the creep frame are shown in Figure 4.7. The strains plotted for each cylinder are the average of the readings from the three sets of Demec points. Shrinkage strains measured from the two shrinkage cylinders are shown in Figure 4.8. The shrinkage values plotted for Cylinder F are the average values determined from the three sets of Demec points. Due to a problem with one set of Demec points on Cylinder E, the data shown are the average shrinkage strains measured with two sets of Demec points.

Average values of total strain at each age where determined from the data in Figure 4.7 for the cylinders in the creep frame. Average shrinkage strains at each age were determined using the data in Figure 4.8. These average shrinkage strains are plotted in Figure 4.9. An elastic strain at each age was determined using the measured applied load and a modulur of elasticity of 6,000,000 psi. This modulus value is representative of

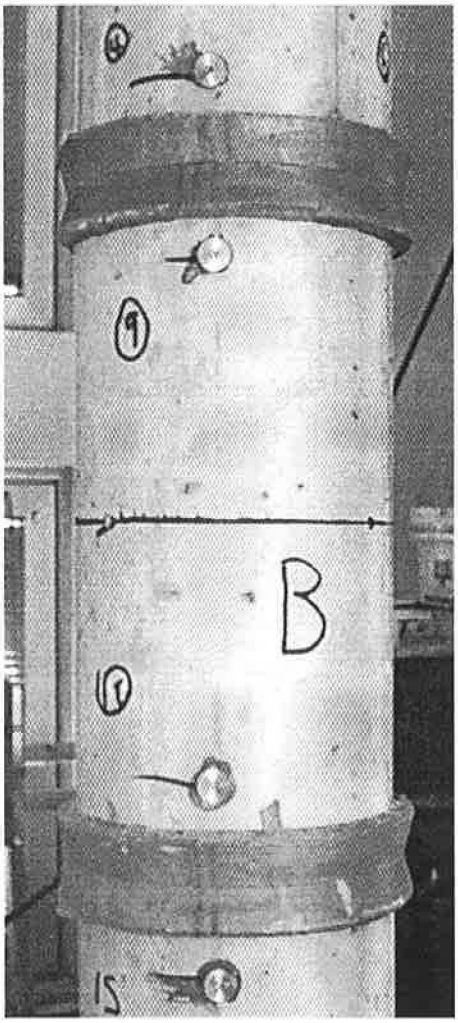

Figure 4.6 Demec Points

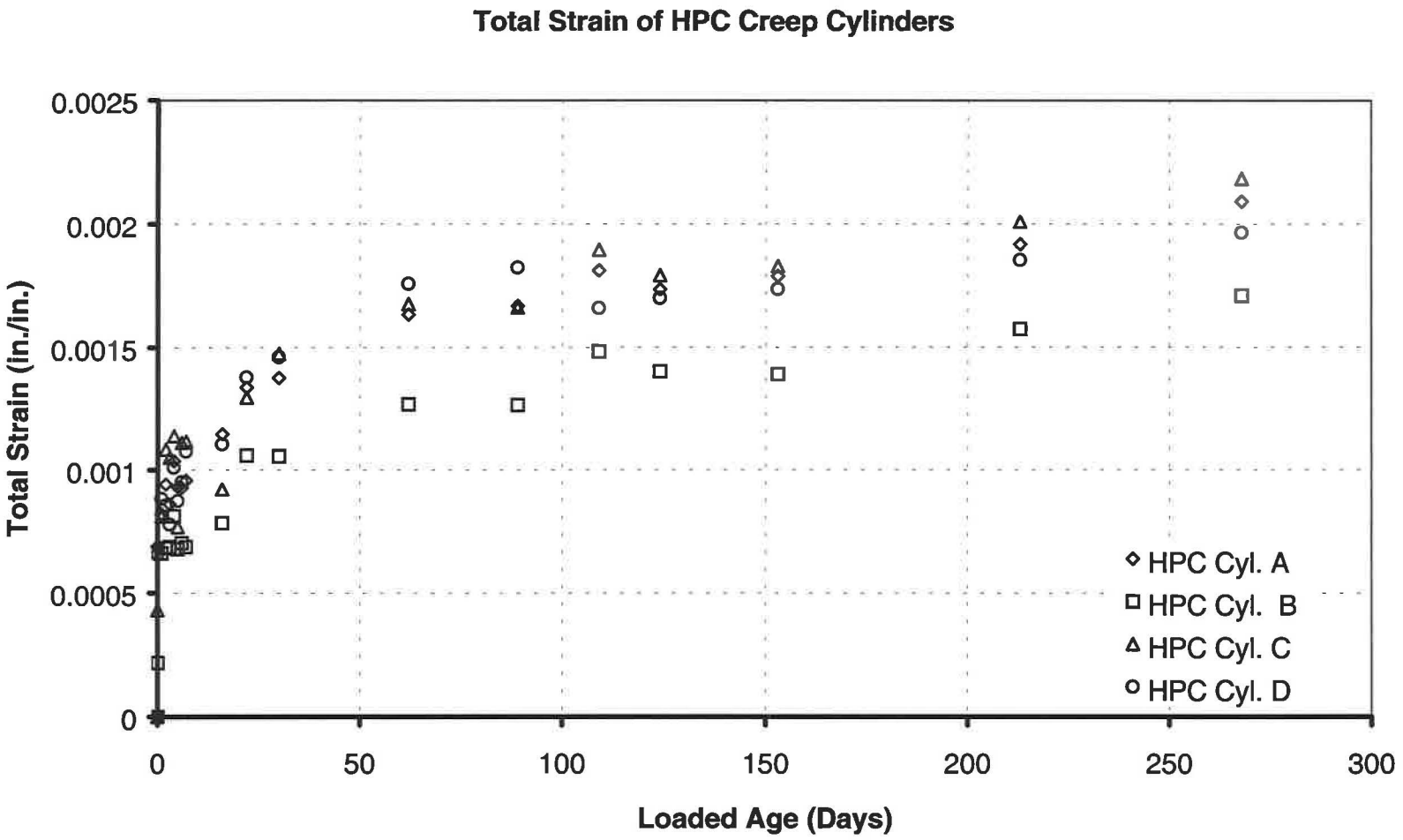

Figure 4.7 Total Strain from HPC Creep Test

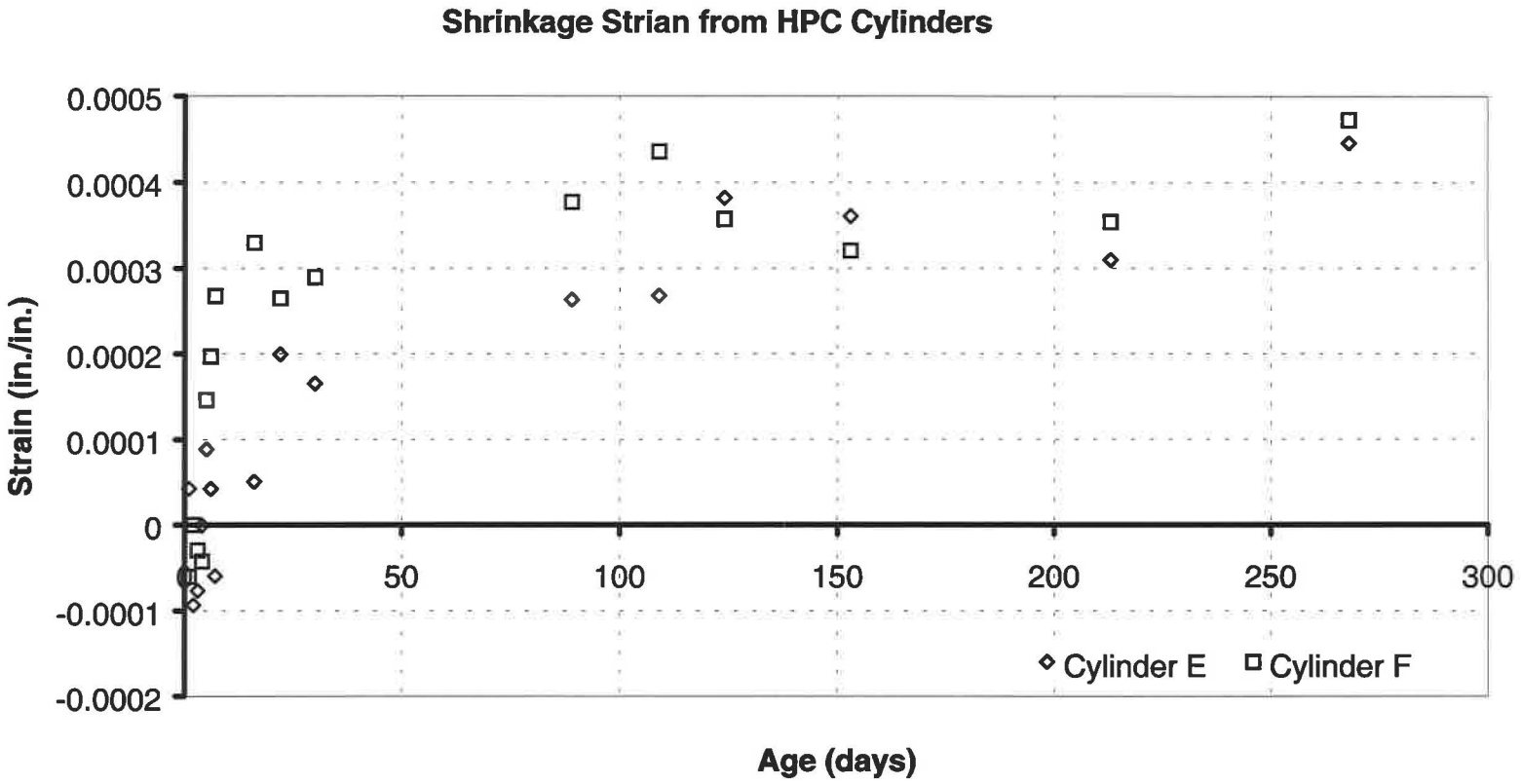

Figure 4.8 Shrinkage Strain from HPC Cylinders

the concrete test cylinders. Creep strains at each age were determined by subtracting the shrinkage strain and elastic strain from the total strain. A creep coefficient was found at each age by dividing the creep strain at each age by the initial elastic strain (at age 1-day) of 0.000691 in./in. The creep coefficients are plotted in Figure 4.10.

Shrinkage strains and creep coefficients calculated using the models discussed in Chapter 2 from ACI 209R-92 (1992) are plotted in Figures 4.9 and 4.10 along with the test data. A summary of the correction factors used to represent the lab test conditions is given in Table 4.4. The average relative humidity in the lab is assumed to be 50% over the duration of the tests. Relative humidity measurements were made periodically, and those measurements ranged from 21% to 70%. The other correction factors in Table 4.4 are based on the volume to surface ratio of the 4 in. diameter cylinders and the materials and characteristics of the HPC mixture.

Table 4.5 contains the creep and shrinkage model parameters determined by least squares fit to the test data. Figures 4.9 and 4.10 illustrate that using the standard parameters from ACI significantly over predicts the creep and shrinkage of the high-performance concrete.

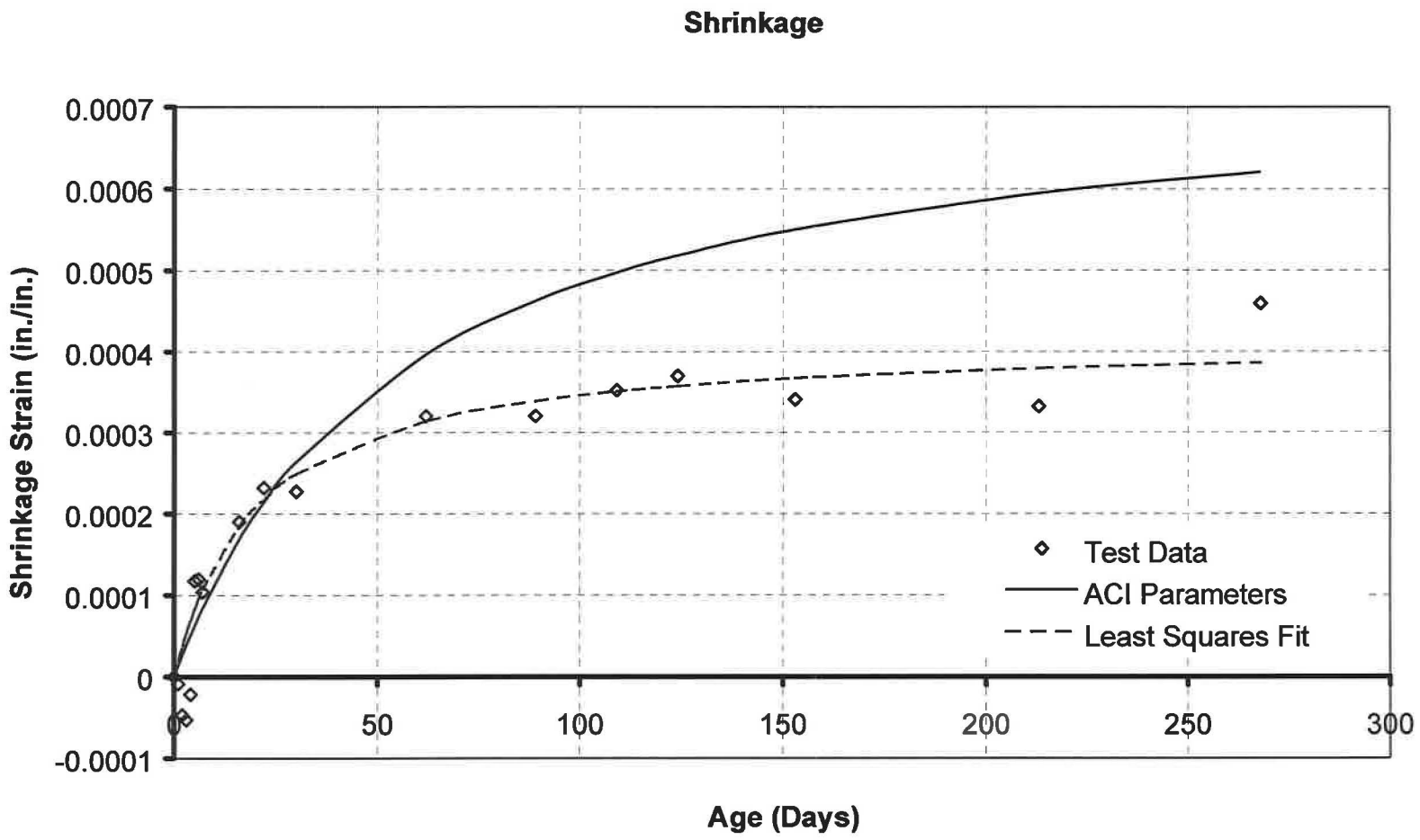

Figure 4.9 Measured and Predicted Shrinkage Strain

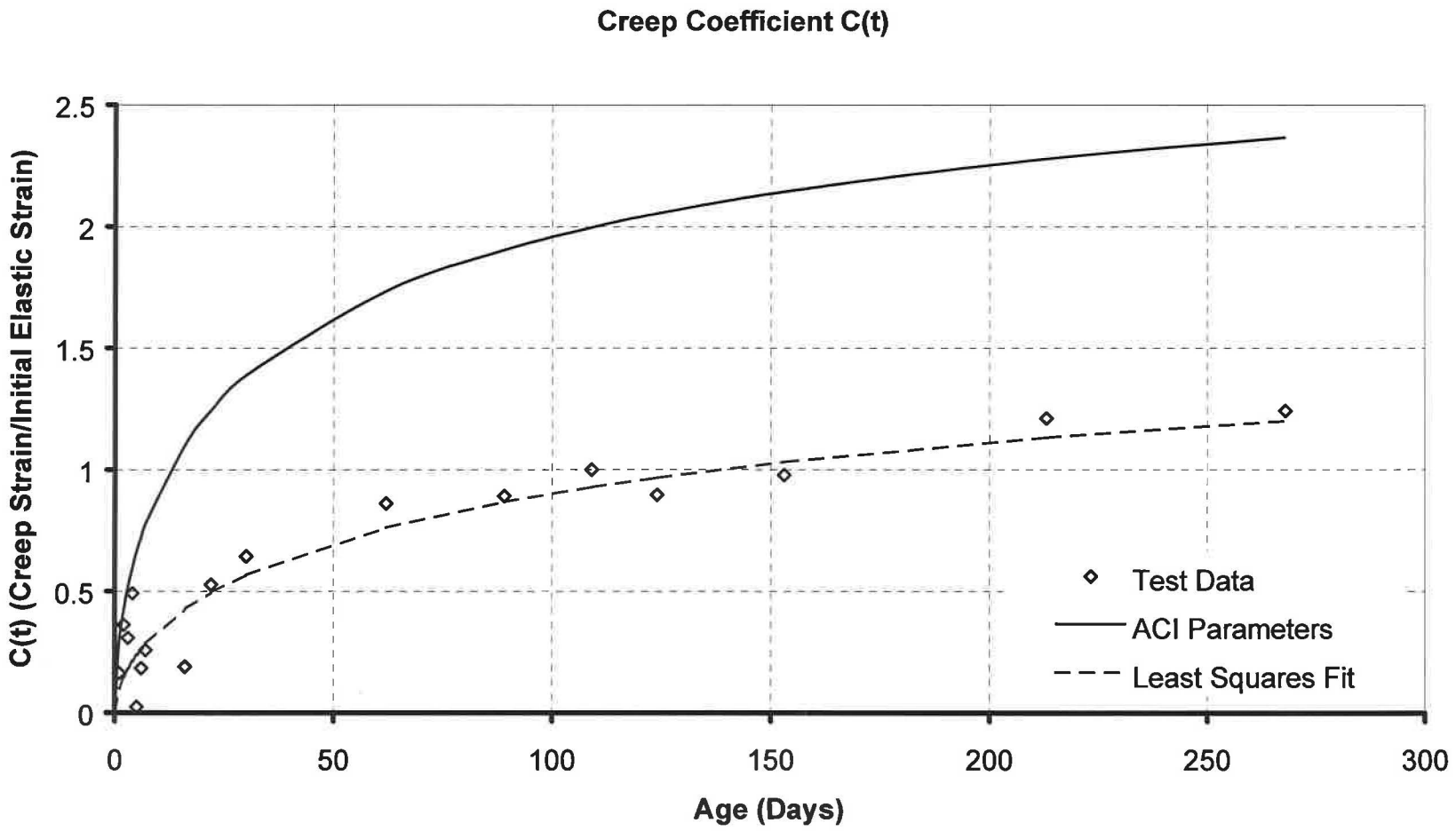

Figure 4.10 Measured and Predicted Creep Coefficients

Table 4.4 Shrinkage and Creep Correction Factors for 4 x 8 in. Cylinders in Lab at 50% Relative Humidity

Factor	Shrinkage	Creep
Relative Humidity, 50%	0.900	0.935
Volume/Surface	1.064	1.106
Slump	1.218	1.356
Fine Aggregate %	0.818	0.969
Cement Content	1.021	NA
Air Content	0.984	1
Product of Factors, γ	0.959	1.359

NA = Not Applicable

Table 4.5 Shrinkage and Creep Parameters from Laboratory Tests of HPC

Parameter	Value
Shrinkage	
α	1
f	20
$(\varepsilon_{sh})_u$ from tests	0.000415 in./in.
$(\varepsilon_{sh})_u$ 6 x 12 cyl. @ H = 40%.	0.000433 in./in.
Creep	
φ	0.6
d	20
C_u from tests	2.037
C_u 6 x 12 cyl. @ H = 40%.	1.97

CHAPTER FIVE

Calculation of Camber, Strains and Losses

Introduction

Camber of prestressed concrete members depends on numerous factors, some of which are time-dependent. All factors cannot be directly accounted for in calculation of camber, but many can. Calculated cambers presented later in this report show very good agreement with measured cambers of the HPC girders. This good agreement indicates that the most important factors are modeled with reasonable accuracy.

Calculated cambers, strains and prestress losses are compared to measured values in the next chapter. A description of the methods used to make those calculations is presented in this chapter. Calculating girder camber requires predictions of the losses of prestress force and modeling of the time dependent changes in member curvature produced by creep. Losses and incremental curvatures are discussed first, followed by a description of how they are used to calculate camber and strains for comparison with the measurements. The procedures presented here are not new and additional discussion can be found in texts on prestressed concrete design such as the one by Nawy (2000). Output from a spreadsheet used to perform the calculations is provided in the Appendix.

Modeling of Prestress Losses

Prestress losses in pretensioned girders of the type considered here result from five primary factors: 1) seating at the strand anchorages, 2) elastic shortening, 3) relaxation of the strand, 4) shrinkage of the concrete, and 5) creep of the concrete.

Modeling of losses requires a definition for the age of zero. Here, age of zero is immediately after release of the prestress force into the girder. Seating at the strand anchorages, relaxation of the strand in the prestressing bed, and elastic shortening of the girder occur prior to age of zero. Seating of the anchorages and relaxation of the strand in the prestressing bed are difficult to quantify and were assumed to equal a loss of 1% of the jacking stress, f_{pj} (75% of the ultimate strength of the strand). For the calculation of camber and strains at midspan, an elastic shortening loss at midspan of 9.96% of the jacking stress was used for the entire span. For girder strain calculations at the quarter span, an elastic shortening loss of 8.66% at the quarter span was used. The elastic shortening losses given above were determined so that the prestress force due to the jacking stress, minus the initial relaxation loss, produced an elastic change in strand stress equal to the elastic shortening loss. Hence, these are refined values of elastic shortening loss. The initial steel stress, f_{pi}, is defined here as the steel stress immediately after release, after the initial relaxation and elastic shortening losses.

Relaxation of the strand is a reduction in strand stress, and force, at a constant strain. The loss in strand stress due to relaxation, Δf_{pR}, was calculated using the common expression applicable to low-relaxation strand:

$$\Delta f_{pR} = f_{pi} \frac{\log(24t)}{45}\left(\frac{f_{pi}}{0.9f_{pu}} - 0.55\right) \qquad (5\text{-}1)$$

where t = age in days; f_{pi} = stress in the steel at time zero; and f_{pu} = ultimate tensile strength of the strand. This expression follows from Eqn. 2-22 where the yield stress is taken as $0.9f_{pu}$, and $\log t_1$ is assumed to be zero.

Shrinkage of the concrete also produces a loss of prestress. The normal strain due to shrinkage was assumed to be uniform across the cross section and along the length of

the member, and the corresponding reduction in strain in the strand was assumed equal to the shrinkage strain. The loss in strand stress due to shrinkage, Δf_{pSH}, is

$$\Delta f_{pSH} = \epsilon_{SH} E_{ps} \tag{5-2}$$

where E_{ps} = 27,500,000 psi is the modulus of elasticity of the prestressing strand. The shrinkage strain in Eqn. 5-2 was calculated using Eqn. 2-2.

Creep of the concrete produces a prestress loss. As will be discussed later, the normal strain due to creep varies across the cross section due the linear variation of concrete stress due to prestress. The reduction in strain of the strand due to creep was taken equal to the concrete creep strain at the level of the prestress force. The loss in strand stress due to creep, Δf_{pCR}, is

$$\Delta f_{pCR} = C(t)\frac{E_{ps}}{E_c} f_{cs} \tag{5-3}$$

where f_{cs} = the stress in the concrete at the level of the prestress force due to the prestress and dead load; and E_c = modulus of elasticity of the concrete. C(t) in Eqn. 5-3 was calculated using Eqn. 2-13.

The total loss of strand stress after release, Δf_p, is the sum of the individual contributions listed above:

$$\Delta f_p = \Delta f_{pR} + \Delta f_{pSH} + \Delta f_{pCR} \tag{5-4}$$

Incremental Curvatures

Curvature for structural members is defined as the angle change due to applied bending moment that occurs between two cross sections that are a unit length apart. Curvature at a cross section is equal to the slope of the strain diagram for the cross section. Camber and deflections of a beam result from curvature along the span. Classical beam deflection calculations typically involve the use of a (M/EI) diagram, where M = the bending moment diagram, E = modulus of elasticity, and I = moment of inertia of the cross section. This (M/EI) diagram is a curvature diagram, or plot of the curvature along the beam span.

Camber of a prestressed girder changes with time as a result of creep and prestress losses. A fundamental method of accounting for these changes is the Incremental Time Steps Method. Application of this method involves calculating the incremental, time-dependent strains that occur for consecutive periods of time after release, and using these strains to calculate incremental curvatures at specific cross sections along the beam. The incremental curvatures are added to the previous totals and used to calculate the girder camber. A description of how to calculate incremental curvatures is given below.

When an eccentric prestress force is released into a girder, linear distributions of elastic stress and strain result at cross sections along the girder, and the girder cambers upward. The prestress force and the girder self-weight cause these stresses and strains. Creep of concrete is strain that occurs at a constant level of stress. Creep strain is assumed directly proportional to the applied stress level for both tensile and compressive stress. Hence, an initial linear distribution of stress across the depth of a girder causes a linear distribution of creep strain at a later age. Fig. 5.1 illustrates a linear distribution of creep strain for an increment of time. The incremental creep strains at the top and bottom

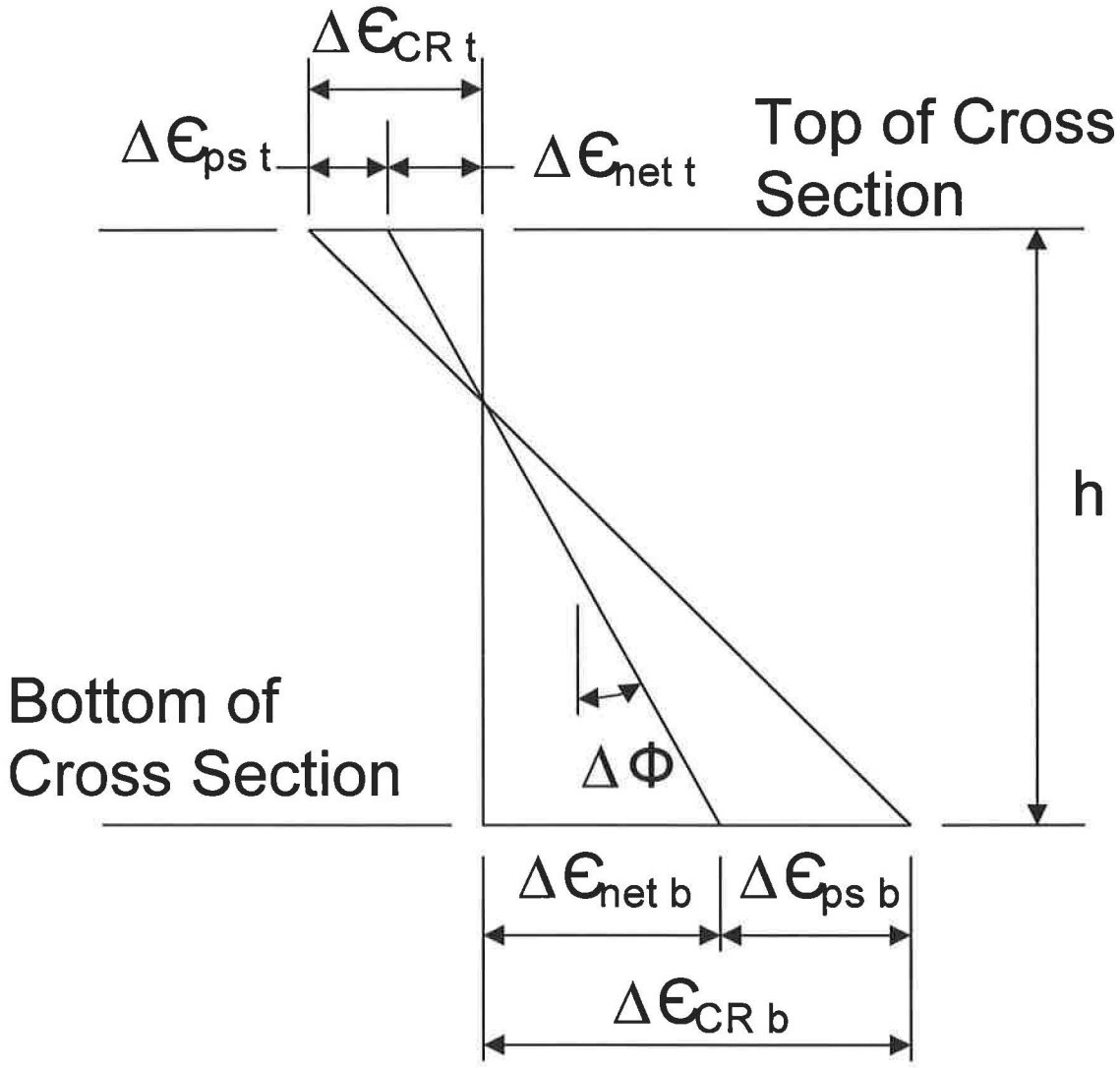

Figure 5.1 Incremental Strains and Curvature

of the cross are indicated by $\Delta\epsilon_{CR\,t}$ and $\Delta\epsilon_{CR\,b}$, respectively. These incremental creep strains are calculated by using the stresses due to the prestress force at the beginning of the time increment.

The loss of prestress force that occurs during a time increment causes a reduction in elastic stresses and strains across the member cross section. Incremental strains at the top and bottom of the cross due to the loss of prestress during the time increment are indicated in Fig. 5.1 by $\Delta\epsilon_{ps\,t}$ and $\Delta\epsilon_{ps\,b}$, respectively. The difference between the incremental creep strains and the incremental strains due to the loss of prestress are defined at the incremental net strains, $\Delta\epsilon_{net\,t}$ and $\Delta\epsilon_{net\,b}$. Incremental curvature at the cross section is determined using the net strains as:

$$\Delta\phi = \frac{\Delta\epsilon_{net\,b} - \Delta\epsilon_{net\,t}}{h} \qquad (5\text{-}5)$$

where h = the thickness of the cross section.

Creep contributes directly to incremental curvature by causing a linear distribution of strain. Shrinkage, strand relaxation, and member self-weight contribute to incremental curvature by affecting the prestress losses. Stresses due to member self-weight also cause creep strains and an additional component of incremental curvature. This self-weight effect is incorporated as described in the following section.

Girder Camber

Camber of a girder at any age is a sum of the upward deflection due to prestressing and the downward deflection due to self-weight and any other applied loads.

These two deflection components are kept separate in the calculations. A primary motivation for keeping them separate is the fact that the curvature diagrams along the span have different shapes for these two components.

Upward deflection at midspan due to prestress in a girder with harped strands with two hold down points is calculated using the expressions shown in Fig. 5.2. Subscripts c in the figure refer to midspan, and subscripts e refer to the support. The second expression is in terms of total curvature at the supports and at midspan. The total curvature is simply the sum of the initial curvature immediately after release plus the sum of all the incremental curvatures up to the age of interest. Calculations of camber by the Incremental Time Steps Method utilized the second expression shown in Fig. 5-2. Implementation of the expression Fig. 5-2 required the calculation of prestress losses and curvatures at midspan and at the supports. The prestress force was assumed to be fully transferred at the centerline of the supports in these calculations.

All camber calculation results presented in the next Chapter are for the HPC girders prior to application of any superposed dead load. The downward deflection at midspan due to self-weight was calculated using the familiar formula for a simple span with uniformly distributed loading. Immediately after release the downward deflection due to self-weight is referred to as δ_D. By assuming that creep strain is directly proportional to stress, the deflection due to self-weight at later ages can be calculated as:

$$\delta = \delta_D [1+C(t)] \qquad (5\text{-}6)$$

where C(t) is defined by Eqn. 2-13.

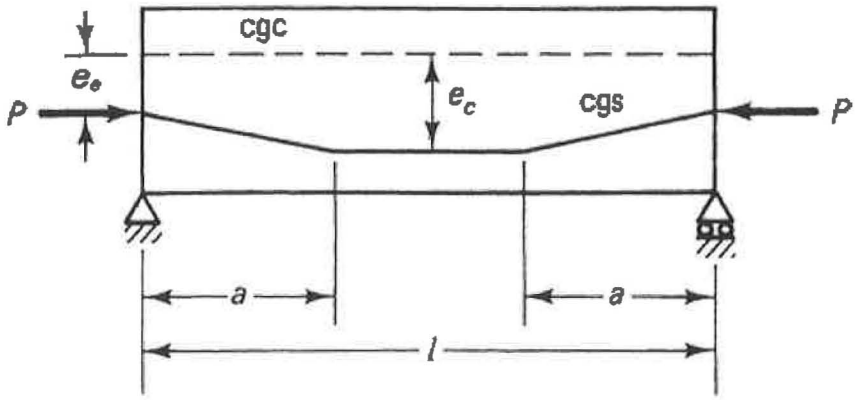

$$\delta = -\frac{Pl^2}{8EI}\left[e_c + (e_e - e_c)\frac{4}{3}\frac{a^2}{l^2}\right]$$

$$= \phi_c \frac{l^2}{8} + (\phi_e - \phi_c)\frac{a^2}{6}$$

Figure 5.2 Upward Deflection due to Prestressing Force (Nawy, 2000)

Girder Strains

Vibrating wire strain gages were embedded in five of the HPC girders as described in Chapter 3, and strain measurements were made until the bridge construction was completed. Comparisons of the measured strains and calculated strains are made in the next Chapter. The zero condition for the strain measurements was immediately before release. Immediately after release, the measured strains included the elastic strains due to the prestress force and the elastic strains due to the self-weight of the girder. At later ages the time dependent factors described above caused changes in the measured strains. Fig. 5-1 illustrates the net strain diagram associated with the incremental curvatures. The net strains for each time increment include the creep strains resulting from the prestress force and the elastic strains associated with loss of prestress. The embedded strain gages measured the net strains plus the creep strains resulting from the self-weight stresses and the shrinkage strains. As part of the Incremental Time Steps calculations, these individual strain contributions were calculated at the locations of the strain gages in the cross sections and summed at the end of each time increment.

Approximate Time Steps Method

Incremental Time Steps Method calculations are tedious to perform, and are only practical when programmed for computer solution. A simplified form of these calculations described by Nawy (2000) is the Approximate Time Steps Method. Camber estimates from this method are compared to measured values in the next Chapter. The camber at any age after release is given by:

$$\delta = \delta_e + 0.5[\delta_e + \delta_i]C(t) + \delta_D [1+C(t)] \qquad (5\text{-}7)$$

where δ_i = upward deflection due to the prestress force immediately after transfer; and δ_e = upward deflection calculated for the prestress force (after losses) at the age of interest.

CHAPTER SIX

Comparison of Calculated and Measured Cambers, Strains and Losses

Introduction

Camber and strains were monitored for five AASHTO BT-54 girders of Alabama's HPC Showcase bridge from release through completion of construction of the bridge. Additionally, camber of 26 of the remaining 30 HPC girders was measured on a single day. Details of the instrumentation and the measurements were presented in Chapters Three and Four. Methods of calculating cambers and girder strains were described in Chapter Five. Comparisons of calculated and measured cambers, strains and prestress losses are made in this chapter.

Material and Geometric Parameters

A summary of the material and geometric parameters used in calculations is provided in Table 6.1. The cross section characteristics are standard values for the AASHTO BT-54. Characteristics of the strand are nominal values based on the project specifications. The girder span length was assumed equal to 112.25 ft which is the distance between centers of the bearings for the instrumented bridge span. This span length is a reasonable estimate of the span length during storage on the production yard. The distance between centers of the supports for two of the seven bridge spans was 1 ft shorter, or 111.25 ft. No distinction is made here when comparing the cambers of those girders to the calculated cambers.

Table 6.1 Summary of Material and Geometric Parameters

Parameter	Value
BT-54 Cross Section	
Thickness, h	54 in.
Area, A	659 $in.^2$
Moment of Inertia, I	268,077 $in.^4$
c bottom	27.63 in.
Prestressing Strands – 0.6-in. dia., low-relaxation	
Number of Strands	42
Strand Area	0.217 $in.^2$
Ultimate Strength, f_{pu}	270 ksi
Modulus of Elasticity, E_s	27,500 ksi
Jacking Stress, f_{pj}	0.75 f_{pu}
Girder Characteristics	
Span Length, L	112.25 ft
Harping Point, a (see Fig. 5.2)	46.125 ft
Eccentricity at Midspan, e_c	21.13 in.
Eccentricity at Supports e_s	9.95 in.
Eccentricity at Quarter Span	16.68 in.
Concrete Properties	
Unit Weight	149.7 lb/ft^3
Modulus of Elasticity, E_c	5,740 ksi

Table 6.1 Summary of Material and Geometric Parameters (Continued)

Parameter	Value
Shrinkage – Standard Parameters (ACI 209R-92)	
α	1
f	55
$(\varepsilon_{sh})_u$	0.00078 in./in.
γ_{sh}	0.586
Shrinkage – HPC Parameters	
α	1
f	20
$(\varepsilon_{sh})_u$	0.000433 in./in.
γ_{sh}	0.585
Creep – Standard Parameters (ACI 209R-92)	
φ	0.6
d	10
C_u	2.35
γ_u	0.860
Creep – HPC Parameters	
φ	0.6
d	20
C_u	1.97
γ_u	0.653

Unit weight and modulus of elasticity values shown in Table 6.1 are averages from test data obtained during production of the HPC girders. Eskildsen (2000) performed a least squares fit with concrete strength test results from production of the HPC girders then used Eqn. 2-21 to calculate the modulus of elasticity as a function of age for use in Incremental Time Steps Calculations. After Eskildsen's work was completed, the authors concluded that this was an over-refinement given the scatter in the modulus of elasticity values measured during production. The value of 5,740 ksi is the average of 32 individual tests of cylinders at various ages from release to 56-days as reported by Glover and Stallings (2000).

Shrinkage and creep parameters for use in Eqn.s 2-2 and 2-13 are shown in Table 6.1. The standard parameter values are based on ACI 209R-92 as outlined in Chapter Two. A full listing of the individual correction factors based on ACI 209R-92 is listed in Table 6.2. Mixture proportions, average air content and average slump for the HPC used in production of the girder are given in Table 6.3. Those proportions and characteristics were used as required to calculate the corrections in Table 6.2. The volume to surface area correction factor and relative humidity correction factor in Table 6.2 are for the AASHTO BT-54 girders at an average relative humidity of 70%. The average relative humidity of 70% was taken from AASHTO LRFD (1993) for the central Alabama area.

Shrinkage and creep parameters in Table 6.1 for the HPC were determined from the lab tests. Parameters $(\varepsilon_{sh})_u$ and C_u are corrected to the standard conditions of 6x12 in. cylinders at 40% relative humidity (see Table 4.5). Correction factors γ_{sh} and γ_c are the products of only the volume to surface area correction factor and the relative humidity

Table 6.2 Correction Factors for AASHTO BT-54 at H = 70% Using ACI 209R-92

Factor	Shrinkage	Creep
Relative Humidity	0.700	0.801
Volume/Surface	0.836	0.815
Slump	1.22	1.36
Fine Aggregate	0.818	0.969
Cement Content	1.02	NA
Air Content	0.984	1
Product, γ	0.586	0.860

NA = Not Applicable

Table 6.3 HPC Mixture

Material	Cubic Yard Proportions
Type III Cement	752 lbs
Type C Fly Ash	152 lbs
#67 Limestone	1822 lbs
#89 Sand	374 lbs
#100 Sand	695 lbs
Water	265 lbs
Superplasticisers	14 oz
Retarder	3 oz
Air Entrainment	4 oz
Air Content	4.20% (Average)
Slump	8 in. (Average)

correction factor since the laboratory shrinkage and creep tests included the affects modeled by all the remaining correction factors.

Camber

A plot of cambers measured for 31 of the HPC girders on the same day is shown in Fig. 6.1. Included in the plot are cambers calculated using the Incremental Time Steps Method with standard parameters and parameters for the HPC. This plot illustrates that using the standard parameters overestimates the measured cambers. The average age for the measured cambers is 200 days; the average camber is 4.44 in., and the standard deviation is 0.271 in. At an age of 200 days, the camber calculated using the HPC parameters is 4.18 in. which is 6% below the average measured camber. Using the standard parameters, the calculated camber at 200 days is 5.49 in. which is 24% above the average measured camber. The error resulting from use of standard parameters is attributed primarily to over estimating the creep effects.

All camber measurements for ages prior to casting of the concrete deck slab are shown in Fig. 6.2. Data plotted include cambers of the instrumented girders along with the camber data shown in Fig. 6.1. Also shown are cambers calculated using HPC parameters in the Incremental Time Steps Method and the Approximate Time Steps Method. Results from these two methods are very similar. At an age of 200 days, cambers from the Incremental Time Steps Method and Approximate Time Steps Method are 4.18 in. and 4.13 in., respectively. The difference between these two values is 1%.

Error bands are included in Fig. 6.2 at plus 35% and minus 15% from the Incremental Time Steps Method results. All of the measured cambers are inside these

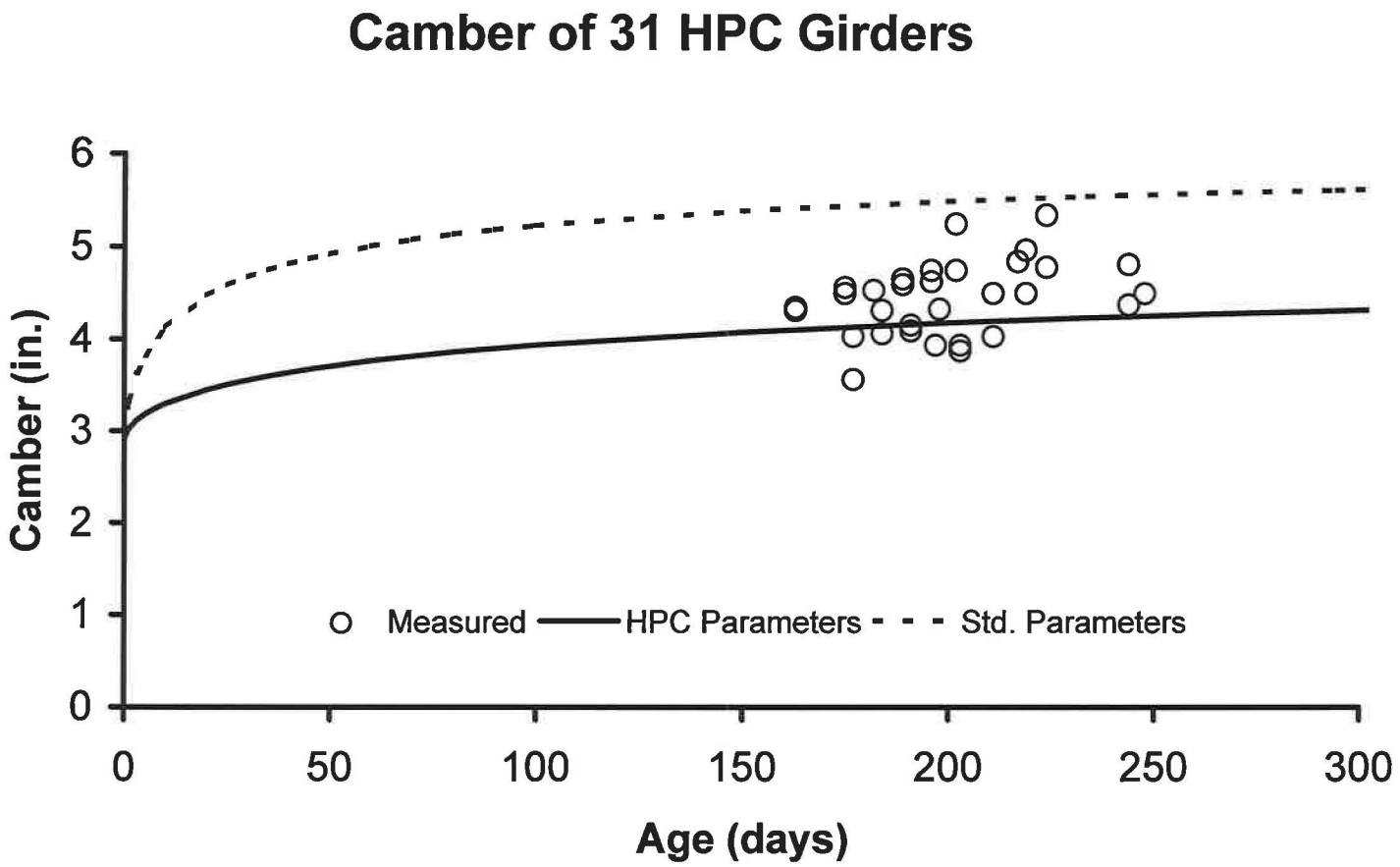

Figure 6.1 Camber of 31 HPC Girders and Calculated Camber

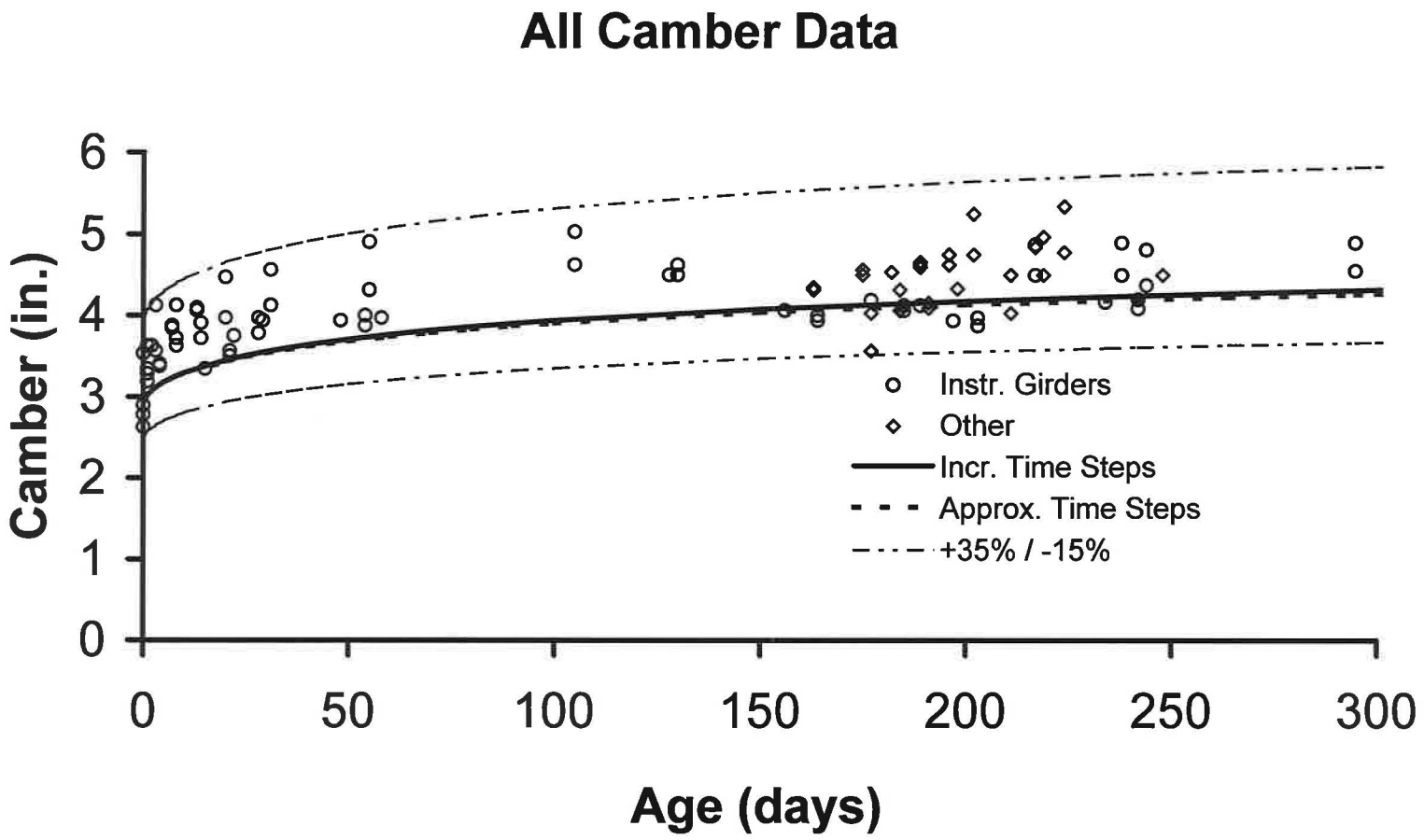

Figure 6.2 All Camber Camber Data and Calculated Camber

error bands. This same conclusion applies for error bands plotted around the cambers calculated using the Approximate Time Steps Method.

Table 6.4 summarizes cambers of the instrumented girders at an age of 1-day and at the last age prior to casting of the deck slab for which camber measurements are available. The cambers at ages greater than 1-day in Table 6.4 were measured while the girders were stored on the production yard, but these values are approximately the cambers at erection. Calculated cambers in Table 6.4 are from the Incremental Time Steps Method using HPC parameters.

At an age of 1-day, percent differences between the measured and calculated cambers in Table 6.4 range from –17% to 8%. The average measured camber at 1-day is 3.36 in., and the calculated camber is 3.02 in. The difference between these two values is –10%. At the later ages shown in Table 6.4, the percent differences between the measured and calculated cambers ranges from –12% to 1% with an average percent difference of -2%.

Simple estimates of camber were made using the PCI Multipliers Method. At erection the estimated camber is 5.71 in., and the final camber is 9.09 in. Erection cambers are generally considered to correspond to ages of 30 to 60 days. Final cambers correspond to long-term cambers years into the future. Inspection of Fig. 6.1 indicates that the estimated erection camber is larger than all the measured cambers at all ages.

ALDOT estimated the erection camber for the HPC girders prior to construction. The camber was shown on the bridge drawings as 5.125 in. This estimate provides a reasonably accurate upper bound to the measured cambers shown in Fig. 6.1.

Table 6.4 Camber of Instrumented HPC Girders

Girder No	Age (days)	Camber (in.) Measured	Camber (in.) Calculated	Percent Difference
1	1	3.34	3.02	-10
	295	4.55	4.31	-5
2	1	3.63	3.02	-17
	295	4.90	4.31	-12
3	1	3.19	3.02	-5
	242	4.09	4.24	4
4	1	3.28	3.02	-8
	242	4.20	4.24	1
5	1	3.34	3.02	-10
	234	4.17	4.23	1

The results in Fig. 6.1 and 6.2 and in Table 6.4 illustrate that both the Incremental Time Steps Method and the Approximate Time Steps Method can produce good estimates of girder cambers when the materials parameters are accurately known. Work on this project and literature study has indicated that modeling the creep characteristics of the concrete is the single most important part of calculating accurate estimates of camber.

Strains

Plots of strains measured at midspan of all five of the instrumented girders prior to construction of the deck slab are shown in Fig. 6.3. Strains measured in the top flange and at the level of the prestress force are shown along with calculated strains. Similar plots for the three girders with strain gages at the quarter span are shown in Fig. 6.4. Calculated strains in these figures were found using the Incremental Time Steps Method with standard parameters and with the HPC parameters.

Similar to the results for camber, use of the standard parameters significantly overestimates the strains. The calculated strains include directly the effects of overestimating the shrinkage and creep by use of the standard parameters.

Fig. 6.5 and 6.6 show the measured and calculated strains along with error bands. The measured midspan strains at the level of the prestress force in Fig. 6.5 are inside the error bands at plus and minus 20% except for a couple of measurements. The top flange strains at midspan are inside error bands at plus and minus 50%, except for some of the measurements at very ages.

Error bands in Fig. 6.6 at plus and minus 20% for the strains at the level of the prestress include all the strain data, except the measurements for Girder 3 at early ages. It

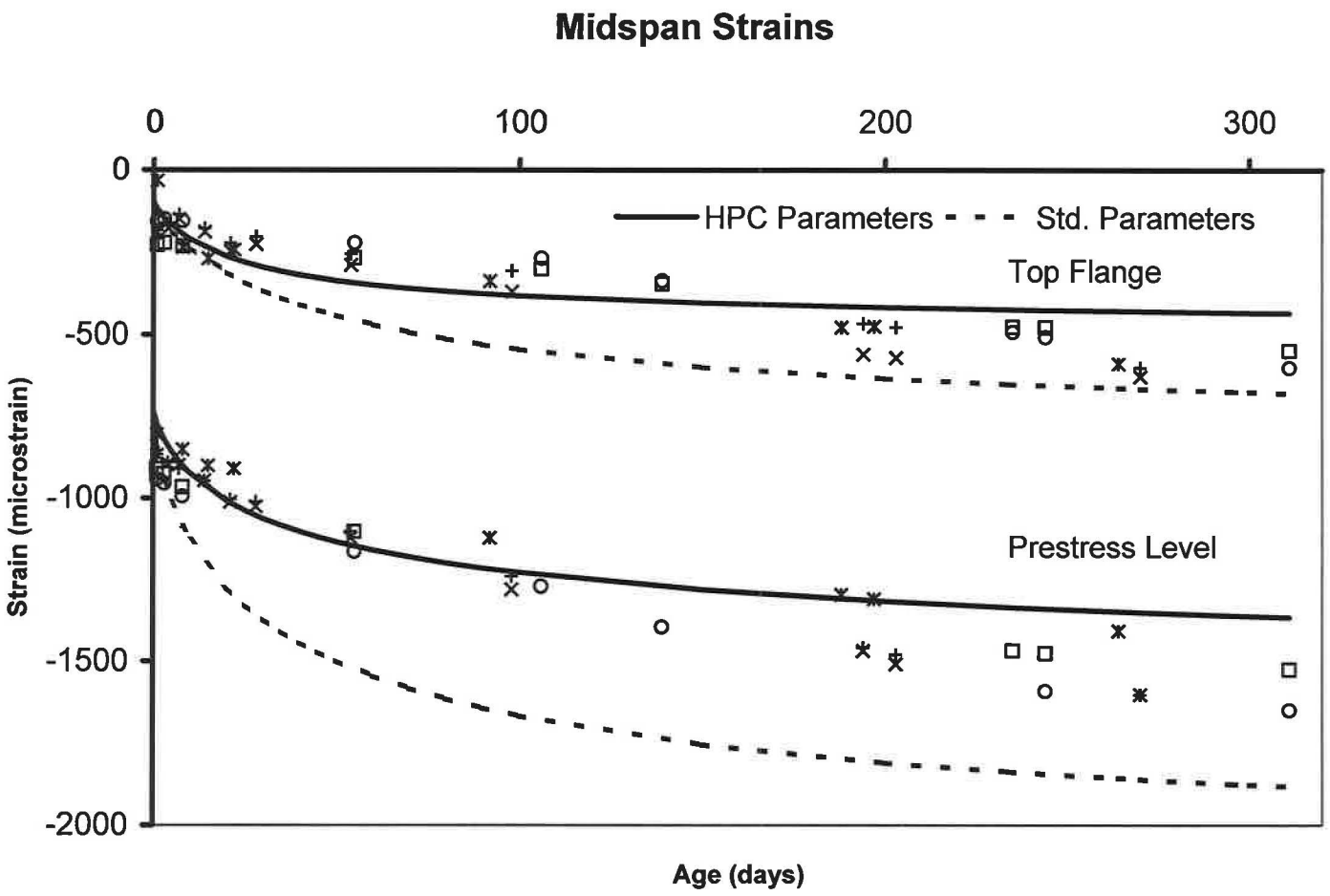

Figure 6.3 Measured and Calculated Strains at Midspan

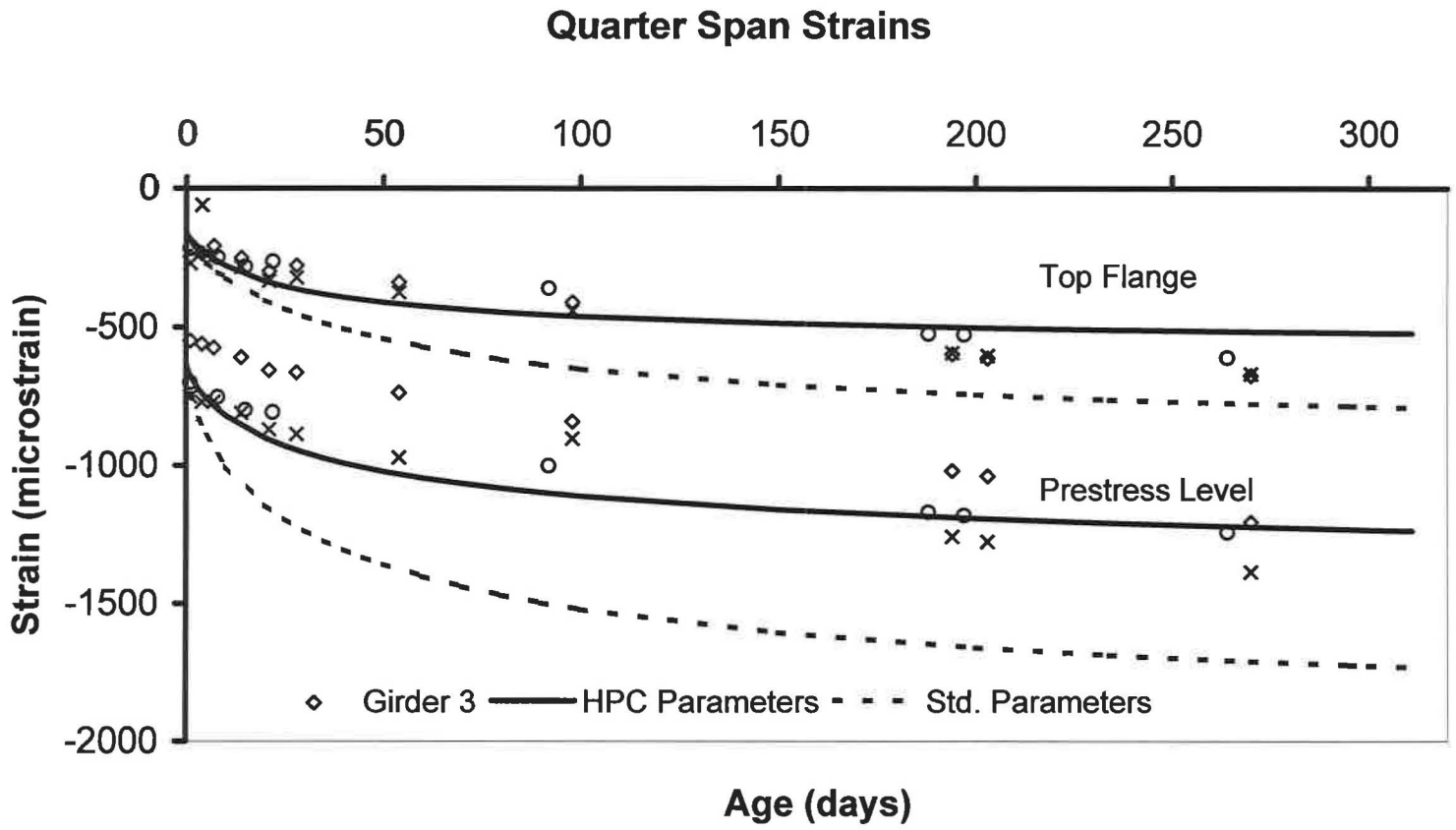

Figure 6.4 Measured and Calculated Strains at Quarter Span

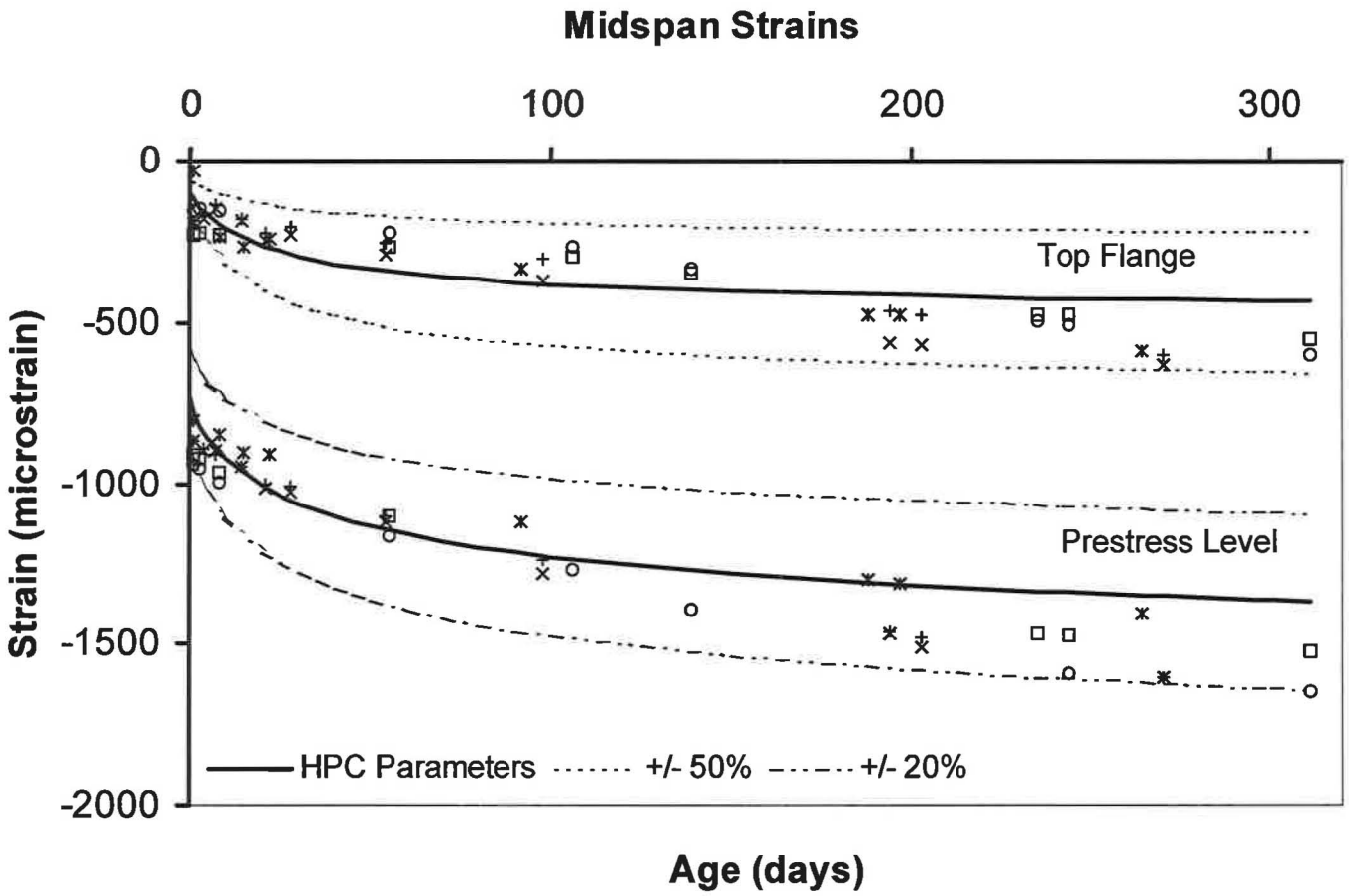

Figure 6.5 Measured Midspan Strains and Calculated Strains with Error Bands

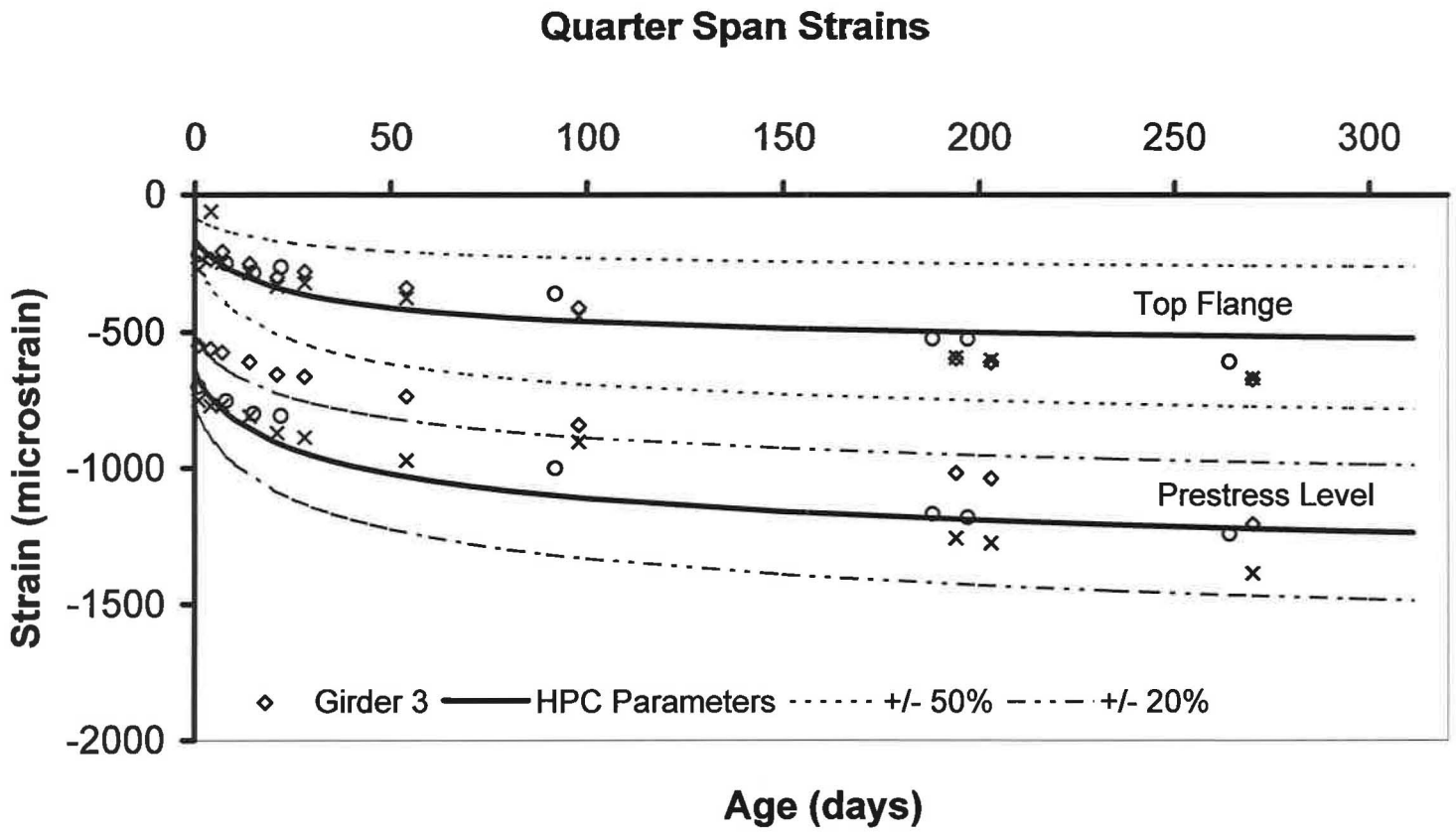

Figure 6.6 Measured Quarter Span Strains and Calculated Strains with Error Bands

is unclear why the measurements for Girder 3 start at a significantly lower strain than for the other two girders. All but one of the top flange strain measurements in Fig. 6.6 are inside error bands at plus and minus 50%.

Strains at ages of 1-day and at the largest age prior to construction of the deck for which strain data is available are shown in Table 6.5 and 6.6. These tabulated strains and percent differences illustrate that the calculated strains at the level of the prestress match the measurements better than the calculated strains at the top flange. At midspan, the average percent difference for strains at the level of the prestress for ages of 264-days to 311-days is –13%. Similarly at the top flange the average percent difference is –27%. At quarter span, the average percent difference of strains at the level of the prestress for ages of 264-days to 311-days is -4%, and at the top flange the average percent difference is -20%.

Overall, the comparisons between the calculated and measured strains show better agreement for the strains at the level of the prestress than for the top flange strains. The calculated strains typically underestimate the measured strains. With only a few exceptions, the strain measurements at the level of the prestress at all ages are inside error bands at plus and minus 20% from the calculated strains.

Prestress Losses

Strain measurements made at the level of the prestress force provide estimates of the loss of prestress force. The change in strain measured for any time period multiplied by the modulus of elasticity for the strand is equal to the loss in prestress due to all effects except relaxation. Losses determined from the measurements in this manner include the

Table 6.5 Strains at Midspan

Girder No.	Age (days)	Top Flange Measured ($\times 10^6$)	Top Flange Calculated ($\times 10^6$)	Top Flange Percent Difference	Prestress Level Measured ($\times 10^6$)	Prestress Level Calculated ($\times 10^6$)	Prestress Level Percent Difference
1	1	-228	-120	-47	-910	-775	-15
	311	-550	-436	-21	-1525	-1366	-10
2	1	-156	-120	-23	-943	-775	-18
	311	-603	-436	-28	-1650	-1366	-17
3	1	-183	-120	-34	-866	-775	-11
	270	-602	-430	-29	-1602	-1351	-16
4	1	-191	-120	-37	-867	-755	-11
	270	-630	-430	-32	-1602	-1351	-16
5	1	-33	-120	264	-806	-755	-4
	264	-590	-429	-27	-1408	-1349	-4

Table 6.6 Strains at Quarter Span

Girder No.	Age (days)	Top Flange Measured ($\times 10^6$)	Top Flange Calculated ($\times 10^6$)	Top Flange Percent Difference	Prestress Level Measured ($\times 10^6$)	Prestress Level Calculated ($\times 10^6$)	Prestress Level Percent Difference
3	1	-248	-183	-26	-549	-677	23
	270	-675	-517	-23	-1209	-1226	1
4	1	-271	-183	-32	-751	-677	-10
	270	-670	-517	-23	-1389	-1226	-12
5	1	-216	-183	-15	-700	-677	-3
	264	-610	-516	-15	-1245	-1224	-2

gain in prestress due to elastic strain resulting from the losses. For example, a loss in prestress force causes a loss in camber and a tensile strain at the level of the prestress. This tensile strain is included in the strain measurements. Relaxation is a loss of stress at constant strain. So, the relaxation loss does not appear directly in the strain measurements, but the elastic tensile strain resulting from the loss does.

Prestress losses are listed in Table 6.7 for the time period starting at an age of 1-day and extending to the last available strain data prior to construction of the deck slab. This time period corresponds with the measurements presented in Table 6.5 and 6.6. Losses from the measurements and the calculated strains were found by taking the difference in strains at the beginning and end of the time period and multiplying by the modulus of elasticity of the strand. The agreement between the calculated and measured losses is good. The calculated losses consistently underestimate the measured losses. At midspan, the average percent difference is –14%. For the three girders were strain measurements were made at the quarter span, the average percent difference between measured and calculate losses is –10%.

Prestress losses in Table 6.7 cover the time from age of 1-day to approximately 10 months. An estimate of total losses to an age of 10 months can be made by adding measured and calculated losses. The average of the measured losses at midspan from Table 6.7 is 18,700 psi. The calculated relaxation loss for this time period is 2780 psi. From time zero to an age of 1-day, the calculated prestress loss is 1070 psi. The sum of these results is an estimate of losses for the instrumented girders of 22,550 psi from release to an age of 10-months. The initial losses at midspan were 1% of the jacking stress from relaxation and 10% from elastic shortening, or 22,200 psi. The sum of the

Table 6.7 Midspan Prestress Losses, Excluding Relaxation

Girder No.	Age Range	Midspan Measured (psi)	Midspan Calculated (psi)	Percent Difference	Quarter Span Measured (psi)	Quarter Span Calculated (psi)	Percent Different
1	1-day to 311-days	16,910	16,270	-4	N.A.	15,500	N.A.
2	1-day to 311-days	19,440	16,270	-16	N.A.	15,500	N.A.
3	1-day to 270-days	20,240	15,850	-22	18,150	15,100	-17
4	1-day to 270-days	20,210	15,850	-22	17,550	15,100	-14
5	1-day to 264-days	16,560	15,780	-5	14,990	15,040	0

N.A. = Not Available

initial loses and losses after age zero gives an estimate of the total losses to an age of 10-months of 44,750 psi.

Losses were calculated using the most rigorous methods provided by AASHTO *LRFD* and the AASHTO *Standard Specifications*. Losses by *LRFD* were 81,400 psi, and losses by the *Standard Specifications* were 83,200 psi. AASHTO specifications provide design estimates of prestress losses which are long-term losses. The AASHTO losses given above are for the girder alone over a normal bridge lifetime without the beneficial effect of the deck dead load on the creep loss. This represents an artificial condition, so comparisons of the AASHTO losses and the measured losses for the relatively short 10 month period are not appropriate.

CHAPTER SEVEN

CONCLUSIONS AND RECOMMENDATIONS

Conclusions

Camber and strains were monitored for five AASHTO BT-54 girders of Alabama's HPC Showcase Bridge from release through completion of construction of the bridge. Camber of 31 of the 35 HPC girders was measured on a single day to simulate the conditions at an artificial erection date. The average age of the 31 girders was 200-days. Test cylinders of the HPC were made and match-cured during production of the girders. Laboratory tests were performed using these match-cured cylinders to determine the strength, modulus of elasticity, creep and shrinkage characteristics of the concrete. These measured materials parameters and standard parameters were used to calculate girder strains, camber and prestress losses up to the time of deck construction at a age of approximately 300-days. Comparisons of the field measurements and the calculated values allow the following conclusions.

Accurate predictions of camber and prestress losses are possible using the Incremental Time Steps Method with materials parameters that are representative of the concrete used to produce the girders.

Cambers calculated by both the Incremental Time Steps Method and the Approximate Time Steps Method with the HPC materials parameters agreed well with the measured cambers. Error bands at plus 35% and minus 15% from the calculated cambers included all measured cambers at all ages up to 300-days. The camber

calculated for an age of 200-days was 6% below the average of 31 measured cambers for girders with an average age of 200-days.

New methods for camber calculations are not required for HPC. But, accurate predictions require accurate materials parameters. Cambers calculated using standard materials parameters were at the upper bound of the measured values. At an age of 200-days, the calculated camber was 24% higher than the average of 31 measured cambers for girders with an average age of 200-days. This error resulted primarily from over-estimating the shrinkage and creep of the concrete.

Measured cambers were significantly smaller than the camber at erection estimated using the PCI Multipliers Method. Cambers at erection by the PCI Multipliers Method correspond to an age of 30-days to 60-days. The calculated camber at erection was 29% larger than the average of measured cambers of 31 girders with an average age of 200-days.

Agreement between calculated and measured strains was best at the level of the prestress force. Strains at the level of the prestressing force at midspan calculated using the Incremental Time Steps Method with HPC materials parameters were generally within 20% of the measured strains for ages up to 300-days. Strains in the top flange were generally with 50% of the measured strains for ages up to 300-days.

Prestress losses calculated using the Incremental Time Steps Method with HPC materials parameters showed good agreement with measured losses. Losses were measured for a period from an age of 1-day to an age that varied from 264-days to 311-days for the individual instrumented girders. For the five girders with midspan strain gages, the calculated losses were consistently less than the measured loss by an average

of 14%. For the three girders with quarter span strain gages, the average percent difference between the measured and calculated losses was 10%.

Recommendations

Camber of prestressed girders can be calculated during the design stage with reasonable accuracy when representative materials parameters are known. The Incremental Time Steps Method or the Approximate Time Steps Method should be used along with representative materials parameters when bridge design details are sensitive to camber estimates. Experiences from this project indicate that only a moderate amount of laboratory testing is needed to obtain the required materials parameters. Given that prestress producers tend to use the same materials sources for long time periods, the development of an adequate database of materials parameters for use by an individual state is practical.

Camber estimates using standard material parameters overestimated the measured cambers. Primarily this resulted from overestimating the effects of creep and shrinkage. This observation suggests that design estimates of prestress losses found using standard materials parameters, or methods such as those of AASHTO, may tend to overestimate the prestress losses that occur in girders made with HPC mixture studied here. Monitoring of Alabama's HPC bridge should be continued for the purpose of evaluating the long-term prestress losses.

References

AASHTO (American Association of State Highway and Transportation Officials). (1996). *Standard Specifications for Highway Bridges*. Sixteenth Edition. Washington, D.C.

AASHTO. (1998). *LRFD Bridge Design Specifications*. Second Edition. Washington, D.C.

American Concrete Institute Committee 209. (1992). "Prediction of Creep, Shrinkage, and Temperature Effects in Concrete Structures." ACI 209R-92 Farmington Hills, Michigan.

American Concrete Institute Committee 318. (1995). "Building Code Requirements for Structural Concrete." ACI 318-95, Farmington Hills, Michigan

American Concrete Institute Committee 363. (1992). "State of the Art Report on High Strength Concrete." ACI 363R-92, Farmington Hills, Michigan.

American Concrete Institute Committee 435. (1995). "Control of Deflection in Concrete Structures." ACI 435R-95, Farmington Hills, Michigan.

American Concrete Institute Committee 435. (1985). "State of the Art Report on Temperature-Induced Deflections of Reinforced Concrete Members." ACI 435.7R-85, Farmington Hills, Michigan.

American Society for Testing and Materials. (1994). "Standard Test Method for Creep of Concrete in Compression." ASTM Annual Book of Standards, Volume 4.02. C512-87.

Bazant, Z.P. (1982). *Creep and Shrinkage in Concrete Structures*. John Wiley and Sons, New York, New York.

Farrington, Burns, and Carrasquillo. (1996). "Creep and Shrinkage of High Performance Concrete." Center for Transportation Research. University of Texas at Austin. Report 580-5.

Glover, J.M. and Stallings, J.M., "High Performance Bridge Concrete," TE-036 Report, ALDOT Research Project 930-373, July 2000, 360 pages.

Glover, Jim. (1999). "Production of High Performance Bridge Concrete." Master's Thesis. Auburn University. Auburn, Alabama.

Nawy, Edward G. (2000). *Prestressed Concrete: A Fundamental Approach.* 3rd Ed., Prentice Hall, Englewood Cliffs, New Jersey.

Neville, A.M. (1983). *Creep of Plain and Structural Concrete.* Construction Press. New York, New York.

Neville, A.M. (1996). *Properties of Concrete*, 4th Ed., John Wiley and Sons, New York, New York.

Precast/Prestressed Concrete Institute (PCI). (1992). *PCI Design Handbook*, 4th Ed., Chicago, Illinois.

Rusch, Hubert, Jungwirth, Dieter, and Hubert K. Hilsdorf. (1983). *Creep and Shrinkage: Their Effect on the Behavior of Concrete Structures*, 1st Ed., Springer-Verlag, New York, New York.

Smerda, Zdenek. (1988). *Creep and Shrinkage of Concrete Elements and Structures.* Elsevier Publishing. New York, New York.

APPENDIX

Spreadsheet for Incremental Time Steps Calculations

Incremental Time Steps Method JMS 2001
Input Data

No. Strands	42			
fpu	270000	psi		
Strand Area	0.217	in.2		
As	9.114	in.2		
Es	27500000	psi		
fpj / fpu	0.750128			
Fj per strand	43950	lbs	**Initial Losses for Camber Calculations**	
Pj jacking force	1845900	lbs	Initial Relaxation Loss =	1 %
Pi initial prestress force	1643578	lbs	Initial Elastic Loss =	9.961 %
ec midspan eccentricity	21.13	in.		9.961
es support eccentricty	9.95	in.		
L span length	1347	in.	112.25	ft
a distance to harping point	553.5	in.	46.125	ft
Unit weight of concrete	149.7	lbs/ft3		
w weight per ft of girder	685.09	lbs/ft		
h concrete section	54	in.		
I concrete section	268077	in. 4		
A concrete section	659	in. 2		
r 2 concrete section	406.79	in.		
c bottom	27.63	in.		
S bottom	9702.39	in.3		
c top	26.37	in.		
S top	10165.98	in.3		

Shrinkage Loss

f	20	f = 20 HPC, 55 ACI
(e sh)u	0.000433	0.000433 HPC, 0.00078 ACI
γ s	0.585	0.585 HPC, 0.586 ACI

Creep Loss

d	20		d= 20 HPC, 10 ACI
Cu	1.97	in/in	Cu= 1.97 HPC, 2.35 ACI
γ c	0.653		0.653 HPC, 0.860 ACI

Prestress Losses for Low Relaxation Strand
At Midspan

PRESTESS EFFECTS ON CURVATURE

Self Wt. Stress @ cgs 1020.58 psi

e midspan 21.13 in.

Ending Age (days)	f'c (psi)	Ec (psi) Inactive	Midspan P End of Incr. (lbs)	Relaxation Loss Factor R	Δ R	Shrinkage Strain (in./in.)	Incr. Shrinkage Strain (in./in.)	Creep C(t)/Ec (in./in.)/psi	Creep Δ e'CR	Prestress Stresses f top (psi)	f bot (psi)	Self Wt. + Prestress f cgs (psi)	Steel Stress Loss (psi)
0	8210	5740000	1643578	0	0	0	0	0.00	0	922.1	-6073.5	-4210.8	
1	8552	5740000	1615001	8.69E-03	8.69E-03	1.21E-05	1.21E-05	1.067E-08	1.06721E-08	906.1	-5967.9	-4119.9	3135.4
3	9547	5740000	1595512	1.17E-02	3.01E-03	3.30E-05	2.10E-05	1.975E-08	9.08119E-09	895.2	-5895.8	-4057.8	2138.3
5	9774	5740000	1582497	1.31E-02	1.40E-03	5.07E-05	1.76E-05	2.602E-08	6.26221E-09	887.9	-5847.7	-4016.4	1428.0
8	9906	5740000	1567754	1.44E-02	1.29E-03	7.24E-05	2.17E-05	3.323E-08	7.21854E-09	879.6	-5793.3	-3969.5	1617.6
10	9952	5740000	1559823	1.50E-02	6.10E-04	8.44E-05	1.21E-05	3.72E-08	3.97079E-09	875.1	-5764.0	-3944.2	870.2
20	10043	5740000	1531713	1.69E-02	1.90E-03	1.27E-04	4.22E-05	5.194E-08	1.474E-08	859.4	-5660.1	-3854.8	3084.3
25	10061	5740000	1521905	1.75E-02	6.10E-04	1.41E-04	1.41E-05	5.748E-08	5.53317E-09	853.9	-5623.8	-3823.5	1076.1
30	10074	5740000	1513726	1.80E-02	4.99E-04	1.52E-04	1.13E-05	6.228E-08	4.79813E-09	849.3	-5593.6	-3797.5	897.4
35	10082	5740000	1506740	1.84E-02	4.22E-04	1.61E-04	9.21E-06	6.652E-08	4.24354E-09	845.4	-5567.8	-3775.3	766.5
40	10089	5740000	1500663	1.88E-02	3.65E-04	1.69E-04	7.68E-06	7.033E-08	3.80757E-09	841.9	-5545.3	-3755.9	666.8
45	10094	5740000	1495300	1.91E-02	3.22E-04	1.75E-04	6.50E-06	7.378E-08	3.45443E-09	838.9	-5525.5	-3738.9	588.5
50	10098	5740000	1490510	1.94E-02	2.88E-04	1.81E-04	5.57E-06	7.694E-08	3.16175E-09	836.3	-5507.8	-3723.6	525.5
60	10105	5740000	1482257	1.99E-02	4.99E-04	1.90E-04	9.05E-06	8.256E-08	5.61797E-09	831.6	-5477.3	-3697.3	905.6
70	10109	5740000	1475347	2.03E-02	4.22E-04	1.97E-04	7.04E-06	8.744E-08	4.87896E-09	827.7	-5451.8	-3675.3	758.2
80	10112	5740000	1469429	2.07E-02	3.65E-04	2.03E-04	5.63E-06	9.175E-08	4.3079E-09	824.4	-5429.9	-3656.5	649.3
90	10115	5740000	1464270	2.10E-02	3.22E-04	2.07E-04	4.61E-06	9.56E-08	3.85253E-09	821.5	-5410.9	-3640.1	566.0
100	10117	5740000	1459711	2.13E-02	2.88E-04	2.11E-04	3.84E-06	9.908E-08	3.48052E-09	819.0	-5394.0	-3625.6	500.3
150	10123	5740000	1442646	2.24E-02	1.11E-03	2.24E-04	1.24E-05	1.127E-07	1.3572E-08	809.4	-5331.0	-3571.3	1872.3
200	10126	5740000	1431183	2.32E-02	7.87E-04	2.30E-04	6.77E-06	1.223E-07	9.64237E-09	803.0	-5288.6	-3534.8	1257.8
234	10128	5740000	1425182	2.36E-02	4.30E-04	2.33E-04	3.08E-06	1.275E-07	5.20766E-09	799.6	-5266.4	-3515.7	658.4
242	10128	5740000	1423923	2.37E-02	9.20E-05	2.34E-04	6.09E-07	1.286E-07	1.10704E-09	798.9	-5261.8	-3511.7	138.2
264	10129	5740000	1420700	2.39E-02	2.38E-04	2.35E-04	1.50E-06	1.315E-07	2.84959E-09	797.1	-5249.9	-3501.4	353.6
270	10129	5740000	1419878	2.40E-02	6.15E-05	2.36E-04	3.69E-07	1.322E-07	7.31953E-10	796.6	-5246.8	-3498.8	90.2
295	10129	5740000	1416673	2.43E-02	2.42E-04	2.37E-04	1.39E-06	1.351E-07	2.86642E-09	794.8	-5235.0	-3488.6	351.7
300	10130	5740000	1416072	2.43E-02	4.60E-05	2.37E-04	2.51E-07	1.356E-07	5.40634E-10	794.5	-5232.8	-3486.7	65.9
311	10130	5740000	1414792	2.44E-02	9.85E-05	2.38E-04	5.26E-07	1.368E-07	1.15446E-09	793.8	-5228.0	-3482.6	140.5

Stresses, Strains, and Curvatures
At Midspan

PRESTESS EFFECTS ON CURVATURE

e midspan 21.13 in.

Ending Age (days)	Δ P (lbs)	Stress and Strain Changes Due to Prestress Losses: Δ f top (psi)	Δ f bot (psi)	Δ e top (in./in.)	Δ e bot (in./in.)	Fiber Gross Strains: Δ eCR top (in./in.)	Δ eCR bot (in./in.)	Net Strains: Δ e top (in./in.)	Δ e bot (in./in.)	Midspan Incremental Curvature (rad./in.)	Midspan Total Curvature (rad./in.)
0								0.0001606	-0.0010581	-2.257E-05	-2.257E-05
1	28576	16.03	-105.60	2.793E-06	-1.840E-05	9.841E-06	-6.482E-05	7.048E-06	-4.642E-05	-9.901E-07	-2.356E-05
3	19489	10.93	-72.02	1.905E-06	-1.255E-05	8.228E-06	-5.420E-05	6.324E-06	-4.165E-05	-8.884E-07	-2.445E-05
5	13015	7.30	-48.09	1.272E-06	-8.379E-06	5.606E-06	-3.692E-05	4.334E-06	-2.854E-05	-6.088E-07	-2.506E-05
8	14743	8.27	-54.48	1.441E-06	-9.491E-06	6.409E-06	-4.221E-05	4.968E-06	-3.272E-05	-6.979E-07	-2.575E-05
10	7931	4.45	-29.31	7.752E-07	-5.106E-06	3.493E-06	-2.300E-05	2.717E-06	-1.790E-05	-3.818E-07	-2.614E-05
20	28110	15.77	-103.88	2.748E-06	-1.810E-05	1.290E-05	-8.496E-05	1.015E-05	-6.686E-05	-1.426E-06	-2.756E-05
25	9808	5.50	-36.24	9.587E-07	-6.314E-06	4.755E-06	-3.132E-05	3.796E-06	-2.500E-05	-5.333E-07	-2.810E-05
30	8179	4.59	-30.22	7.994E-07	-5.265E-06	4.097E-06	-2.698E-05	3.298E-06	-2.172E-05	-4.633E-07	-2.856E-05
35	6986	3.92	-25.81	6.828E-07	-4.497E-06	3.604E-06	-2.374E-05	2.921E-06	-1.924E-05	-4.104E-07	-2.897E-05
40	6077	3.41	-22.46	5.940E-07	-3.912E-06	3.219E-06	-2.120E-05	2.625E-06	-1.729E-05	-3.687E-07	-2.934E-05
45	5363	3.01	-19.82	5.242E-07	-3.453E-06	2.908E-06	-1.916E-05	2.384E-06	-1.570E-05	-3.350E-07	-2.967E-05
50	4789	2.69	-17.70	4.681E-07	-3.083E-06	2.653E-06	-1.747E-05	2.184E-06	-1.439E-05	-3.069E-07	-2.998E-05
60	8254	4.63	-30.50	8.068E-07	-5.314E-06	4.698E-06	-3.094E-05	3.891E-06	-2.563E-05	-5.467E-07	-3.053E-05
70	6910	3.88	-25.53	6.754E-07	-4.448E-06	4.057E-06	-2.672E-05	3.382E-06	-2.228E-05	-4.751E-07	-3.100E-05
80	5918	3.32	-21.87	5.785E-07	-3.810E-06	3.566E-06	-2.349E-05	2.987E-06	-1.968E-05	-4.197E-07	-3.142E-05
90	5158	2.89	-19.06	5.042E-07	-3.321E-06	3.176E-06	-2.092E-05	2.672E-06	-1.760E-05	-3.754E-07	-3.180E-05
100	4559	2.56	-16.85	4.457E-07	-2.935E-06	2.859E-06	-1.883E-05	2.414E-06	-1.590E-05	-3.391E-07	-3.214E-05
150	17064	9.57	-63.06	1.668E-06	-1.099E-05	1.112E-05	-7.321E-05	9.447E-06	-6.222E-05	-1.327E-06	-3.346E-05
200	11464	6.43	-42.36	1.121E-06	-7.380E-06	7.804E-06	-5.140E-05	6.684E-06	-4.402E-05	-9.390E-07	-3.440E-05
234	6001	3.37	-22.18	5.866E-07	-3.863E-06	4.182E-06	-2.754E-05	3.595E-06	-2.368E-05	-5.051E-07	-3.491E-05
242	1259	0.71	-4.65	1.231E-07	-8.106E-07	8.852E-07	-5.830E-06	7.621E-07	-5.020E-06	-1.071E-07	-3.501E-05
264	3222	1.81	-11.91	3.150E-07	-2.075E-06	2.277E-06	-1.499E-05	1.962E-06	-1.292E-05	-2.756E-07	-3.529E-05
270	822	0.46	-3.04	8.036E-08	-5.293E-07	5.834E-07	-3.843E-06	5.031E-07	-3.313E-06	-7.067E-08	-3.536E-05
295	3205	1.80	-11.84	3.133E-07	-2.063E-06	2.283E-06	-1.504E-05	1.970E-06	-1.298E-05	-2.768E-07	-3.564E-05
300	601	0.34	-2.22	5.873E-08	-3.868E-07	4.297E-07	-2.830E-06	3.710E-07	-2.443E-06	-5.212E-08	-3.569E-05
311	1280	0.72	-4.73	1.251E-07	-8.242E-07	9.172E-07	-6.041E-06	7.921E-07	-5.217E-06	-1.113E-07	-3.580E-05

Strains at Vibrating Wire Strain Gage Locations at Midspan

		y bot gage=	21.13	in.			1643578	
Total	Total	y top gage=	-23.66	in.			1643578	
Net	Net	Creep Adjusted Self Wt.		Total	Total			Actual
Strain at	Strain at	Strain at	Strain at	Strain at	Strain at	Ending	Actual	Losses
Top Gage	Bot Gage	Top Gage	Bot Gage	Top Gage	Bot Gage	Age	Prestress	from 1-day
(in./in.)	(in./in.)	(in./in.)	(in./in.)	(in./in.)	(in./in.)	(days)	(psi)	(psi)
Self Weight Stresses =		-1.143E+03	1.021E+03					
9.949E-05	-9.114E-04	-1.991E-04	1.778E-04	-9.960E-05	-7.336E-04	0	180335	
1.039E-04	-9.514E-04	-2.113E-04	1.887E-04	-1.195E-04	-7.747E-04	1	179204	0
1.078E-04	-9.873E-04	-2.217E-04	1.980E-04	-1.469E-04	-8.223E-04	3	177895	1309
1.105E-04	-1.012E-03	-2.288E-04	2.044E-04	-1.690E-04	-8.581E-04	5	176910	2293
1.135E-04	-1.040E-03	-2.371E-04	2.117E-04	-1.959E-04	-9.007E-04	8	175741	3463
1.152E-04	-1.055E-03	-2.416E-04	2.158E-04	-2.108E-04	-9.241E-04	10	175096	4107
1.215E-04	-1.113E-03	-2.585E-04	2.308E-04	-2.636E-04	-1.009E-03	20	172765	6438
1.238E-04	-1.135E-03	-2.648E-04	2.365E-04	-2.817E-04	-1.039E-03	25	171941	7262
1.259E-04	-1.153E-03	-2.703E-04	2.414E-04	-2.964E-04	-1.064E-03	30	171252	7952
1.277E-04	-1.170E-03	-2.751E-04	2.457E-04	-3.086E-04	-1.085E-03	35	170662	8542
1.293E-04	-1.185E-03	-2.795E-04	2.496E-04	-3.190E-04	-1.104E-03	40	170148	9055
1.308E-04	-1.198E-03	-2.834E-04	2.531E-04	-3.280E-04	-1.121E-03	45	169695	9509
1.322E-04	-1.211E-03	-2.870E-04	2.563E-04	-3.358E-04	-1.135E-03	50	169290	9914
1.346E-04	-1.233E-03	-2.934E-04	2.621E-04	-3.489E-04	-1.161E-03	60	168591	10612
1.367E-04	-1.252E-03	-2.990E-04	2.670E-04	-3.594E-04	-1.182E-03	70	168007	11197
1.385E-04	-1.269E-03	-3.039E-04	2.714E-04	-3.681E-04	-1.200E-03	80	167507	11696
1.402E-04	-1.284E-03	-3.083E-04	2.754E-04	-3.754E-04	-1.216E-03	90	167072	12132
1.417E-04	-1.298E-03	-3.123E-04	2.789E-04	-3.817E-04	-1.230E-03	100	166687	12516
1.475E-04	-1.351E-03	-3.278E-04	2.928E-04	-4.038E-04	-1.282E-03	150	165253	13951
1.516E-04	-1.389E-03	-3.388E-04	3.026E-04	-4.175E-04	-1.317E-03	200	164295	14909
1.539E-04	-1.410E-03	-3.448E-04	3.079E-04	-4.243E-04	-1.335E-03	234	163795	15409
1.543E-04	-1.414E-03	-3.461E-04	3.091E-04	-4.257E-04	-1.339E-03	242	163691	15513
1.556E-04	-1.425E-03	-3.493E-04	3.120E-04	-4.292E-04	-1.349E-03	264	163423	15780
1.559E-04	-1.428E-03	-3.502E-04	3.127E-04	-4.301E-04	-1.351E-03	270	163355	15849
1.571E-04	-1.439E-03	-3.534E-04	3.156E-04	-4.336E-04	-1.361E-03	295	163090	16114
1.573E-04	-1.441E-03	-3.541E-04	3.162E-04	-4.342E-04	-1.362E-03	300	163041	16163
1.578E-04	-1.446E-03	-3.554E-04	3.174E-04	-4.356E-04	-1.366E-03	311	162935	16269

PRESTESS EFFECTS ON CURVATURE Self Wt. Stress = 0 at supports

Prestress Losses for Low Relaxation Strand

At Girder Supports e support 9.95 in.

Ending Age (days)	f'c (psi)	Ec (psi) Inactive	P at End (lbs)	Prestress Stresses f top (psi)	f bot (psi)	Prestress f cgs (psi)	Steel Stress Loss (psi)
0	8210	5740000	1643577.5	-885.4	-4179.6	-3101.0	
1	8552	5740000	1617969.5	-871.6	-4114.5	-3052.7	2809.7
3	9547	5740000	1600900.6	-862.4	-4071.0	-3020.5	1872.8
5	9774	5740000	1589506.0	-856.3	-4042.1	-2999.0	1250.2
8	9906	5740000	1576594.6	-849.3	-4009.2	-2974.7	1416.7
10	9952	5740000	1569648.5	-845.6	-3991.6	-2961.5	762.1
20	10043	5740000	1545149.7	-832.4	-3929.3	-2915.3	2688.0
25	10061	5740000	1536636.4	-827.8	-3907.6	-2899.3	934.1
30	10074	5740000	1529561.7	-824.0	-3889.6	-2885.9	776.2
35	10082	5740000	1523538.6	-820.7	-3874.3	-2874.5	660.9
40	10089	5740000	1518315.0	-817.9	-3861.0	-2864.7	573.1
45	10094	5740000	1513717.6	-815.4	-3849.3	-2856.0	504.4
50	10098	5740000	1509622.7	-813.2	-3838.9	-2848.3	449.3
60	10105	5740000	1502591.8	-809.4	-3821.0	-2835.0	771.4
70	10109	5740000	1496727.8	-806.3	-3806.1	-2824.0	643.4
80	10112	5740000	1491721.1	-803.6	-3793.4	-2814.5	549.3
90	10115	5740000	1487368.5	-801.2	-3782.3	-2806.3	477.6
100	10117	5740000	1483529.8	-799.2	-3772.6	-2799.1	421.2
150	10123	5740000	1469250.6	-791.5	-3736.3	-2772.1	1566.7
200	10126	5740000	1459697.3	-786.3	-3712.0	-2754.1	1048.2
234	10128	5740000	1454703.1	-783.6	-3699.3	-2744.7	548.0
242	10128	5740000	1453655.1	-783.1	-3696.6	-2742.7	115.0
264	10129	5740000	1450974.8	-781.6	-3689.8	-2737.6	294.1
270	10129	5740000	1450290.8	-781.3	-3688.0	-2736.3	75.0
295	10129	5740000	1447626.1	-779.8	-3681.3	-2731.3	292.4
300	10130	5740000	1447126.5	-779.6	-3680.0	-2730.4	54.8
311	10130	5740000	1446062.0	-779.0	-3677.3	-2728.4	116.8

Stresses, Strains, and Curvatures
At Girder Supports

PRESTESS EFFECTS ON CURVATURE

e midspan 9.95 in.

Ending Age (days)	Δ P (lbs)	Stress and Strain Changes Due to Prestress Losses				Fiber Gross Strains		Net Strains		Support Incremental Curvature (rad./in.)	Support Total Curvature (rad./in.)
		Δ f top (psi)	Δ f bot (psi)	Δ e top (in./in.)	Δ e bot (in./in.)	Δ eCR top (in./in.)	Δ eCR bot (in./in.)	Δ e top (in./in.)	Δ e bot (in./in.)		
0								-1.542E-04	-7.281E-04	-1.063E-05	-1.063E-05
1	25608.0	-13.79	-65.12	-2.403E-06	-1.135E-05	-9.449E-06	-4.460E-05	-7.046E-06	-3.326E-05	-4.854E-07	-1.111E-05
3	17068.9	-9.19	-43.41	-1.602E-06	-7.562E-06	-7.915E-06	-3.736E-05	-6.313E-06	-2.980E-05	-4.350E-07	-1.155E-05
5	11394.6	-6.14	-28.98	-1.069E-06	-5.048E-06	-5.401E-06	-2.549E-05	-4.331E-06	-2.045E-05	-2.984E-07	-1.185E-05
8	12911.5	-6.96	-32.83	-1.212E-06	-5.720E-06	-6.181E-06	-2.918E-05	-4.969E-06	-2.346E-05	-3.424E-07	-1.219E-05
10	6946.1	-3.74	-17.66	-6.519E-07	-3.077E-06	-3.372E-06	-1.592E-05	-2.721E-06	-1.284E-05	-1.874E-07	-1.238E-05
20	24498.7	-13.20	-62.30	-2.299E-06	-1.085E-05	-1.246E-05	-5.884E-05	-1.016E-05	-4.798E-05	-7.003E-07	-1.308E-05
25	8513.3	-4.59	-21.65	-7.990E-07	-3.772E-06	-4.606E-06	-2.174E-05	-3.807E-06	-1.797E-05	-2.623E-07	-1.334E-05
30	7074.7	-3.81	-17.99	-6.640E-07	-3.134E-06	-3.972E-06	-1.875E-05	-3.308E-06	-1.561E-05	-2.279E-07	-1.357E-05
35	6023.1	-3.24	-15.32	-5.653E-07	-2.668E-06	-3.497E-06	-1.651E-05	-2.931E-06	-1.384E-05	-2.020E-07	-1.377E-05
40	5223.6	-2.81	-13.28	-4.902E-07	-2.314E-06	-3.125E-06	-1.475E-05	-2.635E-06	-1.244E-05	-1.815E-07	-1.395E-05
45	4597.4	-2.48	-11.69	-4.315E-07	-2.037E-06	-2.825E-06	-1.334E-05	-2.394E-06	-1.130E-05	-1.649E-07	-1.412E-05
50	4094.9	-2.21	-10.41	-3.843E-07	-1.814E-06	-2.578E-06	-1.217E-05	-2.194E-06	-1.036E-05	-1.512E-07	-1.427E-05
60	7031.0	-3.79	-17.88	-6.599E-07	-3.115E-06	-4.569E-06	-2.157E-05	-3.909E-06	-1.845E-05	-2.693E-07	-1.454E-05
70	5864.0	-3.16	-14.91	-5.503E-07	-2.598E-06	-3.949E-06	-1.864E-05	-3.399E-06	-1.604E-05	-2.342E-07	-1.477E-05
80	5006.7	-2.70	-12.73	-4.699E-07	-2.218E-06	-3.473E-06	-1.640E-05	-3.004E-06	-1.418E-05	-2.069E-07	-1.498E-05
90	4352.6	-2.34	-11.07	-4.085E-07	-1.928E-06	-3.096E-06	-1.461E-05	-2.687E-06	-1.269E-05	-1.852E-07	-1.516E-05
100	3838.7	-2.07	-9.76	-3.603E-07	-1.701E-06	-2.789E-06	-1.316E-05	-2.428E-06	-1.146E-05	-1.673E-07	-1.533E-05
150	14279.1	-7.69	-36.31	-1.340E-06	-6.326E-06	-1.085E-05	-5.120E-05	-9.506E-06	-4.488E-05	-6.550E-07	-1.598E-05
200	9553.3	-5.15	-24.29	-8.966E-07	-4.232E-06	-7.632E-06	-3.603E-05	-6.735E-06	-3.179E-05	-4.641E-07	-1.645E-05
234	4994.3	-2.69	-12.70	-4.687E-07	-2.213E-06	-4.095E-06	-1.933E-05	-3.626E-06	-1.712E-05	-2.498E-07	-1.670E-05
242	1048.0	-0.56	-2.66	-9.835E-08	-4.643E-07	-8.675E-07	-4.095E-06	-7.692E-07	-3.631E-06	-5.300E-08	-1.675E-05
264	2680.3	-1.44	-6.82	-2.515E-07	-1.187E-06	-2.231E-06	-1.053E-05	-1.980E-06	-9.346E-06	-1.364E-07	-1.689E-05
270	683.9	-0.37	-1.74	-6.419E-08	-3.030E-07	-5.721E-07	-2.701E-06	-5.079E-07	-2.398E-06	-3.500E-08	-1.692E-05
295	2664.7	-1.44	-6.78	-2.501E-07	-1.181E-06	-2.239E-06	-1.057E-05	-1.989E-06	-9.391E-06	-1.371E-07	-1.706E-05
300	499.6	-0.27	-1.27	-4.689E-08	-2.214E-07	-4.216E-07	-1.990E-06	-3.747E-07	-1.769E-06	-2.582E-08	-1.709E-05
311	1064.5	-0.57	-2.71	-9.990E-08	-4.716E-07	-9.000E-07	-4.248E-06	-8.001E-07	-3.777E-06	-5.513E-08	-1.714E-05

Camber Results

Initial Self Weight Deflection
1.590 Down

Ending Age (days)	Midspan Camber due to Prestress (in.)	Creep Adjusted Self Weight (in.)	Total Camber (in.)
0	-4.509	1.590	-2.919
1	-4.708	1.688	-3.020
3	-4.886	1.771	-3.115
5	-5.008	1.828	-3.180
8	-5.149	1.894	-3.255
10	-5.225	1.930	-3.295
20	-5.512	2.065	-3.447
25	-5.619	2.115	-3.504
30	-5.712	2.159	-3.553
35	-5.794	2.198	-3.597
40	-5.868	2.232	-3.636
45	-5.936	2.264	-3.672
50	-5.997	2.293	-3.704
60	-6.107	2.344	-3.763
70	-6.202	2.389	-3.814
80	-6.287	2.428	-3.859
90	-6.362	2.463	-3.899
100	-6.430	2.495	-3.935
150	-6.697	2.619	-4.078
200	-6.886	2.707	-4.179
234	-6.987	2.754	-4.233
242	-7.009	2.764	-4.244
264	-7.064	2.790	-4.274
270	-7.078	2.797	-4.281
295	-7.134	2.823	-4.311
300	-7.145	2.828	-4.316
311	-7.167	2.839	-4.328

Prestress Losses for Low Relaxation Strand
At Quarter Point

Initial Relaxation Loss = 1 %
Initial Elastic Loss = 8.661 %

PRESTESS EFFECTS ON CURVATURE

Self Wt. Stress @ cgs = 599.73 psi
e = 16.68 in.

Ending Age (days)	f'c (psi)	Ec (psi) Inactive	P at the End of Incr. (lbs)	Relaxation Loss Factor R	Δ R	Shrinkage Strain (in./in.)	Incr. Shrinkage Strain (in./in.)	Creep C(t)/Ec (in./in.)/psi	Creep Δ e'CR	Prestress Stresses f top (psi)	Prestress Stresses f bot (psi)	Self Wt. + Prestress f cgs (psi)	Steel Stress Loss (psi)
0	8210	5740000	1667567.6	0	0	0	0	0.00	0	205.6	-5397.3	-3661.4	
1	8552	5740000	1640252.1	8.69E-03	8.69E-03	1.21E-05	1.21E-05	1.06721E-08	1.067E-08	202.3	-5308.9	-3591.6	2997.1
3	9547	5740000	1621889.7	1.17E-02	3.01E-03	3.30E-05	2.10E-05	1.97533E-08	9.081E-09	200.0	-5249.4	-3544.7	2014.7
5	9774	5740000	1609643.1	1.31E-02	1.40E-03	5.07E-05	1.76E-05	2.60155E-08	6.262E-09	198.5	-5209.8	-3513.4	1343.7
8	9906	5740000	1595775.1	1.44E-02	1.29E-03	7.24E-05	2.17E-05	3.3234E-08	7.219E-09	196.8	-5164.9	-3478.0	1521.6
10	9952	5740000	1588316.4	1.50E-02	6.10E-04	8.44E-05	1.21E-05	3.72048E-08	3.971E-09	195.9	-5140.8	-3458.9	818.4
20	10043	5740000	1561944.9	1.69E-02	1.90E-03	1.27E-04	4.22E-05	5.19448E-08	1.474E-08	192.6	-5055.4	-3391.5	2893.5
25	10061	5740000	1552760.9	1.75E-02	6.10E-04	1.41E-04	1.41E-05	5.74779E-08	5.533E-09	191.5	-5025.7	-3368.0	1007.7
30	10074	5740000	1545114.4	1.80E-02	4.99E-04	1.52E-04	1.13E-05	6.22761E-08	4.798E-09	190.5	-5000.9	-3348.5	839.0
35	10082	5740000	1538592.8	1.84E-02	4.22E-04	1.61E-04	9.21E-06	6.65196E-08	4.244E-09	189.7	-4979.8	-3331.8	715.6
40	10089	5740000	1532927.3	1.88E-02	3.65E-04	1.69E-04	7.68E-06	7.03272E-08	3.808E-09	189.0	-4961.5	-3317.4	621.6
45	10094	5740000	1527933.2	1.91E-02	3.22E-04	1.75E-04	6.50E-06	7.37816E-08	3.454E-09	188.4	-4945.3	-3304.6	547.9
50	10098	5740000	1523478.8	1.94E-02	2.88E-04	1.81E-04	5.57E-06	7.69433E-08	3.162E-09	187.9	-4930.9	-3293.2	488.7
60	10105	5740000	1515814.4	1.99E-02	4.99E-04	1.90E-04	9.05E-06	8.25613E-08	5.618E-09	186.9	-4906.1	-3273.6	840.9
70	10109	5740000	1509408.5	2.03E-02	4.22E-04	1.97E-04	7.04E-06	8.74403E-08	4.879E-09	186.1	-4885.4	-3257.3	702.9
80	10112	5740000	1503929.4	2.07E-02	3.65E-04	2.03E-04	5.63E-06	9.17482E-08	4.308E-09	185.5	-4867.6	-3243.3	601.2
90	10115	5740000	1499158.8	2.10E-02	3.22E-04	2.07E-04	4.61E-06	9.56007E-08	3.853E-09	184.9	-4852.2	-3231.1	523.4
100	10117	5740000	1494946.2	2.13E-02	2.88E-04	2.11E-04	3.84E-06	9.90812E-08	3.481E-09	184.3	-4838.6	-3220.3	462.2
150	10123	5740000	1479221.5	2.24E-02	1.11E-03	2.24E-04	1.24E-05	1.12653E-07	1.357E-08	182.4	-4787.7	-3180.1	1725.3
200	10126	5740000	1468674.3	2.32E-02	7.87E-04	2.30E-04	6.77E-06	1.22296E-07	9.642E-09	181.1	-4753.5	-3153.2	1157.3
234	10128	5740000	1463155.3	2.36E-02	4.30E-04	2.33E-04	3.08E-06	1.27503E-07	5.208E-09	180.4	-4735.7	-3139.1	605.6
242	10128	5740000	1461997.1	2.37E-02	9.20E-05	2.34E-04	6.09E-07	1.2861E-07	1.107E-09	180.3	-4731.9	-3136.1	127.1
264	10129	5740000	1459033.8	2.39E-02	2.38E-04	2.35E-04	1.50E-06	1.3146E-07	2.85E-09	179.9	-4722.3	-3128.5	325.1
270	10129	5740000	1458277.7	2.40E-02	6.15E-05	2.36E-04	3.69E-07	1.32192E-07	7.32E-10	179.8	-4719.9	-3126.6	83.0
295	10129	5740000	1455330.7	2.43E-02	2.42E-04	2.37E-04	1.39E-06	1.35058E-07	2.866E-09	179.5	-4710.3	-3119.1	323.4
300	10130	5740000	1454778.1	2.43E-02	4.60E-05	2.37E-04	2.51E-07	1.35599E-07	5.406E-10	179.4	-4708.6	-3117.7	60.6
311	10130	5740000	1453600.9	2.44E-02	9.85E-05	2.38E-04	5.26E-07	1.36753E-07	1.154E-09	179.3	-4704.7	-3114.7	129.2

Stresses, Strains, and Curvatures
At Quarter Point

PRESTESS EFFECTS ON CURVATURE

e = 16.68 in.

Ending Age (days)	Δ P (lbs)	Stress and Strain Changes Due to Prestress Losses: Δ f top (psi)	Δ f bot (psi)	Δ e top (in./in.)	Δ e bot (in./in.)	Fiber Gross Strains: Δ eCR top (in./in.)	Δ eCR bot (in./in.)	Net Strains: Δ e top (in./in.)	Δ e bot (in./in.)	Quarter Point Incremental Curvature (rad./in.)	Total Curvature (rad./in.)
0								3.5825E-05	-0.0009403	-1.808E-05	-1.808E-05
1	27315	3.37	-88.41	5.868E-07	-1.540E-05	2.195E-06	-5.760E-05	1.608E-06	-4.220E-05	-8.112E-07	-1.889E-05
3	18362	2.26	-59.43	3.945E-07	-1.035E-05	1.837E-06	-4.821E-05	1.442E-06	-3.786E-05	-7.278E-07	-1.962E-05
5	12247	1.51	-39.64	2.631E-07	-6.906E-06	1.252E-06	-3.287E-05	9.894E-07	-2.597E-05	-4.992E-07	-2.011E-05
8	13868	1.71	-44.89	2.979E-07	-7.820E-06	1.433E-06	-3.761E-05	1.135E-06	-2.979E-05	-5.726E-07	-2.069E-05
10	7459	0.92	-24.14	1.602E-07	-4.206E-06	7.814E-07	-2.051E-05	6.211E-07	-1.630E-05	-3.134E-07	-2.100E-05
20	26372	3.25	-85.35	5.666E-07	-1.487E-05	2.887E-06	-7.577E-05	2.320E-06	-6.090E-05	-1.171E-06	-2.217E-05
25	9184	1.13	-29.72	1.973E-07	-5.179E-06	1.066E-06	-2.797E-05	8.684E-07	-2.279E-05	-4.382E-07	-2.261E-05
30	7646	0.94	-24.75	1.643E-07	-4.312E-06	9.187E-07	-2.411E-05	7.545E-07	-1.980E-05	-3.807E-07	-2.299E-05
35	6522	0.80	-21.11	1.401E-07	-3.677E-06	8.085E-07	-2.122E-05	6.684E-07	-1.754E-05	-3.373E-07	-2.333E-05
40	5666	0.70	-18.34	1.217E-07	-3.195E-06	7.224E-07	-1.896E-05	6.007E-07	-1.577E-05	-3.031E-07	-2.363E-05
45	4994	0.62	-16.16	1.073E-07	-2.816E-06	6.530E-07	-1.714E-05	5.457E-07	-1.432E-05	-2.753E-07	-2.391E-05
50	4454	0.55	-14.42	9.570E-08	-2.512E-06	5.957E-07	-1.564E-05	5.000E-07	-1.312E-05	-2.523E-07	-2.416E-05
60	7664	0.95	-24.81	1.647E-07	-4.322E-06	1.055E-06	-2.770E-05	8.908E-07	-2.338E-05	-4.495E-07	-2.461E-05
70	6406	0.79	-20.73	1.376E-07	-3.612E-06	9.120E-07	-2.394E-05	7.744E-07	-2.032E-05	-3.907E-07	-2.500E-05
80	5479	0.68	-17.73	1.177E-07	-3.090E-06	8.018E-07	-2.105E-05	6.841E-07	-1.796E-05	-3.452E-07	-2.534E-05
90	4771	0.59	-15.44	1.025E-07	-2.690E-06	7.145E-07	-1.875E-05	6.120E-07	-1.606E-05	-3.088E-07	-2.565E-05
100	4213	0.52	-13.63	9.050E-08	-2.375E-06	6.434E-07	-1.689E-05	5.529E-07	-1.451E-05	-2.790E-07	-2.593E-05
150	15725	1.94	-50.89	3.378E-07	-8.867E-06	2.502E-06	-6.567E-05	2.164E-06	-5.680E-05	-1.092E-06	-2.702E-05
200	10547	1.30	-34.14	2.266E-07	-5.947E-06	1.759E-06	-4.616E-05	1.532E-06	-4.022E-05	-7.731E-07	-2.780E-05
234	5519	0.68	-17.86	1.186E-07	-3.112E-06	9.432E-07	-2.475E-05	8.246E-07	-2.164E-05	-4.161E-07	-2.821E-05
242	1158	0.14	-3.75	2.488E-08	-6.531E-07	1.997E-07	-5.243E-06	1.749E-07	-4.590E-06	-8.823E-08	-2.830E-05
264	2963	0.37	-9.59	6.366E-08	-1.671E-06	5.137E-07	-1.348E-05	4.501E-07	-1.181E-05	-2.271E-07	-2.853E-05
270	756	0.09	-2.45	1.624E-08	-4.264E-07	1.317E-07	-3.457E-06	1.154E-07	-3.030E-06	-5.825E-08	-2.859E-05
295	2947	0.36	-9.54	6.331E-08	-1.662E-06	5.155E-07	-1.353E-05	4.522E-07	-1.187E-05	-2.281E-07	-2.881E-05
300	553	0.07	-1.79	1.187E-08	-3.116E-07	9.702E-08	-2.547E-06	8.515E-08	-2.235E-06	-4.297E-08	-2.886E-05
311	1177	0.15	-3.81	2.529E-08	-6.638E-07	2.071E-07	-5.436E-06	1.818E-07	-4.772E-06	-9.174E-08	-2.895E-05

Strains at Qtr. Span		x =	333	in.				
Strain Gage Locations		y bot gage=	16.68	in.			1667568	
Total	Total	y top gage=	-23.66	in.			1667567	
Net	Net	Creep Adjusted Self Wt.		Total	Total			Actual
Strain at	Strain at	Strain at	Strain at	Strain at	Strain at	Ending	Actual	Losses
Top Gage	Bot Gage	Top Gage	Bot Gage	Top Gage	Bot Gage	Age	Prestress	from 1-day
(in./in.)	(in./in.)	(in./in.)	(in./in.)	(in./in.)	(in./in.)	(days)	(psi)	(psi)
Self Weight Stresses =		-8.507E+02	5.997E+02					
-1.316E-05	-7.424E-04	-1.482E-04	1.045E-04	-1.614E-04	-6.379E-04	0	182968	
-1.375E-05	-7.757E-04	-1.573E-04	1.109E-04	-1.831E-04	-6.769E-04	1	181896	0
-1.428E-05	-8.056E-04	-1.650E-04	1.163E-04	-2.123E-04	-7.223E-04	3	180647	1249
-1.465E-05	-8.261E-04	-1.703E-04	1.201E-04	-2.356E-04	-7.566E-04	5	179702	2194
-1.506E-05	-8.496E-04	-1.765E-04	1.244E-04	-2.639E-04	-7.975E-04	8	178577	3319
-1.529E-05	-8.624E-04	-1.799E-04	1.268E-04	-2.796E-04	-8.201E-04	10	177957	3939
-1.614E-05	-9.105E-04	-1.924E-04	1.356E-04	-3.352E-04	-9.016E-04	20	175717	6179
-1.646E-05	-9.285E-04	-1.971E-04	1.390E-04	-3.543E-04	-9.303E-04	25	174926	6970
-1.674E-05	-9.442E-04	-2.012E-04	1.418E-04	-3.699E-04	-9.543E-04	30	174266	7630
-1.698E-05	-9.580E-04	-2.048E-04	1.444E-04	-3.830E-04	-9.748E-04	35	173701	8194
-1.721E-05	-9.705E-04	-2.080E-04	1.467E-04	-3.941E-04	-9.927E-04	40	173211	8685
-1.741E-05	-9.818E-04	-2.110E-04	1.487E-04	-4.037E-04	-1.008E-03	45	172778	9118
-1.759E-05	-9.921E-04	-2.137E-04	1.506E-04	-4.122E-04	-1.022E-03	50	172392	9504
-1.792E-05	-1.011E-03	-2.184E-04	1.540E-04	-4.263E-04	-1.047E-03	60	171728	10167
-1.820E-05	-1.027E-03	-2.226E-04	1.569E-04	-4.378E-04	-1.067E-03	70	171174	10722
-1.845E-05	-1.041E-03	-2.263E-04	1.595E-04	-4.473E-04	-1.084E-03	80	170701	11195
-1.868E-05	-1.053E-03	-2.295E-04	1.618E-04	-4.555E-04	-1.099E-03	90	170289	11607
-1.888E-05	-1.065E-03	-2.325E-04	1.639E-04	-4.625E-04	-1.112E-03	100	169925	11970
-1.968E-05	-1.110E-03	-2.440E-04	1.720E-04	-4.872E-04	-1.161E-03	150	168575	13321
-2.024E-05	-1.142E-03	-2.522E-04	1.778E-04	-5.028E-04	-1.194E-03	200	167674	14222
-2.054E-05	-1.159E-03	-2.567E-04	1.809E-04	-5.106E-04	-1.211E-03	234	167205	14690
-2.061E-05	-1.162E-03	-2.576E-04	1.816E-04	-5.122E-04	-1.215E-03	242	167107	14788
-2.077E-05	-1.172E-03	-2.600E-04	1.833E-04	-5.163E-04	-1.224E-03	264	166857	15039
-2.081E-05	-1.174E-03	-2.607E-04	1.838E-04	-5.173E-04	-1.226E-03	270	166793	15103
-2.098E-05	-1.183E-03	-2.631E-04	1.855E-04	-5.213E-04	-1.235E-03	295	166544	15352
-2.101E-05	-1.185E-03	-2.636E-04	1.858E-04	-5.220E-04	-1.237E-03	300	166498	15398
-2.108E-05	-1.189E-03	-2.645E-04	1.865E-04	-5.236E-04	-1.240E-03	311	166399	15497